UNIVERSITY OF CALIFORNIA
RIVERSIDE

The Effects of Molecular and Biochemical Disruptions Posed by Harm-Reduction Tobacco Products on Developing Tissues Using Human Pluripotent Stem Cells

A Dissertation submitted in partial satisfaction
of the requirements for the degree of

Doctor of Philosophy

in

Environmental Toxicology

by

Lauren Michelle Walker

June 2019

Dissertation Committee:
Dr. Nicole I. zur Nieden, Chairperson
Dr. David Eastmond
Dr. David Volz

The Dissertation of Lauren Michelle Walker is approved:

_____

_____

_____

Committee Chairperson

University of California, Riverside

ACKNOWLEDGEMENTS

It is with great pleasure that I extend my most enthusiastic appreciation to the small village that made this dissertation possible.

I am grateful for the scientific guidance I received from my principal investigator, Nicole I. zur Nieden. Her enthusiasm for stem cell biology and dedication to research has been inspiring to witness these past few years. Starting my research career in her lab has stimulated a passion in me to do excellent research and make meaningful contributions to the field.

I will also forever remember with fondness the other members of my "lab family," who provided technical advice, graduate school counsel, and too many laughs to count. Thank you, Nicole Sparks and Joey Madrid, for sharing your treats and your jokes—and for making the cell culture room the coolest place to be in lab. Thank you, too, to Eric Wong for your technical instruction on mouse handling. Without a doubt, I have enjoyed the time I spent with my lab mates and lab neighbors on the first floor of Biological Sciences.

Thank you to the Environmental Toxicology Graduate Program and my dissertation committee members Dr. David Eastmond and Dr. David Volz for respectively providing me with a wealth of professional development opportunities and career advice. A very special thank you to Dawn Loyola who was the first person I met my doctoral journey, and who was always willing to lend a cheerful ear.

I would also like to express my gratitude for the funding sources that helped to support me through my graduate school career: The UC Riverside Dean's Distinguished Fellowship, UC Riverside Graduate Research Mentorship Program Fellowship, National Science Foundation Graduate Student Research Fellowship, and National Institutes of Health T32 Training Fellowship.

Thank you to Dr. Prue Talbot and Dr. Frances Sladek (University of California, Riverside) for kindly providing our lab with the mainstream and sidestream tobacco smoke solutions and initial mouse breeding pairs, respectively, that were used in some of my work described herein. Thank you, too, to Dr. Subburaman Mohan (Loma Linda University) for providing technical training in small animal dual-energy x-ray absorptiometry (DXA) for the bone densitometry evaluations described here. The body of this dissertation also benefited from technical, statistical, material, and/or experimental contributions from the following individuals: Julia Ast, Laura Baumgartner, Jolie Carreon, Edward Dominguez, Michael Hanna, Kevin Keller, Joseph Madrid, Ivann Martinez, Veronica Puig-Sanvicens, Beatriz Rodriguez, Tiffany Satoorian, Steven Sera, Nicole Sparks, Susaanne Trettner, and Avani Vaghela.

The text of this dissertation, in part is a reprint of the material as it appears in Toxicology Reports, Volume 2, pages 165–174 (published in 2015). Dr. Nicole I. zur Nieden directed and supervised the research for this work, while my co-authors Laura Baumgartner, Kevin Keller, Julia Ast, and Susanne Trettner provided technical and cell culture expertise.

Last, but certainly not least, I will forever appreciate and be humbled by the loving support that I received from my parents throughout this entire process. Your encouragement and impromptu pep-talks gave me the energy to keep going when the western blots got tough.

ABSTRACT OF THE DISSERTATION

The Effects of Molecular and Biochemical Disruptions Posed
by Harm-Reduction Tobacco Products on Developing Tissues
Using Human Pluripotent Stem Cells

By

Lauren Michelle Walker

Doctor of Philosophy, Graduate Program in Environmental Toxicology
University of California, Riverside, June 2019
Dr. Nicole zur Nieden, Chairperson

Focus on tobacco-related disease concerns has shifted from cigarettes to other forms of tobacco use over the last 20 years. Due to their perception as "safer than a cigarette" by the general public, harm-reduction tobacco products (HRTPs) offer an appealing alternative for women struggling with nicotine addiction who find themselves pregnant. Some studies, however, suggest that HRTPs may increase risk of adverse pregnancy outcomes and hinder fetal skeletal development. To date, the mechanistic etiology of HRTP embryotoxicity is unreported. This thesis aims to address this knowledge gap by answering some of the questions surrounding how HRTPs molecularly and biochemically cause changes in the developing skeleton.

Early in vivo studies reported herein indicated that HRTP exposure directly targets early osteogenesis of the skull following in utero exposure of mouse embryos. To explore the molecular etiology of this outcome, the embryonic stem cell test (EST) protocol was

adapted to an in vitro model of developmental osteogenesis using human pluripotent stem cells (hPSCs). Cultures were concurrently exposed to conventional sidestream cigarette smoke (CSC), harm-reduction sidestream cigarette smoke (HSC), or harm-reduction Snus smokeless tobacco extract (STE). While conventional and harm-reduction extracts both inhibited in vitro osteogenesis, only the HSC and STE harm-reduction extracts did so at sub-cytotoxic doses. Furthermore, inhibitory doses increased cellular levels of reactive oxygen species and reduced endogenous antioxidant enzyme activity. Molecular analysis found that CSC exposure incurred both DNA damage and a concurrent apoptotic response that was absent in cultures exposed to either HRTP extract. Biochemical exploration of HRTP impact on developing cultures found exclusive activation of survival kinase AKT and reduction of stress rescue kinase JNK in STE-exposed cultures. Concurrent treatment with an isoform-specific inhibitor of AKT or JNK activator rescued osteogenesis in STE cultures, implicating the specific misregulation of these kinases in poor osteogenic outcomes. Global proteomic analysis of AKT signaling targets also identified exclusive hyperphosphorylation of FOXO transcription factors—required for oxidative stress defense and adult bone homeostasis—in STE-treated cultures, marking FOXOs for nuclear exclusion. Collectively, our data suggest that HRTPs inhibit normal osteogenesis by disrupting the balance between embryonic osteogenesis, survival, and redox equilibrium mechanisms.

TABLE OF CONTENTS

LIST OF FIGURES

LIST OF TABLES

CHAPTER 1

Addressing the global birth defects burden

Introduction

Each year, over 8 million children are born with a birth defect resulting from genetic causes, maternal nutritional deficiency, or maternal exposure to environmental agents (i.e., chemical, infectious, pharmaceutical) [1]. Of these children, an estimated 3.3 million under the age of 5 die from serious birth defects, with over 300,000 children succumbing within the first month of life [2]. Affected infants who survive past childhood and their families must continue to manage lifelong physical, mental, auditory, and/or visual disabilities. Birth defects may be structural (e.g., cleft palate, heart defects) or functional (e.g., behavioral disorders, muscular dystrophy, etc.) in nature [3]. Some structural and functional defects can be corrected through surgical and pharmacological intervention, respectively. Societal cost of care and medical intervention associated with birth defects, however, can be quite burdensome—especially for low- and middle-income families. For instance, the cost of care for a child born with fetal alcohol spectrum disorder (FASD) in the United States was estimated to be about $23,000 per person annually in addition to productivity losses for caregivers of children born with FASD [4], [5]. More broadly, domestic hospitalization costs alone for individuals with birth defects was estimated to be $23 billion [6]. In this way, long-term disability caused by birth defects can have significant impacts on individuals, their families, health-care systems, and communities (Fig. 1.1).

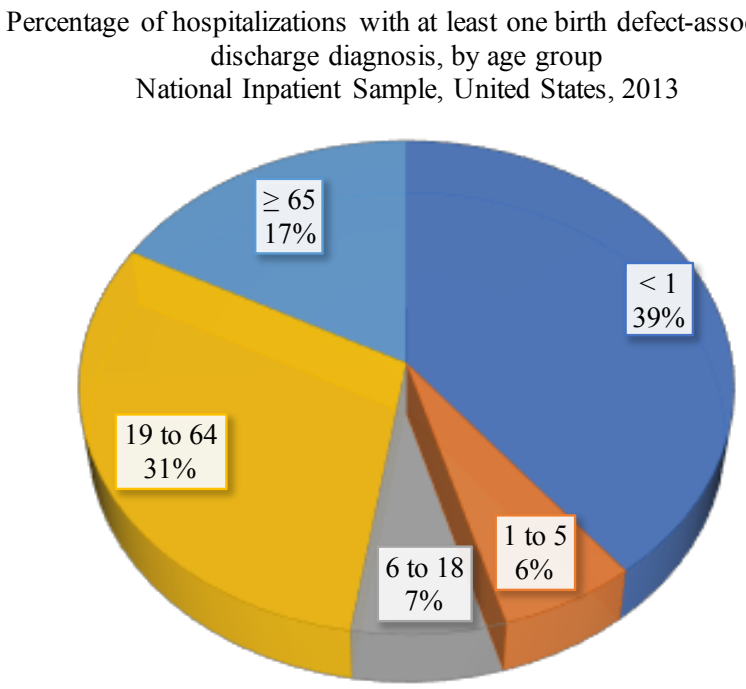

Figure 1.1. Percentage of hospital stays in the United States associated with at least one birth defect-associated diagnosis by age group for 2013 (Arth, 2017).

Birth defects are one of many public health issues that comprise the current global health burden. At present, the causes of about 30% of birth defects are somewhat understood [7]. Given the body of knowledge on the role of environmental factors and adult health [8-11], it follows that the remaining 70% of birth defects may have etiology rooted in environmental conditions and can therefore be preventable with appropriate precautions. To date, environmental contaminants such as industrial solvents, metals, pesticides, and environmental tobacco smoke have all been suggested to disrupt normal development [12]. The full extent of developmental toxicity risks, however, remains unclear. In 2011, a study found that 98% of drugs approved by the US Food and Drug Administration lacked data on whether or not those drugs posed a risk to pregnancy outcomes [13]. In addition, the majority of the commercial chemicals registered for use in the United States lack comprehensive human toxicity and exposure data [14], which also poses a challenge to birth defects prevention. Without sufficient documentation on birth defect etiology, global public health policies are unlikely to change.

In Vitro Solutions to Current Challenges in Birth Defects Research

Traditional approaches to birth defects and developmental biology research utilize animal models to study embryonic developmental processes and associated diseases [15]. The prenatal developmental toxicity test uses pregnant mice, rats, or rabbits to identify chemicals that disrupt normal pregnancy and/or development. This test is also routinely used alongside other *in vivo* methods to establish human exposure guidelines [16-21]. Animal models benefit from generally conserved biological principles governing gene

expression and tissue morphogenesis. Mouse models, in particular, are regarded as the premier system for investigating human organ development as most protein-coding genes are shared between the human and laboratory mouse genome [22]. This similarity is best evidenced by mutant mouse models that recapitulate human disease phenotypes. For instance, null mutations in pancreas specific transcription factor 1a (Ptf1a) result in impaired pancreas development in both mice and humans [23-25]. Despite the overall success of animal models, traditional developmental animal studies still suffer from their expensive and time-consuming nature [26]. Cost and time requirements alone make traditional developmental animal model approaches impractical for use in testing all commercially used chemicals and pharmaceuticals. As such, the rate at which environmental contaminant risks are identified is often slowed. These challenges highlight a need for robust, low-cost, and swift screening methods that can detect and prioritize chemicals that present developmental toxicity risks.

In response to challenges presented by traditional developmental screening approaches, several *in vivo* and *in vitro* screening approaches have been proposed to mitigate challenges posed by traditional methodologies. Each of the *in vivo* assays—the zebrafish embryotoxicity test and the Frog Embryo Teratogenesis Assay (FETAX), and the mouse whole embryo culture assay—operate similarly in that each exposes whole animal embryos to the chemical(s) of interest for 72-120 hours before the developmental stages of specified structures and organs are scored to assess embryotoxic effects [27-30]. In contrast, the *in vitro* limb bud micromass test and mouse embryonic stem cell test (mEST) measure the ability of rat limb bud cells and mid brain cells or mouse embryonic stem cells,

respectively, to successfully differentiate into directed cell types with concurrent chemical exposure [31], [32]. While accuracy data has yet to be reported for the FETAX approach, each of the other methods offer prediction accuracy rates of 70% or higher, with the mouse whole embryo assay at the highest accuracy rate of 80% [27], [29], [33]. Furthermore, the MM test, WEC test, and mEST have been officially validated via independent studies coordinated by the European Center for the Validation of Alternative Methods (ECVAM) [33].

While all of these approaches truncate the completion time for embryotoxicity assessments, only the mEST addresses the cost of routine animal use and subsequent sacrifices. In lieu of whole animal embryos, the EST uses embryonic stem cells to model developmental processes and tissue commitment. Embryonic stem cells (ESCs) are derived by isolating cells from the inner cell mass of a preimplantation blastocyst and cultivating the isolated cells *in vitro* [34], [35] (Fig. 1.2). During normal development, the inner cell mass (ICM) gives rise to all the cell types of the body but does not contribute to placental tissues. Because of this lineage restriction, ICM are regarded as pluripotent instead of totipotent [36]. ESCs are also characterized by their ability to "self-renew" or proliferate indefinitely without differentiating into more specialized cell types [37] (Fig. 1.3). This feature allows for prolonged cell stock maintenance and thus swift, cost-effective generation of starting materials for *in vitro* embryotoxicity assessments. Mouse ESCs (mESCs) can be maintained in in

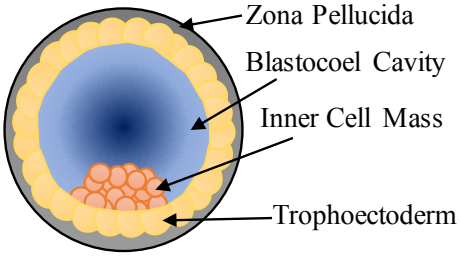

Figure 1.2. Blastocyst illustration demonstrating the inner cell mass (ICM) and trophoectoderm cell populations.

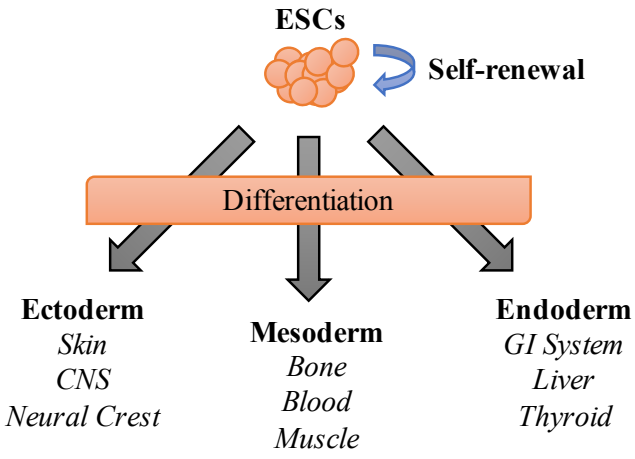

Figure 1.3. Embryonic stem cells (ESCs) have the capacity to self-renew stem cell populations as well as differentiate into specific cell types.

this pluripotent state of self-renewal by supplementing culture medium with cytokine leukemia inhibitory factor (LIF) or by co-culture with murine embryonic fibroblast (MEF) feeder layers that provide a source of LIF [38]. When the LIF source is withdrawn from mESC culture, mESCs pluripotency is lost as the cells differentiate into distinct cell types. mESC differentiation is classically directed through the formation of embryoid body (EB) formation [39]. Here, suspensions of mESCs are allowed to form cell aggregates of densely packed cells with fluid filled cavities [40-42]. EBs execute polarity and tissue regionalization processes that coincide with the sequential activation of genes responsible for gastrulation and early embryo patterning processes [43-45]. The mEST takes advantage of this capacity to recapitulate the gastrulation process with mESCs in the context of embryotoxicity assessments.

In the original mEST protocol, mouse ESCs are induced to differentiate into cardiomyocytes during concurrent chemical exposure and embryotoxic risk is quantitatively measured [46]. Here, mouse D3 ESCs are used to recapitulate embryonic cardiogenesis as they differentiate into actively contracting cardiomyocytes. Differentiation inhibition and cytotoxicity are measured as reductions in formation of functional contractile clusters and cell metabolic activity, respectively. The mEST also accounts for cytotoxic impacts on maternal tissues via the inclusion of 3T3 fibroblasts in the screening protocol. Cytotoxicity in exposed 3T3 cultures is used to identify potential maternal toxicity events that could affect the likelihood of embryotoxicity. Half-maximal inhibitory doses for differentiation (ID_{50}) and cell viability (IC_{50}) are determined from dose-response curves generated from screen endpoints. The values, in turn, are entered into

a biostatistical prediction model which was developed for use with the EST protocol to classify chemicals under evaluation as non-embryotoxic, weakly embryotoxic, or strongly embryotoxic (Fig. 1.4).

Since its ECVAM validation, the mEST has been employed in embryotoxicity screens for a variety of commodities including industrial chemicals [47], [48], pharmaceuticals [49], [50], and cosmetics [51]. The mEST has also been used in embryotoxicity evaluations for a number of environmental contaminants [52-56]. Though the mEST is validated for a cardiomyocyte endpoint, traditional *in vivo* developmental screens evaluate changes in all soft tissues as well as the developing skeleton [16]. Thus, there is a need for additional endpoints in the EST protocol in order to more thoroughly assess the embryotoxic potential of chemicals. Some progress has been made to address these additional needs through the development of defined differentiation protocols. To date, protocols have been reported for directing differentiation of mESCs to bone, neural tissue, and muscle tissue [57-59]. Thus, the mEST protocol can be adapted to address embryotoxicity for chemicals that may additionally or more specifically target tissues other than cardiac tissue.

Updating the mEST with Human Pluripotent Stem Cells

Over the last few decades, most *in vitro* developmental toxicity testing has been predominantly executed using mESCs [33], [50], [60-64]. The first isolation of human ESCs (hESCs) from a human blastocyst [65], however, started a dialogue on the possibility of incorporating hESCs into developmental testing protocols. While the laboratory mouse

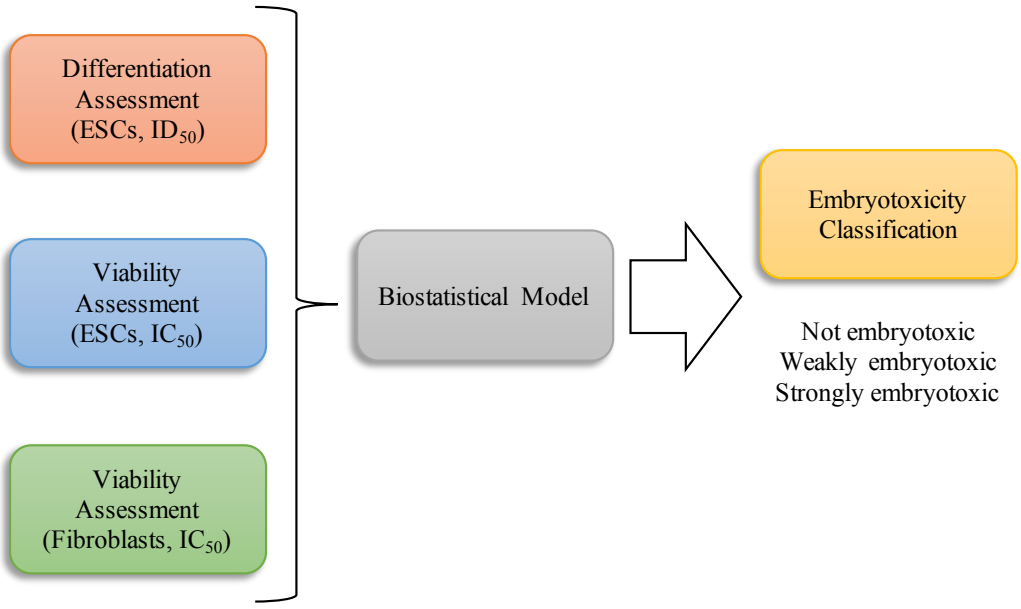

Figure 1.4. Overview of the Embryonic Stem Cell Test. Inhibition of differentiation and cell viability in differentiating embryonic stem cells (ESCs) is compared with inhibition of terminally differentiated fibroblasts in the EST biostatistical model to determine embryotoxicity classification.

and human genome are largely conserved, variations in gene expression patterns and pluripotency maintenance signaling pathways for mouse and human ESCs have been well documented [29], [66], [67]. These discrepancies suggest the potential for additional variations regarding signaling pathways involved in differentiation processes that may have implications for embryotoxicity testing. Differences in metabolism and temporal gene regulation in *in vivo* rodent models have already been documented to sometimes yield inaccurate toxicity assessments and failed human clinical trials [68-71]. Furthermore, *in vivo* mouse models have been shown to not always fully replicate human disease [72].

In light of the potential challenges posed by mouse models, hESCs have been viewed as a means to offer a more biologically relevant approach to *in vitro* developmental modeling and embryotoxicity assessments. Like mESCs, hESCs are pluripotent, capable of self-renewal, and can be directed to differentiate into particular cell types [73–75]. While hESC stocks were previously more challenging to maintain in culture, recent advances in culturing techniques and approaches have made routine hESC culture more accessible [76].

Routine use of hESCs in developmental toxicity evaluations, however, has been slow despite proposed advantages over mESC-based models. One of the main challenges to hESC incorporation into regulatory evaluations has been the ethical and legal debate surrounding hESC derivation, which calls for the destruction of the donor embryo [77], [78]. In response to these concerns, human induced pluripotent stem cells (hiPSCs) have been proposed as "a more ethical alternative" to hESCs as well as an additional route for *in vitro* developmental models and toxicity screens. hiPSCs possess the same defining characteristics of hESCs (i.e., self-renewal, pluripotency) but differ in that they are derived

from biopsied somatic cells that have been genetically reprogrammed to a pluripotent, ESC-like state [79], [80] (Fig. 1.5).

Because these hiPSCs can be derived from various individuals, these cells also offer the additional opportunity to create cell lines of varied genetic and disease backgrounds. In this way, hiPSC-based developmental models could also be used to explore the genetic interplay between toxicant exposure and outcomes. One caveat of hiPSCs, however, is that iPSCs may experience an incomplete reset of DNA methylation patterns during genetic reprogramming that may cause lineage bias during later differentiation [81]. High-efficiency reprogramming protocols and hiPSC stock quality control practices have both been suggested to address this challenge [82], [83]. Nevertheless, which human pluripotent stem cell type—if either—is more advantageous in a developmental model remains to be reported.

Despite strides made in the area of *in vitro* developmental toxicity screens over the last 20 years, hiPSC- and hESC-based developmental toxicity screens have yet to be incorporated into the regulatory framework of embryotoxicity assessments. *In vivo* species-species discrepancies in toxicant response are well-documented [84–86], though it remains to be seen if mESCs are less sensitive than human pluripotent stem cells. Here, additional comparative analysis is required to support claims that human pluripotent stem cells are a superior *in vitro* developmental model system. *hPSCs as a Means to Investigate Birth Defects in Understudied Tissues Like Bone*

The capacity for hPSCs to be differentiated into any of the 3 germ layers formed during gastrulation also creates a potential avenue for studying processes and pathologies

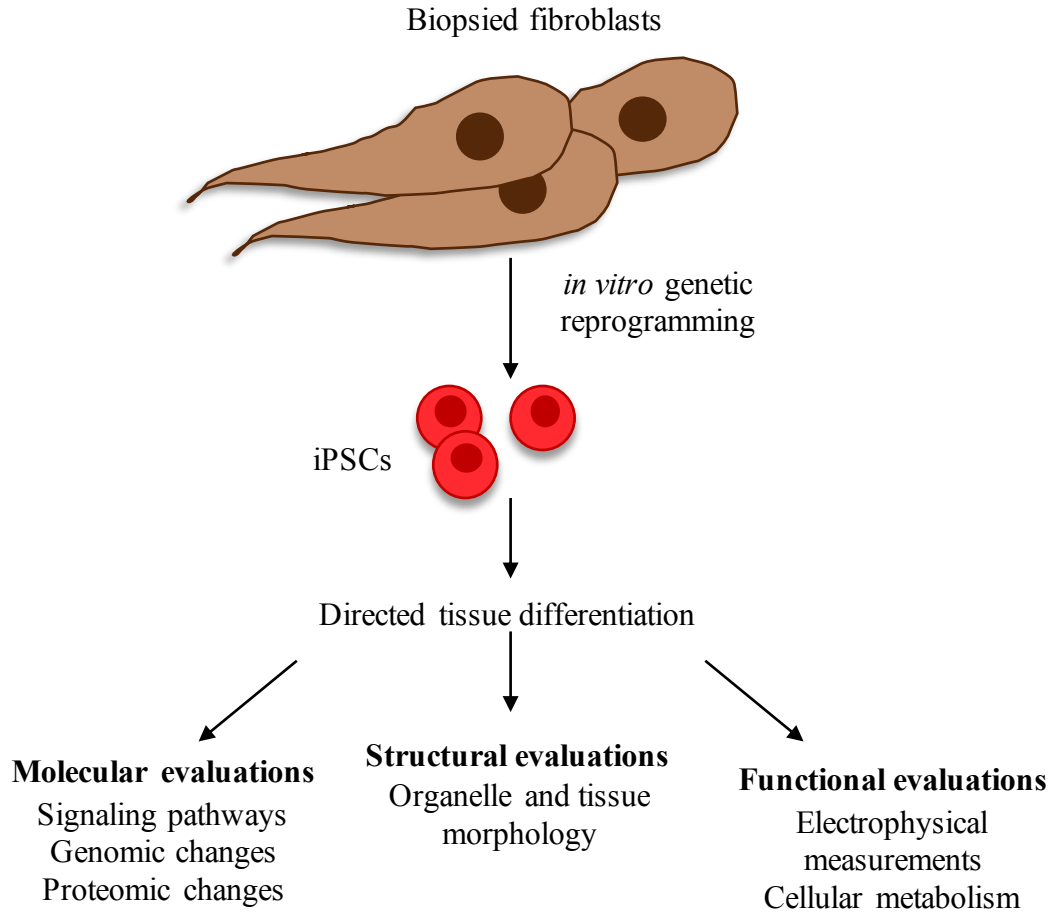

Figure 1.5. How induced pluripotent stem cells (iPSCs) are made and used in research applications. Somatic cells like fibroblasts are biopsied and genetically reprogrammed *in vitro* to create iPSCs. iPSCs can then be used in basic biology, toxicology, and biomedical studies to explore molecular, structural, and functional cell behaviors.

that have been previously difficult to study. One such area is that of skeletal defects and pathologies resulting from disruptions that occur during osteogenesis. Osteogenesis refers to the process by which bone is formed during embryonic development, adult bone homeostasis, or the bone healing process after a fracture event. Depending on the type of bone, osteogenesis can occur predominantly through one of two mechanisms: intramembranous ossification or endochondral ossification [87]. Intramembranous ossification produces the flat bones (i.e., craniofacial skeleton, pelvis). Intramembranous ossification occurs by proliferation and direct differentiation of osteoprogenitor cells into osteoblast bone cells. Endochondral ossification, conversely, produces the long bones (i.e., ribs, spine, humeri, femurs) that make up the axial and appendicular skeleton. During endochondral ossification, bone formation is preceded by chondrogenesis processes that create a cartilaginous base. Osteoprogenitors eventually replace the cartilaginous base with bone cells. With both modes of ossification, bone progenitor cells condense at bone formation sites before ultimately differentiating into osteoblasts that secrete and mineralize extracellular matrix. These osteoblasts later mature into osteocytes.

Bone formation and remodeling through either ossification mechanism is a dynamic process that is tightly regulated between bone-building osteoblasts and bone-absorbing osteoclasts. Osteoblasts are defined by their ability to form a mineralized extra cellular matrix (ECM). Differentiation from pluripotent stem cells to osteoblasts is regulated by temporal expression of specific genes and proteins. *In vitro* approaches to recapitulate this process using ESCs have identified ascorbic acid, β-glycerophosphate and 1,25-$(OH)_2$ vitamin D3 as potent inductors of osteogenic differentiation [88]. Studies in

our group have found mESC-based osteogenesis to recreate temporal expression patterns of osteogenic genes involved in embryonic osteogenesis. During this process, expression of alkaline phosphatase (*ALPL*) is followed by activation of CBFA1, a master regulatory transcription factor [89] for osteogenesis that upregulates runt-related transcription factor 2 (*RUNX2*) and osteopontin (*OPN*) expression. As the differentiation progresses, mature osteoblast markers bone sialoprotein (BSP) and osteocalcin (OCN) are expressed. These developments are followed by expression of osteocyte-affiliated genes *CAPG* and *DESTRIN* [90]. Given the tightly-regulated and timing dependent nature of osteogenesis, it follows that misregulation of any of these key stages during development may lead to skeletal birth defects or pathologies [59], [91].

From a developmental perspective, different gastrulation layers contribute to different skeletal tissues. Neural crest cells arising from the ectoderm germ layer lineage largely contribute to the craniofacial skeleton, while the mesoderm layer ultimately produces the appendicular skeleton (lateral mesoderm) and cranial and axial skeleton (paraxial mesoderm) (Fig. 1.6). At present, the precise relationship between disruption of osteoblast precursor populations during development and adult skeletal function is not well understood. It is recognized, however, that some environmental toxicants can disrupt normal bone metabolism, increasing risk of bone fracture and causing osteoporosis [92-94]. One such environmental toxicant, cigarette smoke, has been associated with a myriad of adverse pregnancy incomes [95]—including low bone mass [96] and increased bone fracture risk [97] for children exposed *in utero.* To date, however, very little investigation of the molecular mechanism of tobacco-related osteotoxicity in developing tissues has been

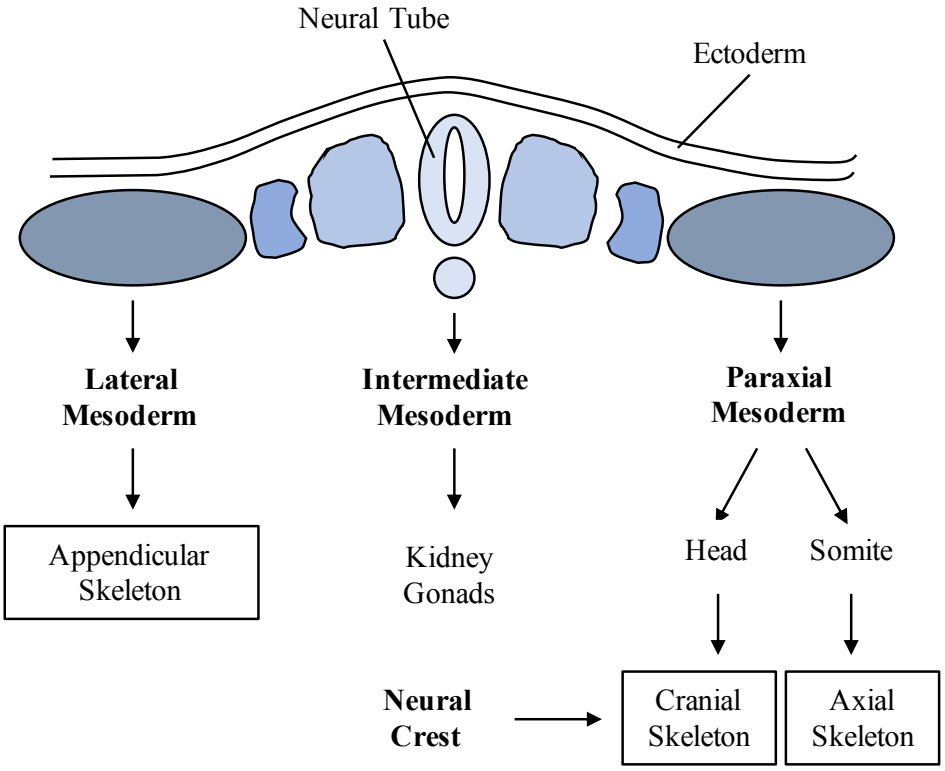

Figure 1.6. Overview of skeletal bone developmental origins in the early embryo. Lateral mesoderm and paraxial mesoderm give rise to the appendicular and axial skeleton, respectively. Neural crest cells give rise to the craniofacial skeleton, though the paraxial mesoderm contributes to other parts of the cranial skeleton.

reported. This dearth of information may be attributable in part at least to the costs and time associated with traditional *in vivo* developmental modeling approaches. It follows, then, that human pluripotent stem cell (hPSC)-based models of osteogenesis could offer a less-expensive and less-time consuming approach to investigating unknown mechanisms of embryotoxicants like tobacco in tissues that are challenging to study *in vivo*.

Conclusion

One of the main challenges to reducing the global birth defects burden is the dearth of knowledge regarding the precise influence of many environmental toxicants on particular developmental processes. Functional defects observed in developmental animal studies long been employed to investigate the potential for embryotoxic effects in humans [98], though this approach fails to provide a clear mode of action for embryotoxic etiology. Use of hESCs or hiPSCs in developmental modeling approaches offers a faster, more cost-effective avenue to investigate molecular changes and embryotoxic mechanisms at play in adverse developmental outcomes. The development of defined differentiation protocols for hPSCs allows for the investigation of understudied embryotoxicity mechanisms like the impact of tobacco on bone.

Aims

The current global birth defects burden exerts an annual toll of billions of dollars in preventable healthcare costs, emotional detriment, and lost economic productivity [5], [6]. Enhancing the traditional developmental toxicity tool kit with robust, biologically-relevant human pluripotent stem cell approaches can help to reduce the bottleneck associated with traditional whole animal approaches. Furthermore, human pluripotent stem cell-based developmental modeling may offer the opportunity to explore embryotoxicant modes of action in a developmentally-relevant system. However, additional research support of hPSC-improved sensitivity compared to mESCs as well as the investigatory capacity of human pluripotent stem cells with regard to complex environmental contaminants remains to be reported. This thesis aims to provide knowledge on the robust nature of hPSCs in embryotoxicity assessments and mode of action studies by addressing three specific aims:

Specific Aim 1: Determine comparative sensitivity of non-human primate and human pluripotent stem cells compared to mESCs (addressed in chapters 2 and 3).

Specific Aim 2: Investigate embryotoxic mechanisms of conventional and harm-reduction cigarettes in developmental osteotoxicity screening model using hESCs (addressed in chapter 4).

Specific Aim 3: Evaluate the biochemical alterations driven by smokeless-tobacco exposure and down-stream ramifications on embryonic bone development (addressed in chapter 5).

References

1. Christianson A and Howson CP. March of Dimes Global Report on Birth Defects. March Dimes Found. 2006.

2. WHO. Disease burden and mortality estimates. 2018. [Online]. Available: http://www.who.int/healthinfo/global_burden_disease/estimates/en/.

3. Parker SE, Mai CT, Canfield MA, Rickard R, Wang Y, Meyer RE, Anderson P, Mason CA, Collins JS, Kirby RS, Correa A, and National Birth Defects Prevention Network. Updated national birth prevalence estimates for selected birth defects in the United States, 2004–2006. Birt. Defects Res A Clin. Mol Teratol. 2010;88(12): 1008–1016.

4. Greenmyer J, Klug MG, Kambeitz C, Popova S, Burd L. A Multi-Country Updated Assessment of the Economic Impact of Fetal Alcohol Spectrum Disorder J Addict Med. 2018;12(6): 466–473.

5. Sokol RJ. A Current Evaluation of the Economic Costs for Fetal Alcohol Spectrum Disorder (FASD): A Comment on the Systematic Review by Greenmeyer et al. J Addict Med. 2018;12(6): 426.

6. Arth AC. Inpatient Hospitalization Costs Associated with Birth Defects Among Persons of All Ages — United States, 2013. MMWR Morb. Mortal. Wkly. Rep. 2017;66.

7. Weinhold B. Environmental Factors in Birth Defects: What We Need to Know. Environ. Health Perspect. 2009;117(10): A440–A447.

8. National Academies of Sciences. Global Health Impacts of Vector-Borne Diseases: Workshop Summary. Washington (DC): National Academies Press (US), 2016.

9. IARC. Arsenic, Metals, Fibres and Dusts. International Agency for Research on Cancer, 2012.

10. Institute of Medicine (US) Committee on the Assessment of Asthma and Indoor Air. Clearing the Air: Asthma and Indoor Air Exposures. Washington (DC): National Academies Press (US), 2000.

11. National Research Council (US) Safe Drinking Water Committee. Drinking Water and Health: Volume 1. Washington (DC): National Academies Press (US), 1977.

12. Stillerman KP, Mattison DR, Giudice LC, Woodruff TJ. Environmental exposures and adverse pregnancy outcomes: a review of the science. Reprod Sci. 2008;15(7): 631–650.

13. Adam MP, Polifka JE, and Friedman JM. Evolving knowledge of the teratogenicity of medications in human pregnancy. Am J Med Genet C Semin Med Genet. 2011;157C(3): 175–182.

14. Judson R, Richard A, Dix DJ, Houck K, Martin M, Kavlock R, Dellarco V, Henry T, Holderman T, Sayre P, Tan S, Carpenter T, Smith E. The toxicity data landscape for environmental chemicals. Environ. Health Perspect. 2009;117(5): 685–695.

15. Franco NH. Animal Experiments in Biomedical Research: A Historical Perspective. Anim. Open Access J. MDPI 2013;3(1): 238–273.

16. OECD. Test No. 414: Prenatal Developmental Toxicity Study. 1981.

17. OECD. Test No. 415: One-Generation Reproduction Toxicity Study. 1983.

18. OECD. Test No. 416: Two-Generation Reproduction Toxicity. 1983

19. OECD. Test No. 421: Reproduction/Developmental Toxicity Screening Test. 1995.

20. OECD. Test No. 422: Combined Repeated Dose Toxicity Study with the Reproduction/Developmental Toxicity Screening Test. 1996.

21. OECD. Test No. 443: Extended One-Generation Reproductive Toxicity Study. 2018.

22. Yue F, Cheng Y, Breschi A, Vierstra J, Wu W, Ryba T, Sandstrom R, Ma Z, Davis C, Pope BD, Shen Y, Pervouchine DD, Djebali S, et al. A comparative encyclopedia of DNA elements in the mouse genome. Nature. 2014;515(7527): 355–364.

23. Kawaguchi Y, Cooper B, Gannon M, Ray M, MacDonald RJ, Wright CV. The role of the transcriptional regulator Ptf1a in converting intestinal to pancreatic progenitors. Nat. Genet. 2002;32(1): 128–134.

24. Krapp A, Knöfler M, Ledermann B, Bürki K, Berney C, Zoerkler N, Hagenbüchle O, Wellauer PK. The bHLH protein PTF1-p48 is essential for the formation of the exocrine and the correct spatial organization of the endocrine pancreas. Genes Dev. 1998;12(23): 3752–3763.

25. Sellick GS, Barker KT, Stolte-Dijkstra I, Fleischmann C, Coleman RJ, Garrett C, Gloyn AL, Edghill EL, Hattersley AT, Wellauer PK, Goodwin G, Houlston RS. Mutations in PTF1A cause pancreatic and cerebellar agenesis. Nat Genet. 2004;36(12): 1301–1305.

26. Meigs L, Smirnova L, Rovida C, Leist M, Hartung T. Animal testing and its alternatives – the most important omics is economics. ALTEX - Altern. Anim. Exp. 2018;35(3): 275–305.

27. Bantle JA, Fort DJ, and James BL. Identification of developmental toxicants using the Frog Embryo Teratogenesis Assay-Xenopus (FETAX). Hydrobiologia. 2004;188577–585.

28. Brown NA and Fabro S. Quantitation of rat embryonic development *in vitro*: a morphological scoring system. Teratology. 1981;24(1): 65–78.

29. Chapin R, Augustine-Rauch K, Beyer B, Daston G, Finnell R, Flynn T, Hunter S, Mirkes P, O'Shea KS, Piersma A, Sandler D, Vanparys P, Van Maele-Fabry G. State of the art in developmental toxicity screening methods and a way forward: a meeting report addressing embryonic stem cells, whole embryo culture, and zebrafish. Birth Defects Res B Dev Reprod Toxicol. 2008;83(4): 446–456.

30. New DA. Whole-embryo culture and the study of mammalian embryos during organogenesis. Biol Rev Camb Philos Soc. 1978;53(1): 81–122.

31. Genschow E, Spielmann H, Scholz G, Pohl I, Seiler A, Clemann N, Bremer S, Becker K. Validation of the embryonic stem cell test in the international ECVAM validation study on three *in vitro* embryotoxicity tests. ATLA-Altern Lab Anim. 2004;32(3): 209–244.

32. Spielmann H, Genschow E, Brown NA, Piersma AH, Verhoef A, Spanjersberg MQ, Huuskonen H, Paillard F, Seiler A. Validation of the rat limb bud micromass test in the international ECVAM validation study on three *in vitro* embryotoxicity tests. ATLA-Altern Lab Anim. 2004;32(3): 245–274.

33. Genschow E, Spielmann H, Scholz G, Seiler A, Brown N, Piersma A, Brady M, Clemann N, Huuskonen H, Paillard F, Bremer S, Becker K. The ECVAM international validation study on *in vitro* embryotoxicity tests: results of the definitive phase and evaluation of prediction models. European Centre for the Validation of Alternative Methods. ATLA-Altern Lab Anim. 2002;30(2): 151–176.

34. Evans MJ and Kaufman MH. Establishment in culture of pluripotential cells from mouse embryos. Nature. 1981;292(5819): 154.

35. Martin GR. Isolation of a pluripotent cell line from early mouse embryos cultured in medium conditioned by teratocarcinoma stem cells. Proc Natl Acad Sci USA 1981;78(12): 7634–7638.

36. Sell S. Stem Cells: What Are They? Where Do They Come From? Why Are They Here? When Do They Go Wrong? Where Are They Going? in Stem Cells Handbook. S. Sell, Ed. Humana Press, 2004.

37. Smith AG. Embryo-derived stem cells: of mice and men. Annu Rev Cell Dev Biol. 2001;17435–462.

38. Smith AG, Heath JK, Donaldson DD, Wong GG, Moreau J, Stahl M, Rogers D. Inhibition of pluripotential embryonic stem cell differentiation by purified polypeptides. Nature. 1988;336(6200): 688.

39. Desbaillets I, Ziegler U, Groscurth P, Gassmann M. Embryoid bodies: an *in vitro* model of mouse embryogenesis. Exp Physiol. 2000;85(6): 645–651.

40. Dang SM, Kyba M, Perlingeiro R, Daley GQ, Zandstra PW. Efficiency of embryoid body formation and hematopoietic development from embryonic stem cells in different culture systems. Biotechnol Bioeng. 2002;78(4): 442–453.

41. Höpfl G, Gassmann M, and Desbaillets I. Differentiating Embryonic Stem Cells into Embryoid Bodies. in Germ Cell Protocols: Volume 2: Molecular Embryo Analysis, Live Imaging, Transgenesis, and Cloning. H. Schatten, Ed. Totowa, NJ: Humana Press, 2004, 79–98.

42. Keller GM. In vitro differentiation of embryonic stem cells. Curr Opin Cell Biol. 1995;7(6): 862–869.

43. Leahy A, Xiong JW, Kuhnert F, Stuhlmann H. Use of developmental marker genes to define temporal and spatial patterns of differentiation during embryoid body formation. J Exp Zool. 1999;284(1): 67–81.

44. Weitzer G. Embryonic stem cell-derived embryoid bodies: an *in vitro* model of eutherian pregastrulation development and early gastrulation. Handb Exp Pharmacol. 2006;(174): 21–51.

45. Yamada G, Kioussi C, Schubert FR, Eto Y, Chowdhury K, Pituello F, Gruss P. Regulated expression of Brachyury(T), Nkx1.1 and Pax genes in embryoid bodies. Biochem Biophys Res Commun. 1994;199(2): 552–563.

46. Spielmann H, Pohl I, Doring B, Liebsch M, Moldenhauer F. The embryonic stem cell test (EST), an *in vitro* embryotoxicity test using two permanent mouse cell lines: 3T3 fibroblasts and embryonic stem cells. In Vitro Toxicol. 1997;(10): 119–127.

47. de Jong E, Louisse J, Verwei M, Blaauboer BJ, van de Sandt JJ, Woutersen RA, Rietjens IM, Piersma AH. Relative developmental toxicity of glycol ether alkoxy acid metabolites in the embryonic stem cell test as compared with the *in vivo* potency of their parent compounds. Toxicol Sci Off J Soc Toxicol. 2009;110(1): 117–124.

48. Estevan C, Fuster E, Del Río E, Pamies D, Vilanova E, Sogorb MA. Organophosphorus Pesticide Chlorpyrifos and Its Metabolites Alter the Expression of Biomarker Genes of Differentiation in D3 Mouse Embryonic Stem Cells in a Comparable Way to Other Model Neurodevelopmental Toxicants. Chem Res Toxicol. 2014;27(9): 1487–1495.

49. Eckardt K and Stahlmann R. Use of two validated *in vitro* tests to assess the embryotoxic potential of mycophenolic acid. Arch Toxicol. 2010;84(1): 37–43.

50. Paquette JA, Kumpf SW, Streck RD, Thomson JJ, Chapin RE, Stedman DB. Assessment of the Embryonic Stem Cell Test and application and use in the pharmaceutical industry. Birth Defects Res B Dev Reprod Toxicol. 2008;83(2): 104–111.

51. Chen R, Chen J, Cheng S, Qin J, Li W, Zhang L, Jiao H, Yu X, Zhang X, Lahn BT, Xiang AP. Assessment of embryotoxicity of compounds in cosmetics by the embryonic stem cell test. Toxicol Mech Methods 2010;20(3): 112–118.

52. Kamelia L, Louisse J, de Haan L, Rietjens IMCM, Boogaard PJ. Prenatal developmental toxicity testing of petroleum substances: Application of the mouse embryonic stem cell test (EST) to compare *in vitro* potencies with potencies observed *in vivo*. Toxicol Vitro Int J Publ Assoc BIBRA. 2017;44303–312.

53. Kong D, Xing L, Liu R, Jiang J, Wang W, Shang L, Wei X, Hao W. Individual and combined developmental toxicity assessment of bisphenol A and genistein using the embryonic stem cell test *in vitro*. Food Chem Toxicol. 2013;60497–505.

54. Stummann TC, Hareng L, and Bremer S. Embryotoxicity hazard assessment of cadmium and arsenic compounds using embryonic stem cells. Toxicology. 2008;252(1–3): 118–122.

55. Stummann TC, Hareng L, and Bremer S. Embryotoxicity hazard assessment of methylmercury and chromium using embryonic stem cells. Toxicology. 2007;242(1–3): 130–143.

56. Zhou R, Cheng W, Feng Y, Wei H, Liang F, Wang Y. Interactions between three typical endocrine-disrupting chemicals (EDCs) in binary mixtures exposure on myocardial differentiation of mouse embryonic stem cell. Chemosphere. 2017;178378–383.

57. Darabi R, Gehlbach K, Bachoo RM, Kamath S, Osawa M, Kamm KE, Kyba M, Perlingeiro RC. Functional skeletal muscle regeneration from differentiating embryonic stem cells. Nat Med. 2008;14(2): 134–143.

58. Thompson RE, Lake A, Kenny P, Saunders MN, Sakers K, Iyer NR, Dougherty JD, Sakiyama-Elbert SE. Different Mixed Astrocyte Populations Derived from Embryonic Stem

Cells Have Variable Neuronal Growth Support Capacities. Stem Cells Dev. 2017;26(22): 1597–1611.

59. zur Nieden NI, Kempka G, Rancourt DE, Ahr HJ. Induction of chondro-, osteo- and adipogenesis in embryonic stem cells by bone morphogenetic protein-2: Effect of cofactors on differentiating lineages. BMC Dev Biol. 2005;5(1): 1.

60. Buesen R, Genschow E, Slawik B, Visan A, Spielmann H, Luch A, Seiler A. Embryonic stem cell test remastered: comparison between the validated EST and the new molecular FACS-EST for assessing developmental toxicity *in vitro*. Toxicol. Sci Off J Soc Toxicol. 2009;108(2): 389–400.

61. Kang HY, Choi YK, Jo NR, Lee JH, Ahn C, Ahn IY, Kim TS, Kim KS, Choi KC, Lee JK, Lee SD, Jeung EB. Advanced developmental toxicity test method based on embryoid body's area. Reprod Toxicol. 2017;7274–85.

62. Panzica-Kelly JM, Brannen KC, Ma Y, Zhang CX, Flint OP, Lehman-McKeeman LD, Augustine-Rauch KA. Establishment of a Molecular Embryonic Stem Cell Developmental Toxicity Assay. Toxicol Sci. 2013;131(2): 447–457.

63. Suzuki N, Ando S, Yamashita N, Horie N, Saito K. Evaluation of novel high-throughput embryonic stem cell tests with new molecular markers for screening embryotoxic chemicals *in vitro*. Toxicol Sci Off J Soc Toxicol. 2011;124(2): 460–471.

64. Uibel F, Mühleisen A, Köhle C, Weimer M, Stummann TC, Bremer S, Schwarz M. ReProGlo: a new stem cell-based reporter assay aimed to predict embryotoxic potential of drugs and chemicals. Reprod Toxicol. 2010;30(1): 103–112.

65. Thomson JA, Itskovitz-Eldor J, Shapiro SS, Waknitz MA, Swiergiel JJ, Marshall VS, Jones JM. Embryonic stem cell lines derived from human blastocysts. Science. 1998;282(5391): 1145–1147.

66. Sato N, Meijer L, Skaltsounis L, Greengard P, Brivanlou AH. Maintenance of pluripotency in human and mouse embryonic stem cells through activation of Wnt signaling by a pharmacological GSK-3-specific inhibitor. Nat Med. 2004;10(1): 55–63.

67. Schnerch A, Cerdan C, and Bhatia M. Distinguishing Between Mouse and Human Pluripotent Stem Cell Regulation: The Best Laid Plans of Mice and Men Stem Cells. 2010.

68. Agoston DV. How to Translate Time? The Temporal Aspect of Human and Rodent Biology. Front Neurol. 2017;8.

69. Knobloch J, Reimann K, Klotz LO, Rüther U. Thalidomide Resistance Is Based on the Capacity of the Glutathione-Dependent Antioxidant Defense. Mol Pharm. 2008;5(6): 1138–1144.

70. Radermacher P and Haouzi P. A mouse is not a rat is not a man: species-specific metabolic responses to sepsis - a nail in the coffin of murine models for critical care research? Intensive Care Med Exp. 2013;1(1): 7.

71. Rangarajan A and Weinberg RA. Opinion: Comparative biology of mouse versus human cells: modelling human cancer in mice. Nat Rev Cancer. 2003;3(12): 952–959.

72. Elsea SH and Lucas RE. The mousetrap: what we can learn when the mouse model does not mimic the human disease. ILAR J. 2002;43(2): 66–79.

73. Guloglu MO and Larsen A. Dopaminergic Differentiation of Human Embryonic Stem Cells on PA6-Derived Adipocytes. in Embryonic Stem Cell Protocols. K. Turksen, Ed. New York, NY: Springer New York, 2016, 235–244.

74. Madrid JV, Sera SR, Sparks NRL, Zur Nieden NI. Human Pluripotent Stem Cells to Assess Developmental Toxicity in the Osteogenic Lineage. Methods Mol Biol. 2018;1797125–145.

75. Xu C, Police S, Rao N, Carpenter MK. Characterization and Enrichment of Cardiomyocytes Derived from Human Embryonic Stem Cells. Circ Res. 2002;91(6): 501–508.

76. Desai N, Rambhia P, and Gishto A. Human embryonic stem cell cultivation: historical perspective and evolution of xeno-free culture systems. Reprod Biol Endocrinol. 2015;139.

77. Isasi R and Knoppers B. Mind the Gap: Policy Approaches to Embryonic Stem Cell and Cloning Research in 50 Countries. Eur J Health Law. 2006;13(1): 9–25.

78. Isasi RM. Policy Interoperability in Stem Cell Research: Demystifying Harmonization. Stem Cell Rev. Rep. 2009;5(2): 108–115.

79. Takahashi K, Tanabe K, Ohnuki M, Narita M, Ichisaka T, Tomoda K, Yamanaka S. Induction of pluripotent stem cells from adult human fibroblasts by defined factors. Cell. 2007;131(5): 861–872.

80. Yu J, Vodyanik MA, Smuga-Otto K, Antosiewicz-Bourget J, Frane JL, Tian S, Nie J, Jonsdottir GA, Ruotti V, Stewart R, Slukvin II, Thomson JA. Induced pluripotent stem cell lines derived from human somatic cells. Science. 2007;318(5858): 1917–1920.

81. Liang G and Zhang Y. Genetic and epigenetic variations in iPSCs: potential causes and implications for application. Cell Stem Cell. 2013;13(2): 149–159.

82. Bock C, Kiskinis E, Verstappen G, Gu H, Boulting G, Smith ZD, Ziller M, Croft GF, Amoroso MW, Oakley DH, Gnirke A, Eggan K, Meissner A. Reference Maps of human ES and iPS cell variation enable high-throughput characterization of pluripotent cell lines. Cell. 2011;144(3): 439–452.

83. Ruiz S, Diep D, Gore A, Panopoulos AD, Montserrat N, Plongthongkum N, Kumar S, Fung HL, Giorgetti A, Bilic J, Batchelder EM, Zaehres H, Kan NG, et al. Identification of a specific reprogramming-associated epigenetic signature in human induced pluripotent stem cells. Proc Natl Acad Sci USA. 2012;109(40): 16196–16201.

84. Ito T, Ando H, and Handa H. Teratogenic effects of thalidomide: molecular mechanisms. Cell Mol Life Sci. 2011;68(9): 1569–1579.

85. Knight A. Systematic reviews of animal experiments demonstrate poor human clinical and toxicological utility. ATLA-Altern Lab Anim. 2007;35(6): 641–659.

86. Schardein JL and Keller KA. Potential human developmental toxicants and the role of animal testing in their identification and characterization. Crit Rev Toxicol. 1989;19(3): 251–339.

87. Provot S, Schipani E, Wu JY, Kronenberg H. Development of the Skeleton. in Osteoporosis (Fourth Edition). R. Marcus, D. Feldman, D. W. Dempster, M. Luckey, and J. A. Cauley, Eds. San Diego: Academic Press, 2013, 97–126.

88. zur Nieden NI, Kempka G, and Ahr HJ. In vitro differentiation of embryonic stem cells into mineralized osteoblasts. Differentiation. 2003;71(1): 18–27.

89. Ducy P, Zhang R, Geoffroy V, Ridall AL, Karsenty G. Osf2/Cbfa1: a transcriptional activator of osteoblast differentiation. Cell. 1997;89(5): 747–754.

90. Ehnes DD, Price FD, Shrive NG, Hart DA, Rancourt DE, zur Nieden NI. Embryonic stem cell-derived osteocytes are capable of responding to mechanical oscillatory hydrostatic pressure. J Biomech. 2015;48(10): 1915–1921.

91. zur Nieden NI, Price FD, Davis LA, Everitt RE, Rancourt DE. Gene profiling on mixed embryonic stem cell populations reveals a biphasic role for beta-catenin in osteogenic differentiation. Mol Endocrinol. 2007;21(3): 674–685.

92. Rodríguez J and Mandalunis PM. A Review of Metal Exposure and Its Effects on Bone Health J Toxicol. 2018;2018.

93. Romero AN, Herlin M, Finnilä M, Korkalainen M, Håkansson H, Viluksela M, Sholts SB. Skeletal and dental effects on rats following *in utero*/lactational exposure to the non-dioxin-like polychlorinated biphenyl PCB 180. PLoS ONE. 2017;12(9): e0185241.

94. Baker AH, Wu TH, Bolt AM, Gerstenfeld LC, Mann KK, Schlezinger JJ. From the Cover: Tributyltin Alters the Bone Marrow Microenvironment and Suppresses B Cell Development. Toxicol Sci. 2017;158(1): 63–75.

95. Centers for Disease Control and Prevention (US). National Center for Chronic Disease Prevention and Health Promotion (US) and Office on Smoking and Health (US). How Tobacco Smoke Causes Disease: The Biology and Behavioral Basis for Smoking-Attributable Disease: A Report of the Surgeon General. Atlanta (GA): Centers for Disease Control and Prevention (US), 2010.

96. Godfrey K, Walker-Bone K, Robinson S, Taylor P, Shore S, Wheeler T, Cooper C. Neonatal Bone Mass: Influence of Parental Birthweight, Maternal Smoking, Body Composition, and Activity During Pregnancy. J Bone Miner Res. 2001;16(9): 1694–1703.

97. Jones G, Riley M, and Dwyer T. Maternal smoking during pregnancy, growth, and bone mass in prepubertal children. J Bone Miner Res. 1999;14(1): 146–151.

98. US EPA. Guidelines for Developmental Toxicity Risk Assessment. Policies and Guidance, 2014.

99. De Bono C, Thellier C, Bertrand N, Sturny R, Jullian E, Cortes C, Stefanovic S, Zaffran S, Théveniau-Ruissy M, Kelly RG. T-box genes and retinoic acid signaling regulate the segregation of arterial and venous pole progenitor cells in the murine second heart field. Hum Mol Genet. 2018;27(21): 3747–3760.

100. Talhout R, Schulz T, Florek E, van Benthem J, Wester P, and Opperhuizen A. Hazardous Compounds in Tobacco Smoke. Int J Environ Res Public. Health. 2011;8(2): 613–628.

CHAPTER 2

Non-human primate and rodent embryonic stem cells are differentially sensitive to embryotoxic compounds

Lauren Walker, Laura Baumgartner, Kevin C. Keller, Julia Ast, Susanne Trettner, and Nicole I. zur Nieden

Abstract

Many industrial chemicals and their respective by-products need to be comprehensively evaluated for toxicity using reliable and efficient assays. In terms of teratogenicity evaluations, the murine-based embryonic stem cell test (EST) offers a promising solution to screen for multiple tissue endpoints. However, use of a mouse model in the EST can yield only a limited understanding of human development, anatomy, and physiology. Non-human primate or human *in vitro* models have been suggested to be a pharmacologically and pathophysiologically desirable alternative to murine *in vitro* models. Here, we comparatively evaluated the sensitivity of embryonic stem cells (ESCs) of a non-human primate to skeletal teratogens with mouse ESCs hypothesizing that inclusion of non-human primate cells in *in vitro* tests would increase the reliability of safety predictions for humans.

First, osteogenic capacity was compared between ESCs from the mouse and a New World monkey, the common marmoset. Then, cells were treated with compounds that have been previously reported to induce bone teratogenicity. Calcification and MTT assays

evaluated effects on osteogenesis and cell viability, respectively. Our data indicated that marmoset ESCs responded differently than mouse ESCs in such embryotoxicity screens with no obvious dependency on chemical or compound classes and thus suggest that embryotoxicity screening results could be affected by species-driven response variation. In addition, ESCs derived from rhesus monkey, an Old World monkey, and phylogenetically closer to humans than the marmoset, were observed to respond differently to test compounds than marmoset ESCs. Together these results indicate that there are significant differences in the responses of non-human primate and mouse ESC to embryotoxic agents.

Introduction

In the United States, one in 28 babies carries congenital anomalies [1]. Although 50% of the causes for such birth defects are unknown, some may be traced back to involuntary environmental chemical exposure. There are more than 80,000 cataloged chemicals in the United States that may be released into the environment and most of them are inappropriately tested for safety. This lack of information is particularly concerning for sensitive populations such as pregnant women and children as adequate safety guidelines cannot always be confidently recommended. Furthermore, given that the developing fetus is especially sensitive to maternal environmental conditions and also that exposure during key points of development can lead to unique effects lasting through multiple generations [2], the potential embryotoxicity and teratogenicity of industrial compounds is of particular concern.

With appropriate data, acceptable exposure levels and actual safety of such products can be established for individuals that are most vulnerable to chemical exposure. Therefore, toxicology programs have been designed to identify toxicities that may potentially be encountered in human embryos. Under the worldwide trend for revision of chemical legislation, it will be necessary to test a large number of chemicals in a short time, which can only be achieved with predictive *in vitro* assays.

A step in the direction of animal sacrifice free embryotoxicity screen was taken when the classic embryonic stem cell test (EST) was first described [3], [4]. This assay relies on embryonic stem cells (ESCs) from the mouse and compares two important aspects of prenatal toxicity. First, the EST has revealed the differences in sensitivity of mouse embryonic stem cells (ESCs) to chemical entities compared to adult fibroblasts. Second, the test determines the ability of a chemical to inhibit the differentiation of the ESCs into a differentiated cell type of interest [5], [6].

Among the many birth defects, the ones that affect musculoskeletal tissues account for 5% of all infant deaths. Thus, skeletal toxicity has become a high priority screening phenotype and is currently integrated into the animal screens that assess general prenatal developmental toxicity (TG414, OECD) [7], [8], [9]. Assessing the inhibition of osteogenic differentiation of the ESCs, the EST may also be exploited to serve as predictor for developmental osteotoxicity [6], [10], [11], [12], [13], [14].

Despite the routine use of rodent models in research, the mouse model as used in the EST can only yield a limited understanding of human development, anatomy and physiology. Accordingly, human *in vitro* models are desirable from a pharmacological and

pathophysiological standpoint. Indeed, ESCs from humans were established around the turn of the century [15]. However, due to ethical considerations, the legality of their use varies widely between countries. A solution comes with human induced pluripotent stem cells (hiPSCs), which are artificially created from somatic cells, and are therefore not ethically challenged, but it is yet unclear how their quality or differentiation potential measures up to bona fide hESCs. Therefore, to provide a legal and ethical alternative to countries, which have banned hESC research, we test here whether the sensitivity of non-human primate ESCs to a small set of classical and skeletal embryotoxic agents is similar to that of mouse ESCs in order to evaluate whether the inclusion of non-human primate cells into the EST would increase the reliability of safety predictions for human use.

Materials and methods

Murine ESC maintenance

Murine D3 embryonic stem cells (American Type Culture Collection, Rockville, MD, USA) were expanded in high glucose DMEM containing L-glutamine (Corning). Media additionally contained 15% batch-tested fetal bovine serum (FBS), 1% non-essential amino acids (NEAA), 50 U/ml penicillin, 50 µg/ml streptomycin, 0.1 mM 2-mercaptoethanol (all Invitrogen) and 1000 U LIF/ml (Millipore). Cells were routinely passaged every 2–3 days with 0.25% Trypsin-EDTA (Life Technologies).

Maintenance culture of non-human primate ESCs

Embryonic stem cells from the common marmoset (cjes001) were cultured in feeder-free conditions as described [16]. Rhesus ESCs (R366.4, WiCell Research Institute) were cultured on mouse embryonic fibroblast feeder layers as previously described [17], [18].

Osteogenic differentiation of ESCs

Murine ESCs were induced to differentiate *via* aggregation into embryoid bodies *via* hanging drops at 750 cells/drop, in the presence of control differentiation medium (CDM, mouse ESC maintenance medium without LIF [19]. Differentiating cells were replated on day 5 as a single cell suspension at a concentration of 50,000 cells/cm^2 [20]. Differentiation of marmoset and rhesus ESCs was initiated from intact ESC colonies in non-adherent conditions as described [16], [17]. In brief, undifferentiated colonies were trypsinized with TrypLE (Invitrogen) into clusters of 20–30 cells. Approximately 100 such clusters were seeded in CDM to one bacteriological grade dish (100 mm diameter). Following 5 days of incubation, cell clusters were transferred onto cell culture plates coated with 0.1% gelatin at an approximate density of 10 cell clusters/cm^2. On day 5 of differentiation, cells from all species received osteogenic differentiation medium containing the induction factors β-glycerophosphate (10 mM), ascorbic acid (25 μg/ml), and 1α,25-$(OH)_2$ vitamin D_3 (5×10^{-8} M) in CDM.

Test compounds

5-fluorouracil, *all-trans* retinoic acid, penicillin G (all Sigma) were selected as control test compounds as the teratogenic potential of each has been well established by previous *in vivo* and *in vitro* investigations [21]. Stock solutions were made in DMSO and diluted to test concentrations in respective cell culture media. Lithium chloride was obtained from Fluka and aluminum chloride was obtained from Sigma. Sodium chloride (Fisher Scientific), lithium acetate (Aldrich), sodium acetate (Sigma), and aluminum hydroxide (Sigma) were included as controls for lithium and aluminum activity. Untreated control cultures containing appropriate vehicle were also included. Osteogenic differentiation was considered valid if the control solvent yielded osteoblast differentiation levels comparable to that of untreated vitamin D_3 induced osteogenic cultures.

Cytotoxicity assay

Cellular viability was evaluated with an MTT assay following 14 days of osteogenic induction as described [22]. In brief, 0.5 mg/ml MTT solution was added to the cultures and cells were incubated at 37 °C for 2 h. Reagent was then aspirated and cells were gently rocked in pre-warmed MTT desorb solution (0.7% SDS in 2-propanol) for 15 min. Absorbance of dissolved blue formazan product was measured spectrophotometrically at 570 nm with a 630 nm reference wavelength. Mitochondrial activity was normalized to solvent only controls and resulting percentages were graphed along the tested concentration range to construct a concentration–response curve. The half-

maximal inhibitory effect (IC_{50}) for each compound was subsequently established *via* linear interpolation of the curve.

Alizarin Red S staining

Attached cells were washed with 1X PBS and fixed with 4% paraformaldehyde in 1× PBS and incubated at 4 °C for 1 h. Residual fixative was quenched *via* incubation with 100 mM glycine for 15 min at room temperature. Samples were then washed three times in 1× PBS and once in dH_2O. Fixed cells were then subjected to a 0.5% Alizarin Red S staining solution for 5 min. Following three washes with dH_2O, subsequent washes were performed with ascending ethanol concentrations (*i.e.* 70%, 80%, 90%, and 100%). Cultures were kept in 100% ethanol for acquisition of images.

Quantification of calcium deposition

Cells were washed twice in 1× phosphate buffered saline (PBS) and lysed in a modified RIPA buffer (1% NP-40, 0.5% sodium deoxycholate, 0.1% sodium dodecyl sulfate in 1× PBS, pH 7.4). Each plate was incubated for 1 h at 4 °C with shaking to ensure complete cell lysis. Ca^{2+} concentration was measured against a set of standards using an Arsenazo III based spectrophotometric assay (Genzyme Diagnostics) at 650 nm as described [23]. The protein concentration in each sample was then measured against a set of standards using a Lowry spectrophotometric assay (Bio-Rad Laboratories) at 750 nm. Ca^{2+} content in each sample was then normalized to the respective protein concentration measured with the Bio-Rad DC protein assay reagent as described [23]. Calcium content

was normalized to solvent only controls and concentration-response curves charted. The half-maximal inhibitory dose (ID_{50}) for each compound was taken from linear interpolation of the curve.

Statistical analysis

Data significance was decided using a web-based one-way ANOVA and Tukey HSD *post hoc* test (http://faculty.vassar.edu/lowry/anova1u.html) or unpaired Student's *t*-test as appropriate. All results are represented as average of five independent replicates ± standard deviation.

Results

Osteogenic differentiation potential of marmoset ESCs

ESCs from the marmoset, *Callithrix jacchus*, a New World monkey, have been previously derived [18], [24], [25] and been shown to be capable of producing osteoblasts that calcify their extracellular matrix [16]. Calcified extracellular matrices had been previously described as dark colored light-dense areas [26]. Those dark areas were observed in cultures from both mouse and marmoset ESCs *via* bright field microscopy on day 30 of osteogenic differentiation (Fig. 2.1A). Alizarin Red S staining of cultures confirmed the presence of calcified extracellular matrix in such dark areas. The overall amount of calcification between the marmoset and the mouse cells was comparable (Fig. 2.1B).

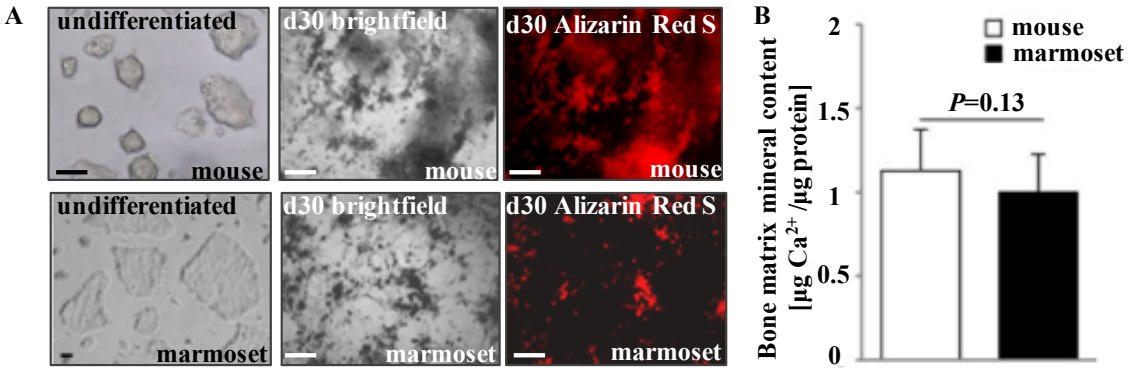

Figure 2.1. Osteogenic differentiation ability in mouse and marmoset ESCs. (A) Brightfield images and Alizarin Red S staining identifying mineralized calcium. (B) Quantification of calcium deposit in osteogenic cultures determined with Arsenazo III, n = 3, five technical replicates each ± SD. p-value was established with a Student's t-test.

Differential sensitivity of mouse and marmoset ESCs to lithium derivatives and controls

Previous literature has suggested that lithium chloride, actively used in psychiatric pharmaceuticals, possesses the capacity for inducing skeletal teratogenicity [27]. In addition, our own research has suggested that lithium derivatives cause skeletal teratogenicity in certain concentration ranges [22]. To test the predictive aptitude of a non-human primate-based EST for lithium derivatives, mouse and marmoset osteogenic ESC cultures were treated with lithium and aluminum compounds. Sodium chloride and lithium acetate served as a control for chloride in lithium chloride to ensure that observed effects were due to lithium activity. Sodium acetate was included as a control for acetate in lithium acetate.

Lithium chloride treatment of mouse ESC osteogenic cultures did not result in the establishment of an ID_{50} value (Fig. 2.2). Instead, calcification was dose-dependently up-regulated over control values in the absence of a cytotoxic effect. In contrast to mouse ESC cultures, LiCl induced a sharp drop in mitochondrial dehydrogenase activity, which is a routinely used and widely accepted test for cytotoxicity [3], [28], [29], in marmoset ESCs at a concentration of 100 μg/ml. LiCl-treated osteogenic marmoset ESC cultures also demonstrated a dose-dependent decrease in calcification as concentration increased with an ID_{50} at 0.4 ± 0.03 μg/ml, almost two orders of magnitude lower than the IC_{50}. These results classify lithium chloride as teratogenic in marmoset, but not in mouse.

Comparatively, murine osteogenic cultures treated with sodium chloride featured consistently elevated calcification levels with a 3-fold increase observed in the lowest tested concentration (Fig. 2.2B). No reduction in calcification was observed in any tested

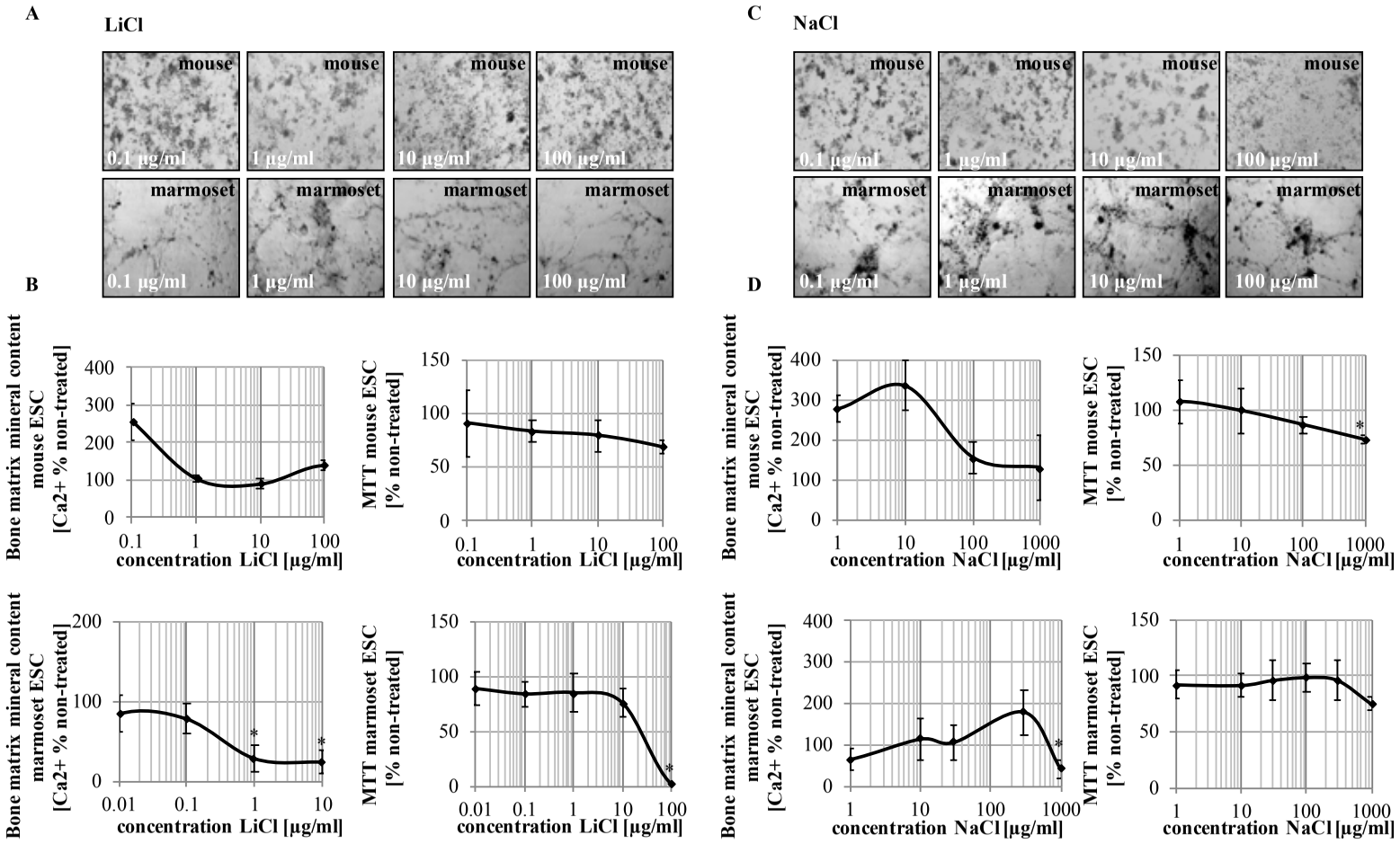

Figure 2.2. Cytotoxicity and bone mineral matrix assessment in mouse and marmoset osteogenic cultures treated with lithium and sodium chloride. (A) Morphology of cultures. (B) Reduction in survival rate and calcium content is given as percentage of non-compound treated cultures (solvent only). Data is represented as means of six technical replicates of n = 3 ± SD. *$p < 0.05$, One-Way ANOVA significantly below untreated solvent control.

concentration. Sodium chloride treated marmoset ESCs, in turn, displayed a half-maximal inhibitory dose at 790 ± 256 μg/ml. Sodium chloride-treated murine and marmoset osteogenic cultures followed relatively similar patterns of dose-dependent decreases in cell viability. In both cases, half maximal viability was approached, but not achieved within the test concentration range. The absent cytotoxicity coupled with a relatively high ID_{50} concentration qualified sodium chloride as non-cytotoxic and non-embryotoxic in neither species.

Lithium acetate treatments resulted in a significant reduction in calcification at the highest tested concentration, while calcification levels remained above the 50% mark in marmoset ESCs for all concentrations tested (Fig. 2.3A and B). No decrease in cellular viability was noted upon exposure with this compound. In contrast, sodium acetate treatment induced a reduction in calcification at concentrations where viability was still around 100% (Fig. 2.3B). Although this effect was noted in both species, marmoset ESCs were more sensitive to sodium acetate than mouse ESCs.

Common sensitivity of mouse and marmoset ESCs to aluminum and controls

In order to further assess response variation between mouse and marmoset ESC osteogenic cultures, effects on calcification levels were also investigated in aluminum chloride, another compound actively used in certain classes of pharmaceuticals with known detrimental effects on the developing skeleton [30], [31], [32]. Cells were treated with aluminum hydroxide as a control for the chloride in aluminum chloride. In aluminum chloride- and aluminum hydroxide-treated mouse ESC cultures, a dose-dependent decrease

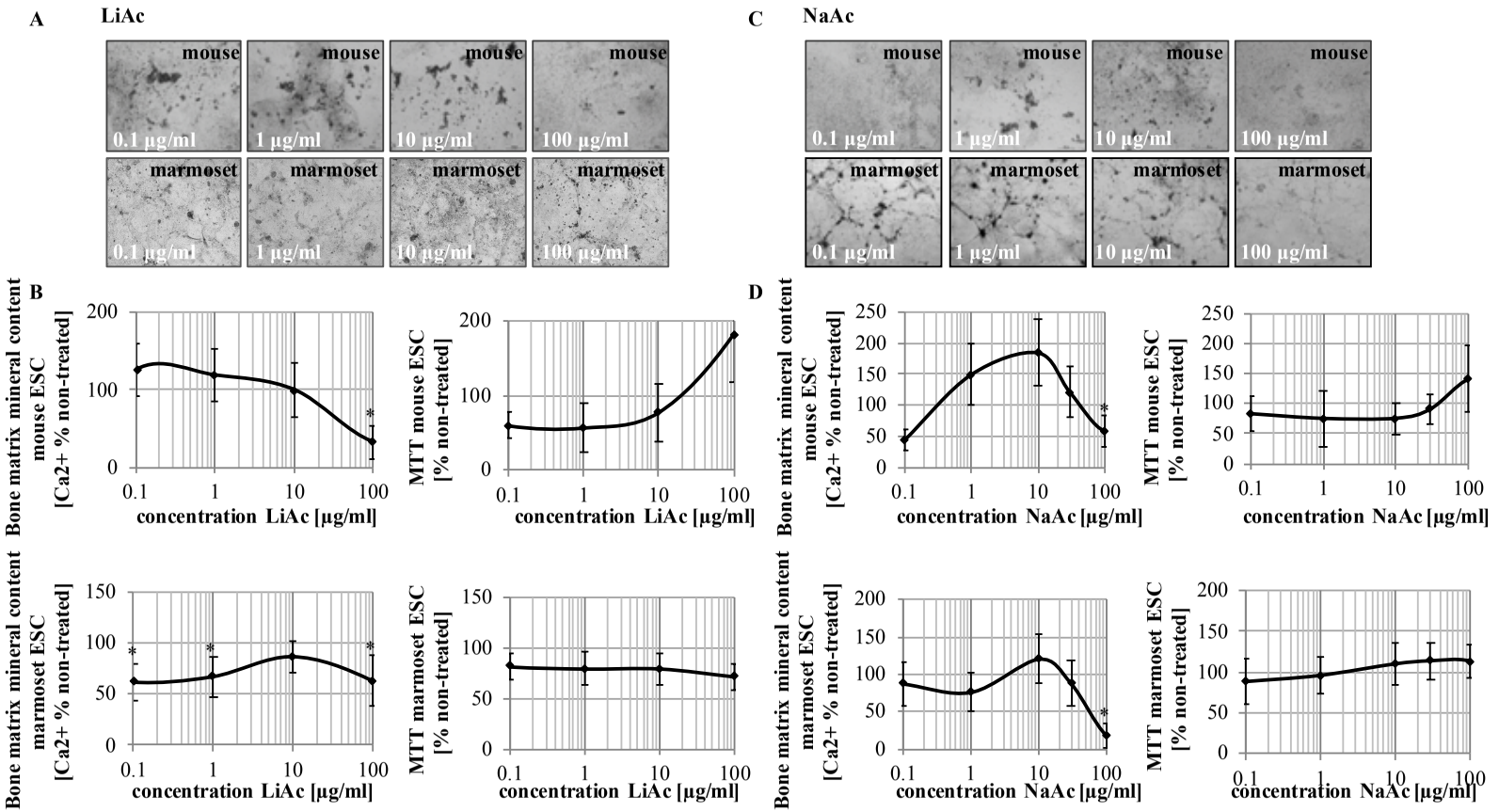

Figure 2.3. Cytotoxicity and bone mineral matrix assessment in mouse and marmoset osteogenic cultures treated with lithium and sodium acetate. (A) Photomicrographs of cultures treated with concentrations of compounds as indicated. (B) Cell viability and calcium deposit in treated cultures is graphed as a function of percent solvent control. Data is represented as means of three independent experiments, each including six technical replicates ± SD. *$p < 0.05$, one-way ANOVA significantly lower than untreated vehicle control.

in calcification was observed with increasing concentration of the test compound (Fig. 2.4). A slightly steeper decrease in calcification was observed in aluminum hydroxide-treated cells. The similar response pattern between the aluminum chloride and hydroxide compounds infers that the observed teratogenic effect may be due to the presence of aluminum at those test concentrations. Comparable dose-dependent decreases in calcification were observed in marmoset ESC osteogenic cultures treated with aluminum chloride or hydroxide. However, calcification reduction in aluminum chloride-treated cultures was not as dramatic compared to osteogenic murine responses.

The similarity between mouse and marmoset ESC responses to treatment with aluminum compounds as summarized in Table 2.1, suggests the potential for response overlap between species utilized for *in vitro* teratogenicity assessments. However, whether or not this overlap occurs may depend on the chemical in question. Lithium is chemically similar to aluminum and yet did not produce similar responses between mouse and marmoset ESC cultures following treatment with lithium compounds (Table 2.1). Therefore, observed variations in response may be due to variability in species sensitivity to particular compounds.

Differential sensitivity to skeletal teratogens in ESCs from Old and New World monkeys

Because of their close phylogenetic relationship with humans, primates share a large number of traits important in human reproduction. However, the reproductive biology of many small primates including *Callithrix*, is distinct from that of humans and Old World monkeys [33]. Because of the closer relationship between humans and Old World

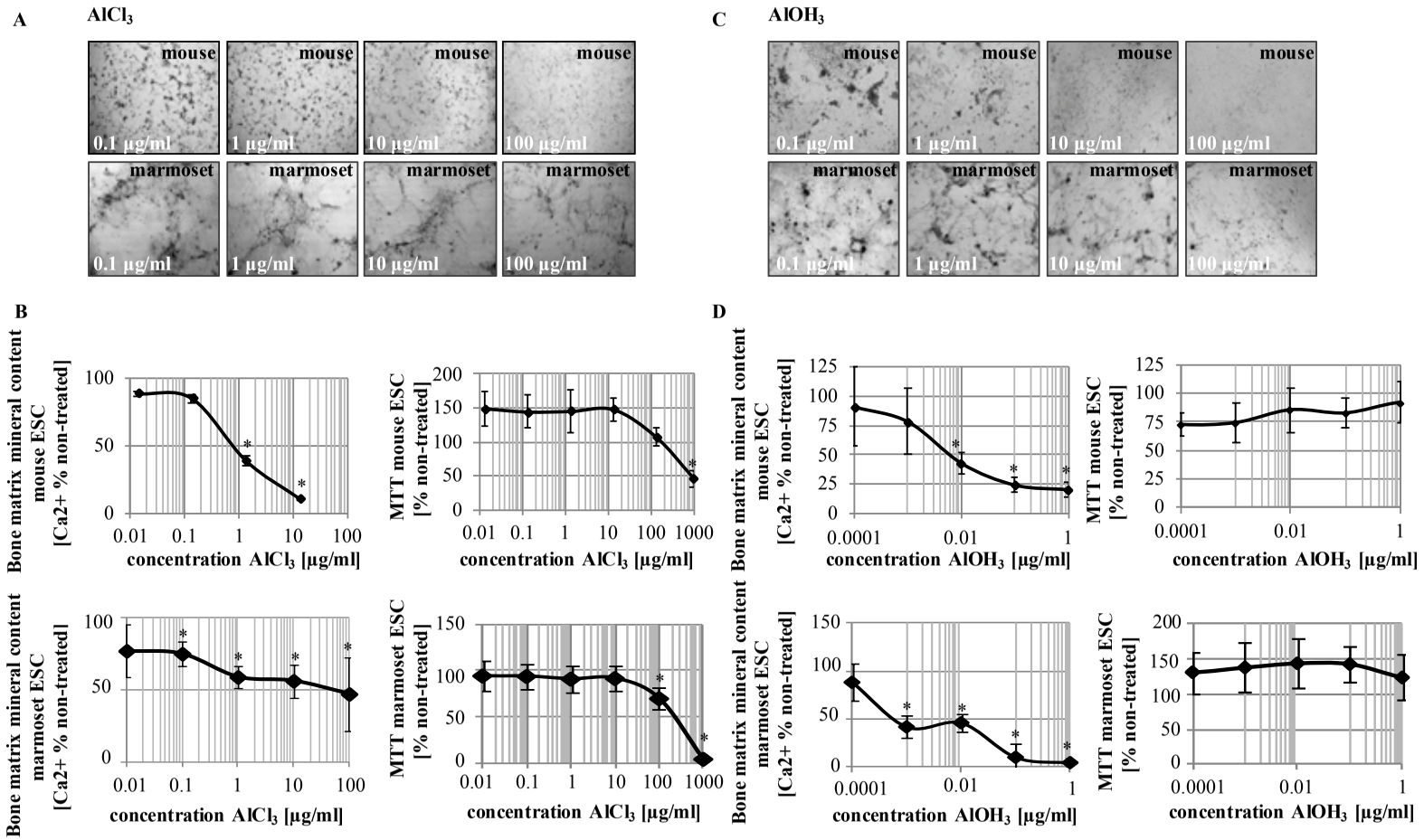

Figure 2.4. Cytotoxicity and differentiation inhibition in aluminum treated mouse and marmoset osteogenic ESC cultures. (A) Morphology on day 14 of differentiation. (B) Values measured for cell viability and calcium deposit were charted in percent of the untreated control. Data is represented as means of six technical replicates of n = 3 ± SD. *$p < 0.05$ below untreated vehicle control, one-way ANOVA.

Compound	ID_{50} (differentiation inhibition, Ca^{2+}) [µg/ml]		IC_{50} (cytotoxicity, MTT) [µg/ml]	
	Mouse	Marmoset	Mouse	Marmoset
LiCl	n/a	0.4 ± 0.03	n/a	24.6 ± 14.8
NaCl	n/a	790 ± 256	n/a	n/a
LiAc	48 ± 11.3	n/a	n/a	n/a
NaAc	100 ± 21	52 ± 9.6	n/a	n/a
$AlCl_3$	0.7 ± 0.02	80 ± 23.8	809 ± 137	204 ± 144
$AlOH_3$	0.0055 ± 0.0035	0.0014 ± 0.0013	n/a	n/a

Table 2.1. Half-maximal inhibitory concentrations of osteogenic differentiation (ID50) and cell viability (IC50) for chloride and aluminum compounds determined with mouse and marmoset ESCs.

monkeys, we next investigated whether ESCs from the rhesus monkey, *Macaca mulatta*, showed similar responses to compounds as the marmoset ESCs. Rhesus ESCs are generally capable of responding to osteogenic triggers with enhanced matrix mineralization [17].

In order to compare the responsiveness of mouse, marmoset and rhesus ESCs to embryotoxic compounds, the embryotoxic potential of 5-fluorouracil (5-FU) and all-trans retinoic acid (*at*RA) in each species were compared against murine ESCs using the skeletal EST protocol [34]. Both compounds were previously shown to act as strong skeletal teratogens in the mouse, both *in vivo* and in the EST [3], [6], [14], [35], [36], [37], [38], [39]. Penicillin G (PenG) was included as a non-embryotoxic compound [21]. Effects on differentiation were assessed *via* calcium deposition quantification assay while cell viability was again measured with the MTT assay.

In 5-FU-treated cells, similar decreases in cell viability were observed in mouse, marmoset and rhesus ESC osteogenic cultures (Fig. 2.5A). However, the mouse ESCs were the most sensitive to the cytotoxic effects of this compound, while marmoset and rhesus ESCs were equally sensitive. Measured calcification patterns in mouse, marmoset and rhesus ESC osteogenic cultures all followed dose-dependent decreases in mineralization with increased 5-FU concentration. Compared to the mouse, the marmoset cells were more sensitive, but the rhesus cells were less sensitive (Fig. 2.5B and C). However, in both primate cells, the $ID_{50}$was approximately two orders of magnitude lower that the IC_{50}, indicating a strong teratogenic effect in both primate cell types.

Exposure to *at*RA treatment again caused cytotoxicity at lower concentrations in mouse ESC cultures than in both primate cell cultures. However, both mouse and rhesus

ESC osteogenic cultures displayed a 2–2.5-fold increase in calcification at lower *at*RA concentrations, followed by a dose-dependent decrease in mineralization as concentration of *at*RA increased (Fig. 2.5A). Calcification levels in *at*RA-treated marmoset ESC osteogenic cultures resembled those of the untreated control at lower concentrations before gradually decreasing dose-dependently. Mouse ESC osteogenic cultures demonstrated the highest sensitivity as calcification at the highest tested concentration in the mouse ESC cultures was significantly lower than mineralization levels observed in marmoset and rhesus cultures at those same concentrations (Fig. 2.5B and C).

According to its role as a non-embryotoxic agent, PenG induced cytotoxicity only at high test concentrations, but failed to cause inhibition of calcification in all species (Fig. 2.5A–C). Results of this assay correctly identified 5-FU and *at*RA as strongly teratogenic compounds across the three species and PenG as non-teratogenic.

Observed differences in primate cell viability and calcification at higher concentrations of 5-FU and *at*RA compared to the mouse ESC osteogenic cultures suggest that both marmoset and rhesus ESCs may be less sensitive than mouse ESCs to particular classes of cytotoxic compounds, while they are more sensitive toward embryotoxic effects of others, again underlining our results obtained with the lithium and aluminum derivatives. Thus, murine-based cytotoxicity and *in vitro* skeletal embryotoxicity assays may provide limited predictivity for extrapolation of results to other species. Though these results indicate that both marmoset and rhesus ESC osteogenic cultures are capable of assessing cytotoxicity and embryotoxicity, the lack of a defined pattern of variability between

A

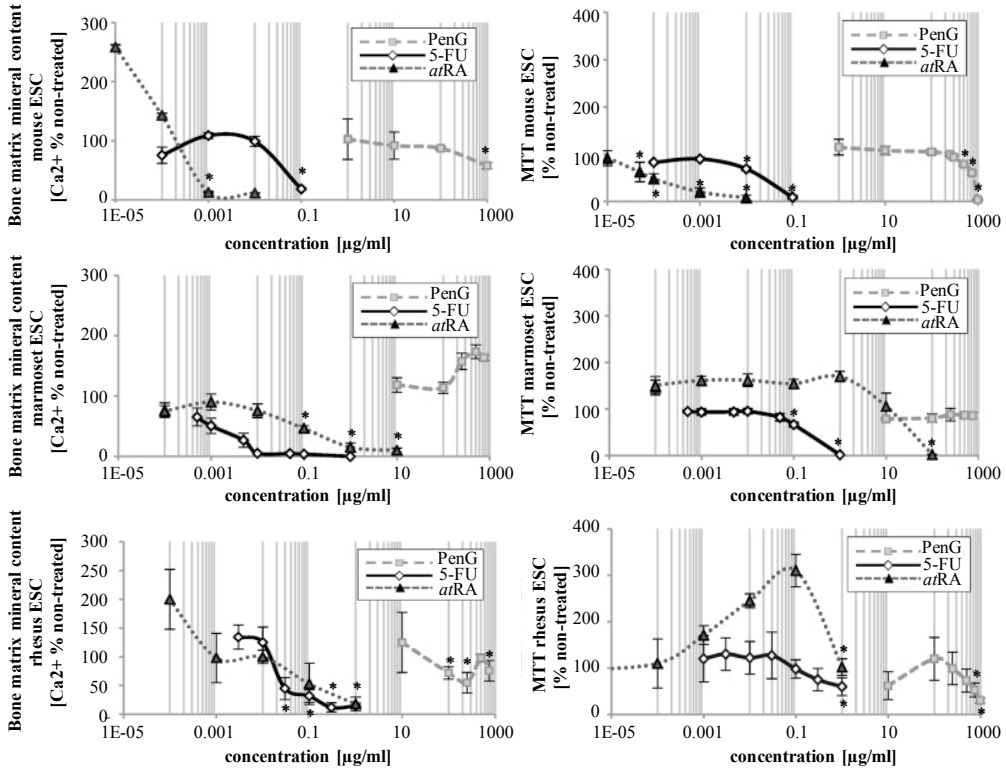

B

	ID_{50} (differentiation inhibition, Ca^{2+}) [µg/ml]	IC_{50} (cytotoxicity, MTT) [µg/ml]
Compound	mouse	
Pen G (class I)	1000	800 ± 10.3
5-FU (class III)	0.04 ± 0.006	0.022 ± 0.0049
atRA (class III)	0.00042 ± 0.000022	$0.00009 \pm 6.6 \times 10^{-6}$
	marmoset	
Pen G (class I)	1000	1000
5-FU (class III)	0.0011 ± 0.00076	0.19 ± 0.045
atRA (class III)	0.07 ± 0.049	30 ± 11
	rhesus	
Pen G (class I)	1000	730 ± 165
5-FU (class III)	0.026 ± 0.015	3.47 ± 2.35
atRA (class III)	0.15 ± 0.14	1.37 ± 0.59

C

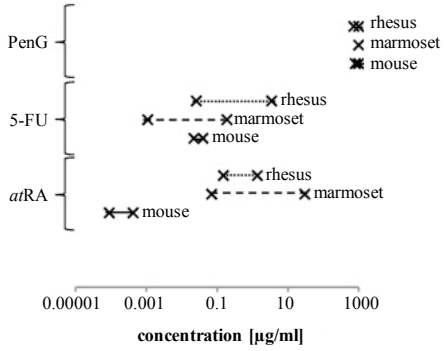

Figure 2.5. Comparison of marmoset and rhesus ESCs for their sensitivity to skeletal embryotoxicants. (A) Juxtaposition of cell viability and mineralization measurements taken from osteogenic mouse, marmoset and rhesus ESC cultures treated with atRA, 5-FU and PenG. *$p < 0.05$ below untreated vehicle control, one-way ANOVA. (B) Table contrasting the resulting IC50 and ID50 values taken from the concentration-response curves. (C) Chart depicting the concentration difference between IC50 and ID50 for each species grouped by compound. The left cross on each line indicates the respective ID50 value, the right cross the IC50 value.

primate osteogenic cultures indicates that response of non-human primate ESCs may also vary between different compound classifications.

Discussion

Since its introduction and subsequent validation, the classic EST has been updated to include additional tissue and molecular endpoints. Such revisions have proven to be extremely useful in allowing for reductions in assay duration as well as providing embryotoxicity responses across tissue types. Skeletal toxicity evaluations in particular stand much to gain from recent improvements as musculoskeletal birth defects account for 5% of all infant deaths. Previous work has demonstrated the capacity of the EST to identify inhibitory effects of toxicants on skeletal development based on the relationship between compound cytotoxicity as measured by reduction in mitochondrial dehydrogenase activity and inhibition of normal differentiation [6], [10].

In developmental toxicology, cytotoxicity of a chemical is often established with MTT assays and previous versions of stem cell based developmental toxicity assays also rely on this read-out measure [4], [40], [41]. However, strictly speaking the MTT assay is a measure for the mitochondrial activity of cells and is therefore only an indirect indicator of cytotoxicity. This could be of concern as mitochondrial activity in stem cells is different than in somatic cells. For instance, stem cells have a low number of mitochondria [42], which increases as cells differentiate concurrently with an increase in mitochondrial DNA content [43]. Future studies will need to compare different endpoints of cytotoxicity, such as apoptosis or proliferative capacity, for their predictivity *in vitro*, which is beginning to be done for other tissue endpoints [44].

One of the main drawbacks of the murine based EST is that it provides a narrow mechanistic understanding of human development and response to toxicants. Yet, potential human sources of cells are either ethically unaccepted in some countries or have been suggested to be of flawed quality. For example, human induced pluripotent stem cells (hiPSCs) often exhibit varying differentiation potential, due to altered global methylation or transcript number of master regulators, which greatly affects their quality and usability [45], [46], [47] and seems dependent on the choice of reprogramming factors [48]. As such, a proposed solution has been to update the EST to feature non-human primate ESCs as a basis for embryotoxicity assessment. Here, we applied a marmoset ESC-based EST in order to evaluate the efficacy of non-human primate ESCs in predicting potential negative side effects on the developing skeletal system. Our proof-of-concept results show that non-human primate ESCs and murine ESCs respond differently in embryotoxicity screens.

Our preliminary comparison screen of murine and non-human primate ESC-based EST assessments indicated that non-human primate ESCs were more tolerant toward the toxic effects of 5-FU and *at*RA compared to murine ESCs. Thus, it is possible that EST embryotoxicity results could be affected by species-driven response variation. Such variations may be attributed to differences in mouse and non-human primate molecular and genomic response to test compounds. Similar species-based discrepancies attributed to variations in molecular and genomic response have been observed in other studies [49]. Discrepancies between the effects of trauma, burns, and exposure to endotoxemia on temporal gene response patterns and inflammation signaling pathways were noted between

mouse models and human patients. Though responses were similar among human subjects, comparison of mouse and human results showed poor correlation of responses between the two groups at the molecular and genomic levels. As all compounds function at the molecular and/or genomic level, these results call into question the extrapolation efficacy of mouse responses as predictors of response in humans [50], [51]. Given the evolutionary closeness between humans and non-human primates [52], it is probable that a mechanism of variation similar to that seen in the Seok et al. [49] study is operating in this study between the murine ESC and marmoset ESC cultures.

Aluminum chloride assay results in murine and marmoset ESCs both demonstrated dose-dependent decreases in calcification. As decreases were observed in both $AlCl_3$- and $AlOH_3$-treated cultures, it is probable that Al^{3+} is responsible for the osteotoxic effects of $AlCl_3$ exposure. Recent studies on aluminum osteotoxicity in infants have reported a strong connection between pre- and perinatal aluminum overexposure and metabolic bone diseases as well as potential long term consequences on bone health and development following exposure to aluminum compounds during critical periods of development [30]. At the molecular level, aluminum has been suggested to antagonize bone formation through activation of the oxidative-stress-mediated c-Jun N-terminal kinase signaling pathway and subsequent induction of apoptosis in osteoblasts [53].

Overall evaluation of cell viability and calcification assay results indicated that lithium chloride and its derivatives possess skeletal teratogenic capacity, though the potency of teratogenic effects may vary depending on the other members of the lithium compound complex. Treatment of marmoset ESC osteogenic cultures with both lithium

chloride and lithium acetate compounds demonstrated noteworthy, but species-specific decreases in calcification, which were absent in sodium chloride. In contrast, sodium acetate was teratogenic in both species. These results suggest lithium to not be the chief skeletal teratogenic component, but rather the combination with the complexed chemical that results in the detrimental outcome on differentiating osteoblasts. Additionally, varied response to lithium and sodium compound treatment between murine and marmoset ESC cultures suggests that species variation in embryotoxic assessments may yield a varied and potentially narrow scope of responses to the compounds under investigation.

Within the cell, lithium chloride has been suggested to operate *via* inhibition of glycogen-synthase-kinase 3beta (GSK3β) to intensify canonical Wnt signaling, which ultimately encourages upregulation of genes required for osteogenic differentiation. Previous studies have reported dose-dependent bone defects incurred by disruption of the canonical Wnt signaling pathway with lithium chloride and support the dose dependent effects of lithium chloride treatment on mouse ESC cultures reported here [54], [55].

Conversely, marmoset ESCs were much more sensitive to the detrimental effects of lithium chloride. Although this may be largely due to increased cytotoxicity of lithium chloride at higher concentrations, the differentiation effect occurred at concentrations that were two orders of magnitude lower than the cytotoxic effect. Considering that other studies have reported variations between mouse and human response at the molecular level, it is likely that a similar explanation stands for the observed differences in lithium chloride response in this study. Lithium chloride is often included in embryotoxicity screens as a control compound in the class of the moderate embryotoxicants [21]. Intriguingly, the

classical EST has a low prediction value for the moderate embryotoxicants [56] and it stands to reason that this low predictivity in this specific class of teratogens stems at least partially from using a less predictive species such as the mouse instead of primate cells.

Of concern are our findings on the differential sensitivity between marmoset and rhesus ESCs that exist even in the small set of chemicals tested here. Although the three control chemicals that were tested exhibited predictive effects, with 5-FU and *at*RA being teratogenic and PenG not, the actual half-maximal inhibitory doses varied substantially. It is thus evident that there may be significant general differences in the responses of different non-human primate cells to drugs and toxicants in a broader screen encompassing more chemicals as is typically done with mouse cells [6], [11]. However, our limited results already suggest that this existing dose discrepancy may make risk predictions for human use and the definition of adverse outcome doses difficult. For the reasons laid out in this manuscript, human embryonic stem cells, which are already beginning to be explored for such purpose [57], [58], [59], may provide the most accurate information regarding the teratogenic potential of chemicals and future studies will need to show whether the ethically accepted human induced pluripotent stem cells are also predictive in such assays.

References

1. Christianson A and Howson CP. March of Dimes Global Report on Birth Defects. March of Dimes Foundation. 2006.

2. Woodruff TJ, Zota AR, and Schwartz JM. Environmental chemicals in pregnant women in the United States: NHANES 2003-2004. Environ. Health Perspect. 2011;119(6): 878–885.

3. Scholz G. et al. Results of the first phase of the ECVAM project "prevalidation and validation of three *in vitro* embryotoxicity tests." ALTEX. 1998;15(1): 3–8.

4. Spielmann H. et al. The embryonic stem cell test (EST), an *in vitro* embryotoxicity test using two permanent mouse cell lines: 3T3 fibroblasts and embryonic stem cells. In Vitro Toxicol. 1997;(10): 119–127.

5. Festag M. et al. An *in vitro* embryotoxicity assay based on the disturbance of the differentiation of murine embryonic stem cells into endothelial cells. II. Testing of compounds. Toxicol In Vitro. 2007;21(8): 1631–1640.

6. zur Nieden NI, Kempka G, and Ahr HJ. Molecular multiple endpoint embryonic stem cell test--a possible approach to test for the teratogenic potential of compounds. Toxicol Appl Pharmacol. 2004;194(3): 257–269.

7. Hansen JM. In vivo models of developmental toxicology. Methods Mol Biol 2012;8897–13.

8. Meyer O and Svendsen O. Animal models in pharmacology and toxicology. in Handbook of Laboratory Animal Science. II.J. Hau and G. van Hoosier, Eds. CRC Press, 2003, 11–401.

9. Toppari J. et al. Male reproductive health and environmental xenoestrogens. Environ Health Perspect. 1996;104 Suppl 4741–803.

10. de Jong E, van Beek L, and Piersma AH. Comparison of osteoblast and cardiomyocyte differentiation in the embryonic stem cell test for predicting embryotoxicity *in vivo*. Reprod Toxicol. 2014;4862–71.

11. de Jong E, van Beek L, and Piersma AH. Osteoblast differentiation of murine embryonic stem cells as a model to study the embryotoxic effect of compounds. Toxicol In Vitro. 2012;26(6): 970–978.

12. Pulyanina P and zur Nieden N. Pluripotent stem cells as tools to assess developmental toxicity. in Advances in Medicine and Biology. Bernhardt, Ed. Nova Science. Publishers, Inc., 2012.

13. zur Nieden NI. ESCs for the prediction of developmental toxicity in pharmacological screening. in Multiparameteranalytics – Methods, Applications, Perspectives. K. Conrad, W. Lehman, U. Sack, and U. Schedler, Eds. Lengerich: MPabst Science. Publishers, 2008, 198–220.

14. zur Nieden NI, Davis LA, and Rancourt DE. Comparing three novel endpoints for developmental osteotoxicity in the embryonic stem cell test. Toxicol Appl Pharmacol. 2010;247(2): 91–97.

15. Thomson JA. et al. Embryonic stem cell lines derived from human blastocysts. Science. 1998;282(5391): 1145–1147.

16. Trettner S. et al. Osteogenic induction from marmoset embryonic stem cells cultured in feeder-dependent and feeder-independent conditions. Osteoporos Int. 2014;25(4): 1255–1266.

17. Dienelt A and zur Nieden NI. Hyperglycemia impairs skeletogenesis from embryonic stem cells by affecting osteoblast and osteoclast differentiation. Stem Cells Dev. 2011;20(3): 465–474.

18. Sasaki E. et al. Establishment of novel embryonic stem cell lines derived from the common marmoset (*Callithrix jacchus*). Stem Cells. 2005;23(9): 1304–1313.

19. zur Nieden NI, Kempka G, and Ahr HJ. In vitro differentiation of embryonic stem cells into mineralized osteoblasts. Differentiation. 2003;71(1): 18–27.

20. zur Nieden NI, Davis LA, and Rancourt DE. Monolayer cultivation of osteoprogenitors shortens duration of the embryonic stem cell test while reliably predicting developmental osteotoxicity. Toxicology. 2010;277(1–3): 66–73.

21. Brown NA. Selection of test chemicals for the ECVAM international validation study on *in vitro* embryotoxicity tests. European Centre for the Validation of Alternative Methods. Altern Lab Anim. 2002;30(2): 177–198.

22. zur Nieden NI and Baumgartner L. Assessing developmental osteotoxicity of chlorides in the embryonic stem cell test. Reprod Toxicol. 2010;30(2): 277–283.

23. Davis L, Dienelt A, and zur Nieden NI. Absorption-Based Assays for the Analysis of Osteogenic and Chondrogenic Yield. in Embryonic Stem Cell Therapy for Osteo-Degenerative Diseases. NI zur Nieden, Ed. Humana Press, 2011, 255–272.

24. Müller T. et al. A novel embryonic stem cell line derived from the common marmoset monkey (*Callithrix jacchus*) exhibiting germ cell-like characteristics. Hum Reprod. 2009;24(6): 1359–1372.

25. Thomson JA. et al. Pluripotent cell lines derived from common marmoset (*Callithrix jacchus*) blastocysts. Biol Reprod. 1996;55(2): 254–259.

26. zur Nieden NI. et al. Gene profiling on mixed embryonic stem cell populations reveals a biphasic role for beta-catenin in osteogenic differentiation. Mol Endocrinol. 2007;21(3): 674–685.

27. Jacobson SJ. et al. Prospective multicentre study of pregnancy outcome after lithium exposure during first trimester. Lancet. 1992;339(8792): 530–533.

28. Schoonen W, Westerink W, and Horbach J. High-throughput screening for analysis of *in vitro* toxicity. EXS. 2009;99401–452.

29. Seiler A and Spielmann H. The validated embryonic stem cell test to predict embryotoxicity *in vitro*. Nat Protocols. 2011;6(7): 961–978.

30. Fanni D. et al. Aluminum exposure and toxicity in neonates: a practical guide to halt aluminum overload in the prenatal and perinatal periods. World J Pediatr. 2014;10(2): 101–107.

31. Firling CE, Hill TA, and Severson AR. Aluminum toxicity perturbs long bone calcification in the embryonic chick. Arch Toxicol. 1999;73(7): 359–366.

32. Severson AR. et al. Influence of short-term aluminum exposure on demineralized bone matrix induced bone formation. Arch Toxicol. 1992;66(10): 706–712.

33. Fischer KE and Austad SN. The development of small primate models for aging research. ILAR J. 2011;52(1): 78–88.

34. Kuske B, Pulyanina PY, and zur Nieden NI. Embryonic stem cell test: stem cell use in predicting developmental cardiotoxicity and osteotoxicity. Methods Mol Biol. 2012;889147–179.

35. Dagg CP. Sensitive stages for the production of developmental abnormalities in mice with 5-fluorouracil. Am J Anat. 1960;10689–96.

36. Eichele G. Retinoids and vertebrate limb pattern formation. Trends Genet. 1989;5(8): 246–251.

37. Fernhoff PM and Lammer EJ. Craniofacial features of isotretinoin embryopathy. J Pediatr. 1984;105(4): 595–597.

38. Shuey DL. et al. Biologically based dose-response modeling in developmental toxicology: biochemical and cellular sequelae of 5-fluorouracil exposure in the developing rat. Toxicol Appl Pharmacol. 1994;126(1): 129–144.

39. Stephens JD. et al. Multiple congenital anomalies in a fetus exposed to 5-fluorouracil during the first trimester. Am J Obstet Gynecol. 1980;137(6): 747–749.

40. Genschow E. et al. Validation of the embryonic stem cell test in the international ECVAM validation study on three *in vitro* embryotoxicity tests. Altern Lab Anim. 2004;32(3): 209–244.

41. Seiler A. et al. Improvement of an *in vitro* stem cell assay for developmental toxicity: the use of molecular endpoints in the embryonic stem cell test. Reprod Toxicol. 2004;18(2): 231–240.

42. Prigione A and Adjaye J. Modulation of mitochondrial biogenesis and bioenergetic metabolism upon *in vitro* and *in vivo* differentiation of human ES and iPS cells. Int J Dev Biol. 2010;54(11–12): 1729–1741.

43. Mandal S. et al. Mitochondrial function controls proliferation and early differentiation potential of embryonic stem cells. Stem Cells. 2011;29(3): 486–495.

44. Hayess K. et al. The DNT-EST: a predictive embryonic stem cell-based assay for developmental neurotoxicity testing *in vitro*. Toxicology. 2013;314(1): 135–147.

45. Jiang J. et al. Different developmental potential of pluripotent stem cells generated by different reprogramming strategies. J Mol Cell Biol. 2011;3(3): 197–199.

46. Kim K. et al. Epigenetic memory in induced pluripotent stem cells. Nature. 2010;467(7313): 285–290.

47. Polo JM. et al. Cell type of origin influences the molecular and functional properties of mouse induced pluripotent stem cells. Nat Biotechnol. 2010;28(8): 848–855.

48. Buganim Y. et al. The Developmental Potential of iPSCs Is Greatly Influenced by Reprogramming Factor Selection. Cell Stem Cell. 2014;15(3): 295–309.

49. Seok J. et al. Genomic responses in mouse models poorly mimic human inflammatory diseases. Proc Natl Acad Sci USA 2013;110(9): 3507–3512.

50. Bailey J. Non-human primates in medical research and drug development: a critical review. Biogenic Amines. 2005;19(4): 235–255.

51. Schardein JL, Schwetz BA, and Kenel MF. Species sensitivities and prediction of teratogenic potential. Environ Health Perspect. 1985;6155–67.

52. Chimpanzee Sequencing and Analysis Consortium. Initial sequence of the chimpanzee genome and comparison with the human genome. Nature. 2005;437(7055): 69–87.

53. Li X. et al. Aluminum induces osteoblast apoptosis through the oxidative stress-mediated JNK signaling pathway. Biol Trace Elem Res. 2012;150(1–3): 502–508.

54. Lindsley RC. et al. Canonical Wnt signaling is required for development of embryonic stem cell-derived mesoderm. Development. 2006;133(19): 3787–3796.

55. Rodda SJ and McMahon AP. Distinct roles for Hedgehog and canonical Wnt signaling in specification, differentiation and maintenance of osteoblast progenitors. Development. 2006;133(16): 3231–3244.

56. Genschow E. et al. Development of prediction models for three *in vitro* embryotoxicity tests in an ECVAM validation study. In Vitr Mol Toxicol. 2000;13(1): 51–66.

57. Adler S. et al. Testing potential developmental toxicants with a cytotoxicity assay based on human embryonic stem cells. Altern Lab Anim. 2008;36(2): 129–140.

58. Jung E-M. et al. Evaluation of developmental toxicity using undifferentiated human embryonic stem cells. J Appl Toxicol. 2015;35(2): 205–218.

59. West PR. et al. Predicting human developmental toxicity of pharmaceuticals using human embryonic stem cells and metabolomics. Toxicol Appl Pharmacol. 2010;247(1): 18–27.

CHAPTER 3

Embryonic stem cell test revised: an evaluation of human induced pluripotent stem cells to test for cardiac developmental toxicity and comparison of differential embryotoxicity

Lauren M. Walker, Nicole RL Sparks, Veronica Puig-Sanvicens, Beatriz Rodrigues, Nicole I. zur Nieden

Abstract

Traditional embryotoxicity approaches are challenged by low throughput and species-species variation risks. The validated embryonic stem cell test (EST) developed in murine embryonic stem cells (mESCs) addressed the former problem over 10 years ago. Here, we address biological relevance by updating the EST protocol with human induced pluripotent stem cells (hiPSC). hiPSC-EST embryotoxicity screens with 5-flurouracil and all-trans retinoic acid inhibited cardiac differentiation at lower concentrations than in the mESC-EST, yielding accurate and more sensitive embryotoxicity classifications. The hiPSC-EST was also responsive to complex toxicants, represented here by cigarette smoke and smokeless Snus tobacco extract. Tobacco treatment inhibited cardiac differentiation at sub-cytotoxic doses. Expression of early cardiac marker *Tbx5* yielded toxicity patterns like those observed in the full-length hiPSC-EST. Together, the presented findings support the use of hiPSCs and early molecular endpoints in the EST as a higher throughput,

biologically relevant embryotoxicity screening approach for individual chemicals and mixtures.

Introduction

The mammalian developmental stage is a sensitive and highly-regulated period of life. During this time, developing mammalian organisms are subject to many complex processes that are critical for proper formation. As such, exposure to some chemicals, pharmaceuticals, or other agents during particular pregnancy windows could result in adverse developmental outcomes such as growth retardation, structural and/or functional abnormalities, and/or embryo lethality. Current regulations require commercially available industrial chemicals and pharmaceutical products to be evaluated for developmental repercussions [1,2]. For instance, industrial chemicals are subject to *in vivo* reproductive and developmental screening tests as outlined by the Organisation for Economic Co-operation and Development (OECD) [3-8]. These screening approaches evaluate adverse pregnancy outcomes in relation to maternal toxicity to determine the overall embryotoxic specificity of the agent, if any. While traditional *in vivo* screening approaches offer a wealth of information regarding the developmental toxicity of an agent, exclusively animal-based screens are time-consuming, low throughput, expensive, and require a large number of animals to complete statistical evaluations. In recent decades, *in vitro* screening approaches have been sought as higher throughput alternatives to animal-based screens.

Early iterations of *in vitro* developmental toxicity assays employed a variety of cell and tissue cultures, including primary embryonic cell cultures and whole mammalian

embryos to determine general embryotoxicity and specific malformations, respectively [9]. Discovering the capacity of mouse blastocyst-derived pluripotent embryonic stem cells (ESCs) to be established and maintained in culture [10], however, revolutionized *in vitro* toxicity screening approaches. Given their unspecialized nature, pluripotent ESCs can recapitulate key steps of the developmental process *in vitro* through directed differentiation into particular cell types. To date, numerous differentiation protocols using pluripotent ESCs have been reported to recapitulate a variety of processes including myogenesis, hematopoiesis, and osteogenesis [11-13]. The original embryonic stem cell test (EST) capitalizes on this ability by using differentiating mouse ESC cultures to evaluate the embryotoxicity of an agent without the requirement for routine animal sacrifice [14]. Here, mouse D3 ESCs are differentiated into contracting cardiac muscle cells and simultaneously exposed to the agent under evaluation. Differentiation inhibition imparted by the agent is determined by a reduction in active contractile clusters and is also compared to the cytotoxic impact on the ESCs to determine if an agent is predominantly embryotoxic (i.e., birth defect-inducing) or cytotoxic. Effects on ESCs are also compared to differentiated 3T3 fibroblast cells to determine embryotoxic specificity. Here, 3T3 fibroblasts are included to mimic maternal tissues and identify maternal toxicity that could influence embryotoxicity outcomes. Results from all three endpoints are ultimately entered into a biostatistical prediction model developed by the ZEBET unit of The Federal Institute for Risk Assessment (Germany) to determine and rank the embryotoxicity of the agent as non-embryotoxic, weakly embryotoxic, or strongly embryotoxic [15-16].

While the mouse EST prediction model approach was successfully validated by the European Center for the Validation of Alternative Methods (ECVAM) for *in vitro* embryotoxicity screens [15-16], it is limited by the possibility of species-species variation in response to particular agents. This, in turn, presents the risk of false negative results.

Our group previously reported an *in vitro* study that assessed the sensitivity of non-human primate and mouse-derived ESC lines in determining chemical embryotoxicity [17]. Notably, non-human primate ESCs showed differential sensitivity to assorted classes of compounds compared to mouse ESCs. Our results highlighted the analytical limitations introduced by species variation and highlight the need for robust methods that are as biologically relevant as possible to humans.

The establishment of human pluripotent cell lines offers a biologically relevant alternative to the traditional mouse D3 line. Particularly promising are human induced pluripotent stem cells (hiPSCs) as such lines can be induced to differentiate like ESCs, without the potential ethical or legislative challenges presented by routine use of human ESC lines. hiPSCs are already routinely used as *in vitro* models of human cardiotoxicity and disease [18-19], though reported use of hiPSCs in the EST protocol for screening potential real-world toxicants is limited.

In this study, we evaluate the sensitivity of hiPSCs in the EST prediction model against the traditional mESC-based EST using the traditional contractile assay and cell viability parameters. Moreover, we report the promise of using early molecular markers to increase assay throughput without reducing sensitivity and test our hiPSC-EST protocol in a proof-of-concept embryotoxicity screen.

Materials and Methods

Culture of human induced pluripotent stem cells (hiPSCs)

The hiPSC cell line Riv9 was obtained from the Stem Cell Core at the University of California, Riverside. hiPSCs were seeded on Matrigel (Corning)-coated tissue culture plates and maintained in a pluripotent state in mTeSR® medium (Stem Cell Technologies). Cells were cultured under a humidified atmosphere of 5% CO_2 at 37^{o}C, and passaged for maintenance or to seed for experiments approximately every 5 days as previously described [20-21].

Cardiac Differentiation of hiPSCs

After cells reached 70% confluency (designated day 0), media was changed to control differentiation media supplemented with 0.06 mg/ml ascorbic acid (Sigma) to induce cardiac differentiation (Puig-Sanvicens et al., 2015). Control differentiation media was comprised of: Dulbecco's modification of Eagle's medium (DMEM with 4.5 g/L glucose, L-glutamine and sodium pyruvate; Corning cellgro) supplemented with 18% FBS (PAA), 0.8% penicillin/streptomycin (10,000 units/10,000 units, Gibco), 0.12% non-essential amino acids (NEAA; Gibco), 0.1 mM β-mercaptoethanol (Gibco). Cultures were cultured in differentiation media for 25 days, starting from day 0.

Culture of human foreskin fibroblasts (hFFs)

Human foreskin fibroblasts were gifted from Dr. Derrick Rancourt (University of Calgary). hFFs were seeded onto 0.1% gelatin-coated tissue culture plates and maintained

in Dulbecco's modification of Eagle's medium (DMEM with 4.5 g/L glucose, L-glutamine and sodium pyruvate; Corning cellgro) supplemented with 10% FBS (Atlanta Biologicals) and 0.5% penicillin/streptomycin (10,000 units/10,000 units, Gibco).

Immunocytochemistry

hiPSC-derived cardiomyocytes were washed with sterile commercially available 1x PBS (Gibco), and fixed with 4% paraformaldehyde (Sigma) 4°C for 30 minutes. Fixed cultures were then washed three times with 1x PBS for 5 min. Cell membranes were permeabilized with 0.1% Triton X-100 in 1x PBS (Fisher Scientific) for 15 min at room temperature before being washed three more times with 1x PBS for 5 min. Cultures were incubated in a blocking solution of 10% fetal bovine serum (PAA) and 0.5% bovine serum albumin (Fisher Scientific, BP1600-100) in 1x PBS for 1 h at room temperature. Primary antibodies against mouse anti-Myosin Heavy Chain (MHC, abcam, ab15, 1:500) and/or rabbit anti-Troponin I (Trop I, Santa Cruz, sc-15368, 1:200) were added directly to the blocking buffer solution following the initial blocking period and allowed to incubate overnight at 4°C. Cultures were washed with 1x PBS three times for 5 min prior to secondary antibody incubation. Cells were incubated with 20 μg/ml DAPI (4'-6-Diamidino-2- Phenylindole, Sigma, D9542), anti-mouse 546 conjugated florescent antibody (ThermoFisher, A10036) and/or anti-rabbit 488 conjugated fluorescent antibodies (ThermoFisher, A21206) for 2 h at room temperature. Cells were washed three times in 1x PBS to remove background from non-specific secondary antibody binding prior to imaging on a Nikon Eclipse Ti inverted fluorescence microscope.

Preparation of 5-fluorouracil, retinoic acid, and penicillin G solutions

5-flurorouracil (5-FU), all-trans retinoic acid (*at*RA), and penicillin G (PenG) were selected from a subset of chemicals used in the original EST validation study [22-23]. 5-FU and *at*RA were selected as positive test compounds due to their established embryotoxic potential while PenG was used as a negative control. All chemicals were purchased from Sigma. Stock solutions were prepared in DMSO and filtered through a 0.2 micron Acrodisc® PSF Syringe Filter (Pall Corporation, Port Washington, NY), aliquoted into sterile microcentrifuge tubes and stored at -20°C until use. Test chemicals were serially diluted to final concentrations in differentiation media. *at*RA concentrations (μg/ml): 100, 1, 10^{-2}, 10^{-3}, 10^{-6}, and 10^{-8}. 5-FU concentrations (μg/ml): 10^{-2}, 10^{-3}, 10^{-4}, 10^{-5}, and 10^{-6}. PenG concentrations (μg/ml): 600, 700, 800, 900, 1000. Cardiogenic cultures were treated with designated chemicals through day 25 of differentiation and hFF cultures were treated with each compound for a 25-day duration period. Compounds were replenished with each media change.

Preparation of Marlboro Red tobacco smoke extract

A University of Kentucky smoking machine was used to produce smoke extract solutions from commercially available conventional Marlboro Red 100 brand cigarettes as previously described [24-25]. The smoking machine took a 2.2 second puff of mainstream (MS) smoke every minute. Smoke solution concentrations were made in puff equivalents (PE), which are the number of cigarette puffs dissolved in 1 ml of medium. MS smoke

solutions were produced by pulling 30 puffs of MS smoke through 10 ml of DMEM. Resulting 3 PE smoke extracts were filtered through a 0.2 micron Acrodisc® PSF Syringe Filter (Pall Corporation, Port Washington, NY), aliquoted into sterile microcentrifuge tubes, and stored at -80°C until use. Serial dilutions were performed in differentiation medium to reach desired final exposure concentrations: 1 PE, 0.3 PE, 0.1 PE, 0.03 PE, 0.01 PE, 0.003 PE, and 0.001 PE. Cardiogenic cultures were treated with smoke solutions through 25 days of differentiation. Smoke solutions were replenished with each media change.

Preparation of Camel Snus smokeless tobacco extract

A 10% (w/v) Camel Snus extract was prepared as previously described [25]. Ten grams of Snus was added to 85 ml of DMEM and allowed to incubate at 37°C for 2 hours. This initial extract solution was centrifuged for 10 min at 4500×g. Supernatant from the first round of centrifugation was then centrifuged again at 13,000×g for 1 hour. The resulting supernatant was collected and pH adjusted to 7.4. 15 ml of FBS was added to the pH-adjusted Snus extract to produce a 10% stock solution of Snus tobacco extract (STE). The stock solution was then sterile-filtered with a 0.22 μm vacuum filter system. STE was aliquoted into sterile microcentrifuge tubes and stored at -80°C until use. Serial dilutions were performed in differentiation medium to reach desired final exposure concentrations of 0.001%, 0.01%, 0.1%, 1%, 3%, and 5%. Cardiogenic cultures were treated with STE through 25 days of differentiation. STE was replenished with each media change.

Cardiac viability assay

Cardiomyocyte survival following concurrent exposure to each compound was evaluated by -[4,5-dimethylthiazol-2-yl]-2,5-diphenylterazolium bromide (MTT) assay. On day 25 of differentiation, cells were incubated with MTT (5 mg/ml) for 2 h at 37°C. MTT supernatant was removed and replaced with a desorb solution of 0.7% SDS in 2-propanol. The absorbance of the solution was measured at 570 nm in an iMark™ microplate reader (Bio-Rad) with 655 nm as a reference wavelength. Here, mitochondrial dehydrogenase activity on the MTT in solution is directly proportional to a blue-purple product that is detected at 570 nm. Hence, a decrease in absorbance is interpreted as a direct measurement of any reduction in the number of viable cells [17, 25-27].

Cardiac contractile assay

Contractile cardiac clusters and individual contractile, or "beating", cells were counted and recorded on days 15, 20, and 25 of differentiation as previously described [28]. Individual beating cells and beating cell clusters were cumulatively quantified between measurement time points. Untreated control cells served as a baseline for normal contractile incidence for each differentiation. Changes in beating incidence between treatment groups and days were reported as a percentage of beating incidence in solvent controls.

Real-time Quantitative PCR (qPCR)

RNA was extracted using the protocol from NucleoSpin RNA II kit (Macherey Nagel). Quantification of RNA was determined by NanoDrop® 1000 spectrophotometer (Thermo Scientific) at 260 nm. 25 ng of total RNA was used as a template for cDNA synthesis with a mastermix including 5 µL 5x reaction buffer, 1.25 µL 10mM dNTPs, 1.25 µL 400 U/µL RNase inhibitor, 0.1 µL 200 U/µL reverse transcriptase, 0.1 µL 3 µg/µL random primer, and 1.5 µL DEPC H_2O for a total of 25 µL per reaction. 25 ng cDNA transcripts were used for quantitative polymerase chain reaction (qPCR) SYBR green technology on the MyiQ cycler (Bio-Rad). The reactions were setup for 10 minutes of denaturing at 94°C (initial), followed by 40 cycles of denaturing at 94°C, and annealing at 60°C each 45 seconds. The n-fold expression in target samples was calculated with the ΔΔCT method by standardizing Ct values to *GAPDH* expression [29]. Primer sequences for human *GAPDH* were 5'-GAGTCAACGGATTTGGTCGT-3' and 5'-TTGATTTTGGAGGGATCTCG-3'. Target genes were cardiogenic markers *TBX5* and *MEF2c*. Primer sequences for human *TBX5* were 5'- CTGGACACCCCTAAACTGGA-3' and 5'- TCCCACAGAGCTGAACTCCT-3' and primer sequences for human *MEF2c* were 5'- CCATTGGACTCACCAGACCT-3' and 5'- AGCACACACACACACTGCAA-3' [30].

Statistical Analysis

Half-maximal inhibitory compound doses of differentiation (ID_{50}) and cytotoxicity (IC_{50}) were determined from concentration-response curves. ID_{50} and IC_{50} values were used to classify chemical embryotoxicity via a biostatistical prediction model developed

specifically and reported previously for the EST protocol [14-16]. The lowest concentrations at which cardiac contractile function or cell viability registered below that of the untreated control were also identified with one-way analysis of variance (ANOVA) statistical analysis and a subsequent post hoc test as appropriate. *P*-values below 0.05 were considered significant.

Results

hiPSCs efficiently differentiate into cardiomyocytes

Prior to testing the efficacy of the hiPSC-based EST, Riv9 hiPSC cultures were evaluated for their cardiac differentiation potential and efficiency following a 25-day differentiation protocol (Fig. 3.1A). Successful differentiation into cardiomyocytes was visually confirmed with the generation of active contractile clusters on days 20 and 25 of differentiation. The cardiac identity of these clusters was confirmed molecularly via mature cardiomyocyte markers. Immunocytochemistry stains of differentiated cell cultures on day 25 revealed positive staining for myosin heavy chain (MHC) and Troponin I (Trop I) in contractile clusters (Fig. 3.1B). Moreover, RT-PCR analysis of cardiac-specific transcription factors at differentiation day 10 showed a significant upregulation of *TBX5* and *MEF2c* in hiPSC cultures induced to a cardiac cell fate (Fig. 3.1C). Together, these results indicated that Riv9 hiPSCs successfully and efficiently differentiate into cardiomyocytes under the appropriate culture conditions.

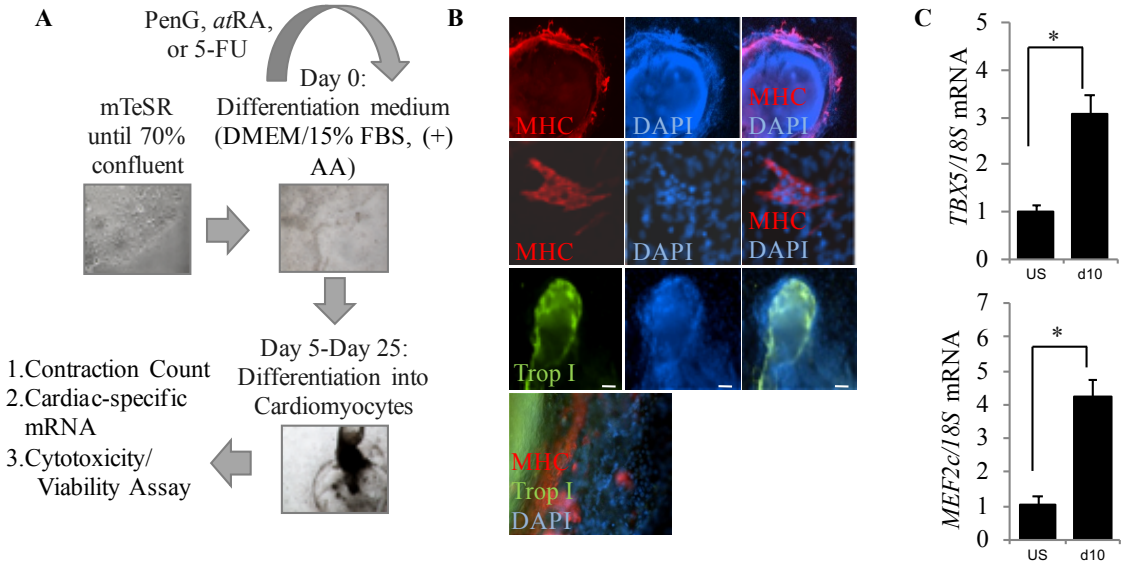

Figure. 3.1. hiPSCs consistently and robustly differentiated into cardiomyocytes. Differentiated cardiomyocytes were assessed for cardiomyocyte-specific markers and gene expression. A) Schematic protocol for cardiomyocyte differentiation and embryotoxicity screen. B) Immunocytochemistry stains of differentiated cultures confirmed cardiomyocyte identity via myosin heavy chain (MHC) and Troponin I (Trop I). C) Differentiated cardiomyocytes expressed cardiac-specific genes *TBX5* and *MEF2c* as measured by qPCR. hiPSC, human induced pluripotent stem cell; MHC, myosin heavy chain; Trop I, Troponin I.

The hiPSC-based EST is more sensitive to embryotoxic compounds than the mESC-based EST

To evaluate the sensitivity of hiPSCs in the validated EST protocol, cardiogenic differentiation was induced in hiPSC cultures with concurrent treatment of one of the following compounds of known toxicity or nontoxicity in humans: PenG (non-toxic), 5-FU (cytotoxic) and *at*RA (embryotoxic). Over the course of the differentiation, hiPSC-derived cardiomyocytes were then subjected to visual quantitation of active contractile cells and clusters on days 15, 20, and 25. At the conclusion of the differentiation, cultures were also evaluated for changes in cell viability.

While no actively contracting cells or clusters were observed on day 15 of differentiation for any treatment group, differences in contraction incidence were readily observed between days 20 and 25 of differentiation for 5-FU- and *at*RA-treated cultures compared to the untreated control. 5-FU exposure negatively impacted the formation of contractile structures at concentrations above 1×10^{-6} μg/ml (Fig. 3.2A) by day 20 and returned a half-maximal inhibitory dose (ID_{50}) for differentiation of 2.7×10^{-6} μg/ml on day 25 (Fig. 3.2B). *at*RA-treated cells failed to form contractile clusters or cells at concentrations above 1×10^{-3} μg/ml (Fig. 3.2A), and exhibited significantly reduced contractile activity in doses above 1×10^{-8} μg/ml (Fig. 3.2B). The resulting ID_{50} value for *at*RA on day 25 was 1.65×10^{-7} μg/ml. Treatment with PenG did not inhibit the formation of contractile structures (Fig. 3.2A) and did not negatively impact contractile activity at most of the tested concentrations (Fig. 3.2B). Dips in contractile incidence were observed at 800 μg/ml and 900 μg/ml doses, though these reductions were not statistically

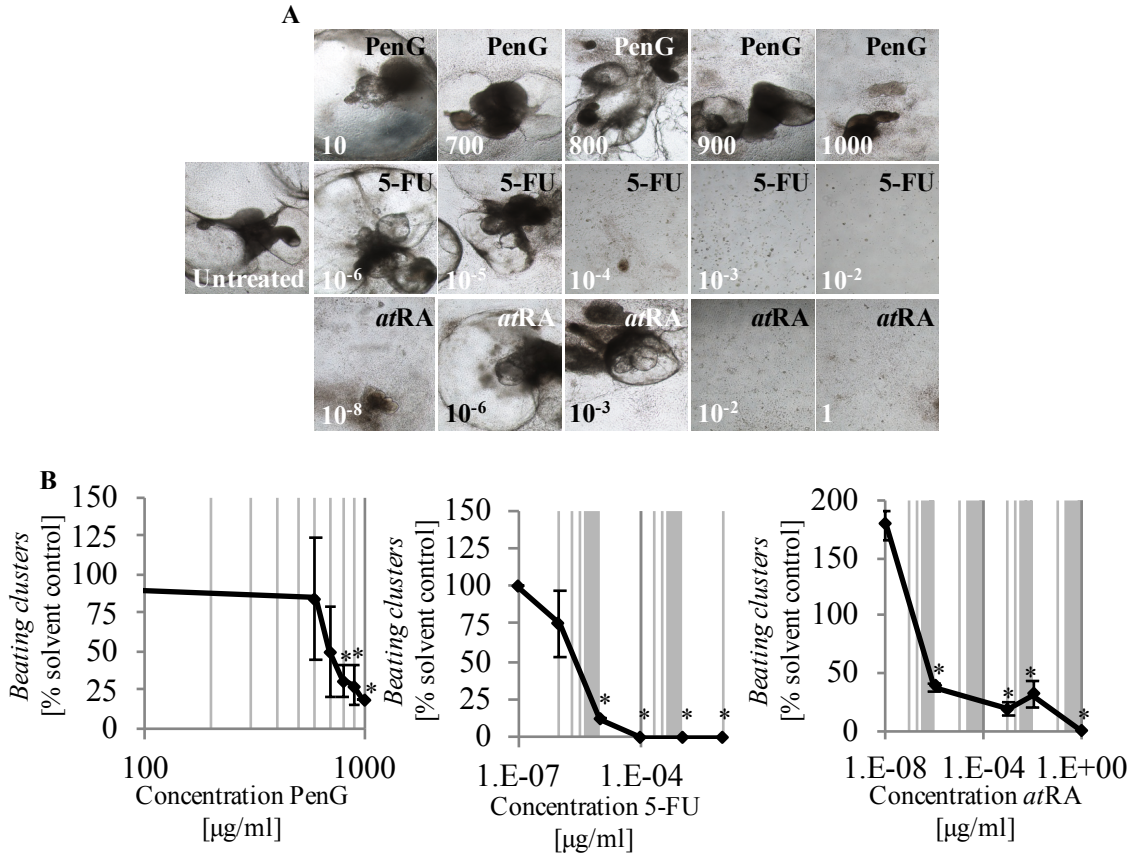

Figure. 3.2. Treatment with embryotoxicants 5-FU and *at*RA impeded cardiomyocyte differentiation. hiPSCs were treated with different concentrations of 5-FU, *at*RA, or PenG and evaluated for differentiation inhibition by visually scoring the number of actively contracting cardiomyocyte clusters. A) Contractile cardiomyocyte clusters. B) Contractile cardiomyocyte cluster screens for 5-FU, *at*RA, and PenG. Each data point represents the mean of three independent experiments ± standard deviation. $^{*}P<0.05$ = the lowest concentration significantly below the untreated control group as determined by One-Way ANOVA. hiPSC, human induced pluripotent stem cell; 5-FU, 5-fluorouracil; *at*RA, all-trans retinoic acid; PenG, penicillin G.

significant. Furthermore, contractile activity at 700 μg/ml and 1000 μg/ml were similar despite the difference in dosage which suggests that the dips seen at 800 μg/ml and 900 μg/ml are likely anomalies. Because dosages above 1000 μg/ml are not physiologically relevant, validated EST protocol does not test compounds above a dose of 1000 μg/ml. As follows, an ID_{50} value was not determined for PenG.

Cell viability assessments did not find reduced cell survival in PenG-treated cultures at the conclusion of differentiation (Fig. 3.3A). 5-FU treatment, however, produced significant reductions in cell viability at concentrations above 1×10^{-6} μg/ml (Fig. 3.3A) and returned a half-maximal inhibitory concentration for cell viability (IC_{50}) of 4.7×10^{-5} μg/ml. Because 5-FU-driven reductions in cell viability were observed around the same doses at which contractile activity was inhibited, these results together suggest that the inhibitory impact of 5-FU primarily driven by cytotoxic activity rather than teratogenic. *at*RA-treated cultures only displaced reductions in cell viability at the highest tested concentrations of 1 and 100 μg/ml (Fig. 3.3A). Unlike 5-FU, *at*RA-driven inhibition of differentiation occurred at much lower concentrations than where cytotoxicity was observed. This outcome indicates that *at*RA operates predominantly through a teratogenic mechanism that inhibits differentiation without conveying outright cytotoxicity. The IC_{50} value for *at*RA was 3 μg/ml.

The impact of the tested compounds in differentiating hiPSCs was also compared against treatment of differentiated hFF cells to determine embryotoxic specificity. Both 5-FU- and *at*RA-treated hFF cells demonstrated a dose-dependent reduction in cell viability. Significant reductions were observed for 5-FU and *at*RA above concentrations of 1×10^{-4}

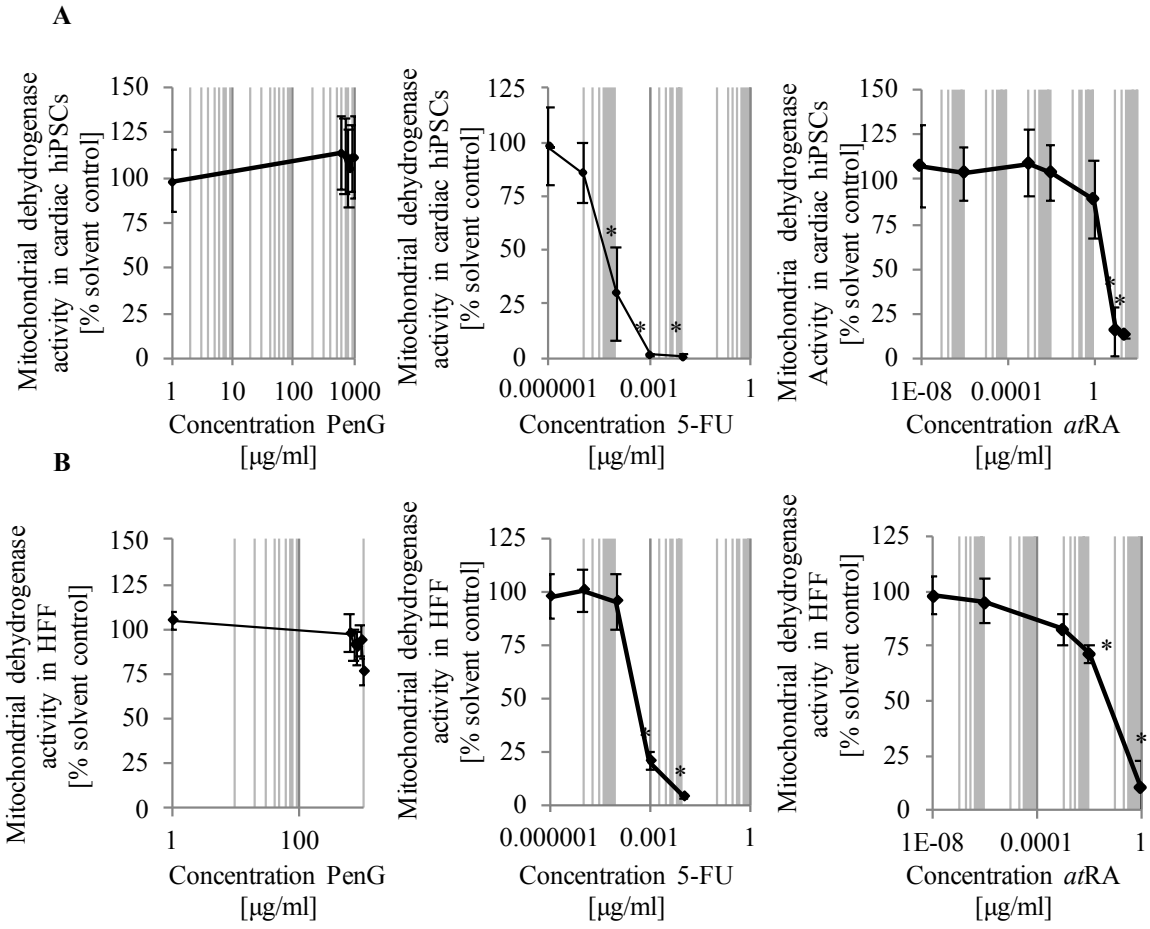

Figure 3.3. 5-FU and *at*RA treatment reduced hiPSC-cardiomyocyte and hFF viability in a dose-dependent manner as assessed via MTT assay. A) hiPSC viability screens for 5-FU, *at*RA, and PenG, n=3 ± SD. $^{*}P<0.05$ = the lowest concentration significantly below the untreated hiPSC control group as determined by One-Way ANOVA. B) hFF viability screens for 5-FU, *at*RA, and PenG, n=3 ± SD. $^{*}P<0.05$ = the lowest concentration significantly below the untreated hFF control group as determined by One-Way ANOVA. hiPSC, human induced pluripotent stem cell; MTT, mitochondrial dehydrogenase activity assay; 5-FU, 5-fluorouracil; *at*RA, all-trans retinoic acid; PenG, penicillin G; hFF, human foreskin fibroblast.

μg/ml and 0.01 μg/ml, respectively. Dosing hFF cultures with 5-FU returned an IC_{50} value of 4 x 10^{-4} μg/ml, which was larger than the IC_{50} value produced by hiPSC-cardiomyocyte evaluations. Observed differential outcomes in hFF and hiPSC-cardiomyocyte cultures exposed to 5-FU support the notion that developing cells (as represented by hiPSC-cardiomyocytes) are more sensitive to cytotoxicants than terminally differentiated cells. hFF cells treated with *at*RA experienced significant cell death at the highest tested concentration of 1 μg/ml. atRA-dosed hFFs produced an IC_{50} value of 0.045 μg/ml, which was lower than the IC_{50} value found in the hiPSC-cardiomyocyte assessment. Here, hFFs may possess differences in cellular metabolic functions that may encourage a slightly higher sensitivity to the cytotoxic impact of *at*RA. PenG-treated hFF cultures did not display a reduction in cell viability at any tested concentration.

To classify compounds under evaluation, the validated EST applies a biostatistically based prediction model to classify compounds as non-embryotoxic, weakly embryotoxic, or strongly embryotoxic based on differentiation and cell viability assay outcomes. The prediction model uses a series of equations to perform a linear discriminant analysis using determined IC_{50} and ID_{50} values determined from dose-response curves [31]. Using this model with the results of the hiPSC-EST resulted in the accurate classification of PenG as non-embryotoxic and 5-FU and *at*RA as embryotoxic (Table 3.1). More specifically, 5-FU was classified as strongly embryotoxic while *at*RA was classified as weakly embryotoxic. Comparing our findings to that of the mESC-based EST [32] (Table 3.1) revealed the hiPSC-based EST to be a more sensitive method of identifying compounds that inhibit differentiation, based on the chemicals tested. Notably, the mESC-

Cell Type	Toxicity Parameter	Penicillin G	5-Flurouracil	*all-trans* Retinoic acid
mESCs[1]	ID_{50} (μg/ml)	> 1000	5.5×10^{-2}	3.1×10^{-4}
	IC_{50} (μg/ml)	> 1000	4.7×10^{-2}	1.25×10^{-3}
	3T3 IC_{50} (μg/ml)	695	0.25	13.5
hiPSCs	ID_{50} (μg/ml)	> 1000	2.7×10^{-6}	1.65×10^{-7}
	IC_{50} (μg/ml)	> 1000	4.7×10^{-5}	3
	hFF IC_{50} (μg/ml)	> 1000	4×10^{-4}	4.5×10^{-2}
mESC Biostatistical Embryotoxicity Classification		Not embryotoxic	Weakly embryotoxic	Weakly embryotoxic
hiPSC (Day 25) Biostatistical Embryotoxicity Classification		Not embryotoxic	Strongly embryotoxic	Weakly embryotoxic

Table 3.1. Comparison of mESC- and hiPSC-EST IC_{50} and ID_{50} values and embryotoxicity classifications. mESC-EST conclusions were pulled from previously published data [32]. Inhibition of differentiation (ID_{50}) was determined from dose-response curves as 50% inhibition of functional cardiomyocytes in the control. Inhibition of cell viability (IC_{50}) was determined from dose-response curves as 50% inhibition of viable cells in control cultures. hiPSC-EST correctly classified all-trans retinoic acid and 5-flurouracil as embryotoxic. mESC, murine embryonic stem cell; hiPSC, human induced pluripotent stem cell; EST, embryonic stem cell test.

EST classified both 5-FU and *at*RA as weakly embryotoxic. Higher ID_{50} values and 3T3 mouse fibroblast IC_{50} values observed in the mESC-EST suggest some resistance to the toxic effects of both chemicals in mESC and 3T3 cultures, respectively. While hiPSC-derived cardiomyocytes were more susceptible to 5-FU-driven cytotoxicity compared to mESC-derived cardiomyocytes, mESC-derived cardiomyocytes were more sensitive to *at*RA-driven cytotoxicity. hFF response was also found to be more sensitive than 3T3 cell viability outcomes, with lower IC_{50} values yielded from 5-FU and *at*RA treatment.

Compared to the mESC-based EST, the hiPSC-based EST showed a higher capacity to discern between a strong embryotoxicant (due to the strong cytotoxic nature of 5-FU) and a weak embryotoxicant (due to the differentiation inhibition in the absence of a strong cytotoxic response).

hiPSC-EST models embryotoxicity of environmental toxicant mixtures

Given their well-reported embryotoxicity, 5-FU and atRA were selectively tested in aforementioned comparison studies between the mESC-based and hiPSC-based EST assays. To test how well the hiPSC-based EST evaluated real-world embryotoxicants, the assay was used to classify two different types of tobacco products: conventional cigarette smoke (Marlboro Red 100) and Snus smokeless tobacco (Camel Snus). Tobacco was selected as a model embryotoxicant as maternal smoking has previously been linked to a suite of negative effects on fetal development including low birth weight, congenital heart defects, and negative impact on bone growth and bone mass [33]. Frequently advertised as

a harm-reducing alternative to cigarettes, Snus smokeless tobacco has also been linked to impaired embryonic development following use during pregnancy [33-36].

Contractile assays found dose-dependent reductions in the formation of active contractile clusters and structures for both Marlboro Red 100 mainstream (MS) smoke (Fig. 3.4A) and Camel Snus (Fig. 3.4B) extract. Contractile assay dose-response curves returned ID_{50} values for 0.014 puff equivalent (PE) and 0.0054% w/v Camel Snus Extract. The viability of differentiating hiPSCs during concurrent tobacco exposure was not negatively impacted by either product in the tested concentration ranges. Viability of hFF cultures exposed to Marlboro Red 100 MS smoke and Camel Snus extract was reduced in a dose-dependent manner. An IC_{50} value for Marlboro Red exposed hFF cultures was not determined within the dose range under evaluation, but was expected to occur at a dose above 0.1 PE. Camel Snus hFF exposure returned an IC_{50} value of 0.022% extract. Because hiPSCs failed to develop cardiomyocyte structures at sub-cytotoxic concentrations (Table 3.2) with regard to both hiPSC and hFF MTT outcomes, these results collectively suggest that both products have embryotoxic characteristics.

hiPSC-EST yields accurate early toxicity classifications based on TBX5 mRNA expression

One of the main critiques of traditional whole animal developmental toxicity assays is the length of time it takes to complete toxicity evaluations. With the average gestation period for laboratory mice ranging from 18.5 to 21 days, the process of collection and evaluating pups is encumbered by slow throughput and variability due to subjective scoring methods. As such, a shorter, quantifiable, and accurate *in vitro* embryotoxicity assessment

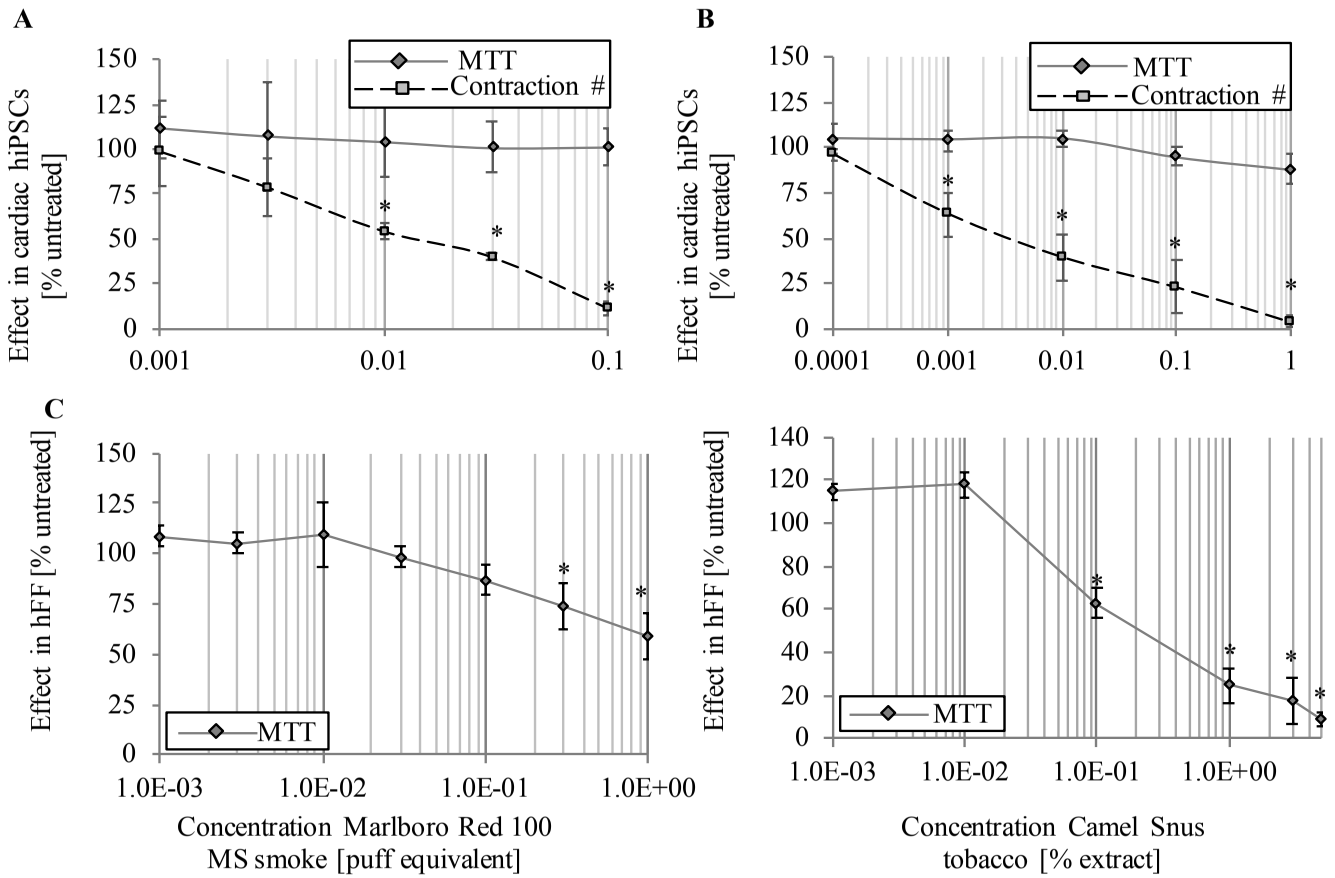

Figure 3.4. Effects of cigarette smoke and Snus smokeless tobacco on developing cardiomyocytes. A) Contractile and viability screens for hiPSCs exposed to MS cigarette smoke using contractile and MTT assay, n=3 ± SD. B) Contractile and viability screens for hiPSCs exposed to Snus smokeless tobacco using contractile and MTT assay, n=3 ± SD. C) Viability screen for hFFs exposed to MS cigarette smoke using MTT assay, n=3 ± SD. hiPSC, human induced pluripotent stem cell; MTT, mitochondrial dehydrogenase activity assay; MS; mainstream; hFF, human foreskin fibroblast.

Toxicity Parameter	Marlboro Red 100 MS (PE)	Camel Snus (%)
hiPSC IC_{50}	>0.1	>1%
hiPSC ID_{50}	0.014 ± 0.0047	0.0054%
hFF IC_{50}	>0.1	0.022 %

Table 3.2. List of IC_{50} and ID_{50} values determined from concentration-response curves for mainstream cigarette smoke and Snus smokeless tobacco. hiPSC, human induced pluripotent stem cell; hFF, human foreskin fibroblast.

approach could improve throughput without sacrificing accuracy. Given the accurate predictions of our full length hiPSC-based EST, we next investigated if our approach could be modified with an earlier, qPCR-based endpoint to determine differentiation inhibition. Here we selected two cardiogenesis-specific transcription factors, *TBX5* and *MEF2c* [37-39], to determine if the adverse differentiation outcomes on day 25 of differentiation would be detectable as changes in *TBX5* and *MEF2c* expression on day 10 of differentiation.

Similar to the pattern observed in the contractile cluster assay, 5-FU-treated cultures demonstrated a dose-dependent reduction in *TBX5* mRNA expression with an ID_{50} value of 5×10^{-4} μg/ml (Fig. 3.4). However, d10 *TBX5* mRNA expression was more dramatically reduced at concentrations above 1×10^{-4} μg/ml, compared to the lower dose of 1×10^{-6} μg/ml observed in the contractile assay. It is possible, however, that our d10 analysis timepoint captured the beginnings of the full apoptotic response that were able to be fully manifested and observed in cultures on d25 of differentiation. It follows, then, that embryotoxicants would be the most detectable at d10 of differentiation in stronger concentrations with middle range doses producing a more moderate response.

Cells exposed to *at*RA also showed a dose-dependent downregulation of *TBX5* mRNA expression. In these cultures, tested concentrations above 1×10^{-6} μg/ml featured significantly downregulated *TBX5* and produced an ID_{50} value of 1.5×10^{-3} μg/ml (Fig. 3.5). *at*RA treatment at 1×10^{-6} and 10^{-8} μg/ml yielded a significant upregulation in *TBX5* mRNA expression. This upregulation correlates with the almost 2-fold increase in contractile cluster incidence seen in cultures treated with 1×10^{-8} μg/ml *at*RA (Fig. 3.2B). As retinoic acid is a well-reported regulator of *TBX5* expression in developing tissues, it is

possible that exposure of differentiating hiPSCs to low levels of *at*RA exposure may have encouraged *TBX5* mRNA expression [99], while *at*RA exposure above a particular threshold elicited an embryotoxic response. While the response pattern in *TBX5* mRNA expression mirrored that which was observed in the contractile assay, differentiation inhibition was more readily detected at mid- and high range concentrations compared to the lower concentrations seen with the contractile assay. Here, as with the 5-FU-treated cultures, it is possible that the early inhibitory impact of *at*RA at d10 of differentiation is readily observed via qPCR in middle and high concentration ranges. Lower ranges, however, may be better detected at a later timepoint. Treatment with the negative control PenG did not significantly impact *TBX5* mRNA expression (Fig. 3.5).

In contrast to expression patterns observed with *TBX5* mRNA, *MEF2c* mRNA expression yielded inconsistent responses to compound treatment. No reductions in *MEF2c* mRNA expression were observed for any 5-FU-treated group compared to the untreated control (Fig. 3.5) and thus no ID_{50} value could be determined. In cells dosed with *at*RA, however, *MEF2c* mRNA transcripts were dose-dependently downregulated in differentiating cardiomyocytes (Fig. 3.5). Here, a steady decline in *MEF2c* mRNA expression was observed at doses above 1×10^{-3} μg/ml with a final ID_{50} of 4×10^{-2} μg/ml. *MEF2c* mRNA expression in cells dosed with PenG remained largely unchanged from that of the untreated control, though slight upregulation was observed at 800 and 900 μg/ml. Given the lack of altered *MEF2c* mRNA expression in cultures exposed to cytotoxic 5-FU compared to *at*RA, it is likely that *MEF2c* is an inconsistent indicator of early

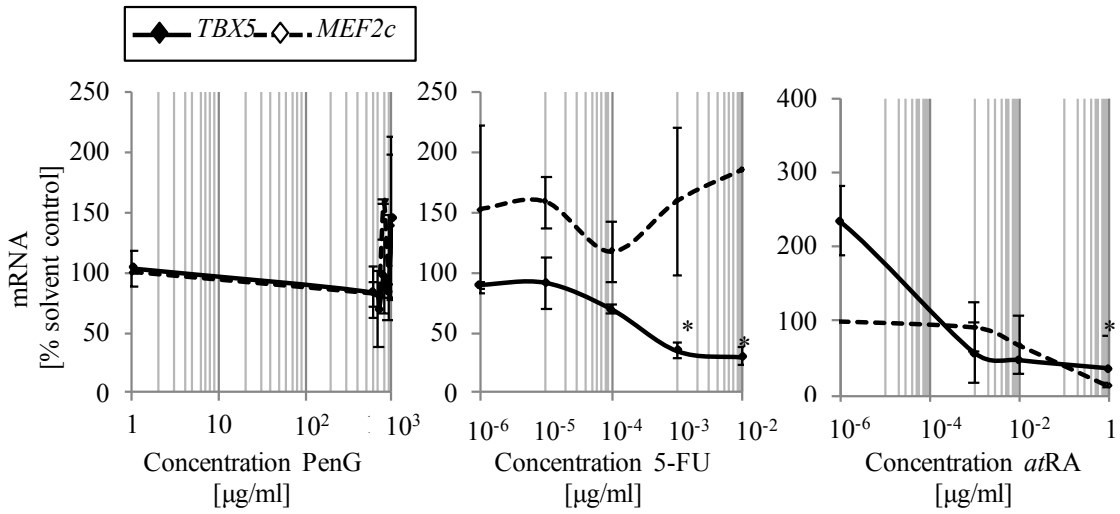

Figure 3.5. Treatment with embryotoxicants 5-FU and *at*RA impeded cardiomyocyte differentiation as measured by day 10 *TBX5* gene expression in hiPSCs. hiPSCs were treated with different concentrations of 5-FU, *at*RA, or PenG and evaluated for *TBX5* or *MEF2c* expression via qPCR. Inhibition of differentiation (ID_{50}) was determined from dose-response curves as 50% reduction of gene expression in the control. hiPSC, human induced pluripotent stem cell; 5-FU, 5-fluorouracil; *at*RA, all-trans retinoic acid; PenG, penicillin G.

differentiation inhibition in cardiomyocytes. In contrast, *TBX5* mRNA expression patterns suggest that *TBX5* may be a better candidate for early differentiation inhibition assessment.

To compare the relative sensitivity of qPCR-based embryotoxicity classifications versus contractile assay-based classifications, the ID_{50} values generated from 5-FU and *at*RA *TBX5* mRNA dose-response curves were compared against the ID_{50} values from the contractile assay curves in the EST biostatistical model. Despite the slight reduction in sensitivity observed in the qPCR approach, both methods produced the same embryotoxicity classifications for 5-FU, *at*RA, and PenG of strongly embryotoxic, weakly embryotoxic, and non-embryotoxic, respectively (Table 3.3).

Discussion

Here, we have shown hiPSCs can be induced to produce a robust and consistent cardiac differentiation model suitable for embryotoxicity screening as outlined by the original EST protocol. Using the EST biostatistical model and chemical agents used in the original EST protocol, this hiPSC-based EST model correctly classified the embryotoxicants, 5-FU and *at*RA, as embryotoxic and our negative control, PenG, as non-embryotoxic. Moreover, the hiPSC-EST model demonstrated improved sensitivity over the original mESC-based EST in determining ID_{50} values by several magnitudes. Mixed cytotoxicity sensitivity was observed in the hiPSC-EST, however. While hiPSC determined IC_{50} values indicated improved sensitivity for determining 5-FU-driven cytotoxicity, reduced sensitivity in cytotoxic assessment was observed for *at*RA treatment in the hiPSC-EST compared to the mESC-based EST. This could be driven by metabolic differences between the cell lines used in both studies. While studies comparing the metabolic efficiencies of mouse and

human pluripotent stem cells have yet to be reported, differential cytotoxic sensitivity between human and mouse has been previously observed in neuroblastoma cell lines exposed to organophosphate insecticides [40]. Such differences may be due to variations in the activation efficiency or robustness of biochemical processes related to apoptotic or necrotic responses. These differences underscore the importance of considering cellular vigor when selecting cell lines for toxicity screens and comparisons. However, in our study, the reduced cytotoxic sensitivity observed for *at*RA-treated cultures did not seem to impact the correct classification of *at*RA as a weak embryotoxicant.

The observed discrepancies in assay sensitivity between the mouse- and human-EST may be explained by molecular differences between species that influence how cells respond to particular agents. This is most readily observed in the case of *at*RA, which acts as a signaling molecule during development and governs critical early embryonic processes including axial patterning, proliferation, apoptosis, and cellular differentiation [41]. Moreover, excessive or deficient retinoic acid levels during development inhibit normal tissue development [42-45]. While retinoic acid signaling is conserved between mammals, it is plausible that these mechanisms may have precise, species-specific thresholds at which an excess of retinoic acid disrupts differentiation versus provoking cytotoxicity. 5-FU, in contrast, is a base analogue that mimics uracil and thymine and can be readily incorporated into DNA and RNA. In this way, 5-FU hinders normal nucleoside metabolism and consistently causes cytotoxicity and cell death regardless of species. While both chemicals are embryotoxic, 5-FU imparts embryotoxicity through cell death while *at*RA can cause embryotoxicity through differentiation inhibition or cell death. Thus, the nature of a

Cell Type	Toxicity Parameter	Penicillin G	5-Flurouracil	*all-trans* Retinoic acid
hiPSCs[a] (d25)	ID_{50} (μg/ml)	> 1000	2.7×10^{-6}	1.65×10^{-7}
	IC_{50} (μg/ml)	> 1000	4.7×10^{-5}	3
hiPSCs (d10 *Tbx5*)	ID_{50} (μg/ml)	> 1000	5×10^{-4}	$1.5 \times 10^{--3}$
hFF	IC_{50} (μg/ml)	> 1000	4×10^{-4}	4.5×10^{-2}
hiPSC (Day 25 cluster) Biostatistical Embryotoxicity Classification		Not embryotoxic	Strongly embryotoxic	Weakly embryotoxic
hiPSC (Day 10 qPCR) Biostatistical Embryotoxicity Classification		Not embryotoxic	Strongly embryotoxic	Weakly embryotoxic

Table 3.3. List of IC_{50} and ID_{50} values and embryotoxicity classifications determined from concentration-response curves for contractile and d10 qPCR assay endpoints. [a]Data from Table 3.1. hiPSC, human induced pluripotent stem cell; hFF, human foreskin fibroblast.

chemical as well as differences in tissue developmental requirements influence the precise embryotoxicity classification in the EST.

Given the correct classification of the test embryotoxicants by the hiPSC-EST, we also assessed the ability of our model to determine the embryotoxicity of cigarette smoke and Snus tobacco toxicants connected to adverse pregnancy outcomes following prenatal maternal exposure (see citations). In the concentration ranges tested, the hiPSC-EST successfully identified ID_{50} values for both Marlboro Red and Camel Snus that were considerably lower than where cytotoxicity was observed in hFF-treated cultures. Our results harmonize with epidemiological studies that connect maternal tobacco use with congenital heart defects [46] and collectively suggest a molecular basis for the embryotoxicity of both tobacco products that operates through differentiation inhibition rather than cytotoxic effects on differentiating cardiomyocytes. Given this outcome and the robustness of our cardiac differentiation, the hiPSC-EST model could plausibly be used for molecular follow up analysis to determine root causes of environmental toxicant-elicited embryotoxicity observed at the screening phase. Furthermore, considering that cigarette smoke is a mixture of over 5000 chemicals [100], our results suggest that the hiPSC-EST model is also suitable for assessing embryotoxicity of environmental toxicant mixtures in addition to screens of individual toxicants. This feature could prove useful in risk assessment applications where the developmental toxicity potential of commercial, industrial, and/or environmental chemical moistures is sought.

In addition to providing a biologically-relevant platform for developmental toxicity screens, the model presented here was able to be modified with the addition of molecular

endpoints to shorten the overall screen duration and increase assessment throughput. Evaluation of cardiac gene expression at day 10 of differentiation produced higher IC_{50} values than that observed in the traditional cardiac contractile assessment at day 25, which suggests a reduction in sensitivity with regard to lower dose ranges. This outcome suggests that the chemical(s) under study and the test concentration range is critical and should be carefully considered when using the qPCR-based hiPSC-EST. This is well-evidenced by 1 $x10^{-8}$ μg/ml *at*RA-dosed cells, which showed elevated *TBX5* expression and contractile clusters. While *at*RA exposure can antagonize *TBX5* expression [48], it can also work together with *TBX5* in early tissue development—particularly in developing cardiac tissue [49]. Our results therefore show a threshold effect where very low doses of *at*RA enhanced cardiogenesis and mid-to-high concentrations inhibited cardiac differentiation. Similar concentration-range responses were obtained for chondrogenic and osteogenic endpoints [13].

The differential response in expression between the two cardiac markers chosen for this study, *TBX5* and *MEF2c*, also underscore the importance of carefully selecting tissue and timepoint specific markers for assessment in this screening model. Changes in *TBX5* expression patterns mirrored that of the contractile assay dose-response curve, while *MEF*2c expression patterns were not consistent between all of the tested chemicals. While *MEF2c* expression is specifically detectable in differentiating cardiomyocytes at day 10 of differentiation, additional studies by our group (not shown) have found that *MEF2c* expression is highest on day 25 of differentiation. Thus, it is possible that before day 25 of differentiation, *MEF2c* expression is not yet at a robust enough level of expression to

generate a consistent dose-response curve in actively differentiating cells. It should be noted, however, that the qPCR-derived ID_{50} values still successfully yielded the same embryotoxicity classifications for 5-FU, *at*RA, and PenG as the contractile assay when calculated with the EST biostatistical model.

Conclusion

In summary, we have shown that hiPSCs may be used as a more biologically-relevant and robust replacement for mESCs in the EST embryotoxicity evaluation protocol. The hiPSC-based EST protocol is responsive in embryotoxicity screens using environmental embryotoxicants and chemical mixtures such as cigarette smoke and could serve as an *in vitro* model system of developmental disease, thereby reducing the number of animals required for developmental studies. Moreover, incorporating early tissue marker endpoints as outlined in this protocol also offers an opportunity to reduce the time commitments surrounding traditional animal embryotoxicity screens and the *in vitro* contractile assay to increase throughput with an opening for automated assessments and reduced culture time.

References

1. U.S. Department of Health and Human Services. Guidance for Industry Reproductive and Developmental Toxicities — Integrating Study Results to Assess Concerns. 2011.

2. U.S. Food and Drug Administration Redbook 2000: IV.C.9.b Guidelines for Developmental Toxicity Studies. 2000.

3. OECD. Test No. 414: Prenatal Developmental Toxicity Study. 1981.

4. OECD. Test No. 415: One-Generation Reproduction Toxicity Study. 1983.

5. OECD. Test No. 416: Two-Generation Reproduction Toxicity. 1983.

6. OECD. Test No. 421: Reproduction/Developmental Toxicity Screening Test. 1995.

7. OECD. Test No. 422: Combined Repeated Dose Toxicity Study with the Reproduction/Developmental Toxicity Screening Test. 1996.

8. OECD. Test No. 443: Extended One-Generation Reproductive Toxicity Study. 2018.

9. Augustine-Rauch K, Zhang CX, and Panzica-Kelly JM. In vitro developmental toxicology assays: A review of the state of the science of rodent and zebrafish whole embryo culture and embryonic stem cell assays. Birth Defects Res C Embryo Today Rev. 2010;90, 87–98.

10. Evans MJ., and Kaufman MH. Establishment in culture of pluripotential cells from mouse embryos. Nature. 1981;292, 154.

11. Barberi T. et al. Derivation of engraftable skeletal myoblasts from human embryonic stem cells. Nat Med. 2007;13, 642–648.

12. Hwang Y, Broxmeyer HE, and Lee MR Generating autologous hematopoietic cells from human-induced pluripotent stem cells through ectopic expression of transcription factors. Curr Opin Hematol. 2017;24, 283–288.

13. zur Nieden NI. et al. Induction of chondro-, osteo- and adipogenesis in embryonic stem cells by bone morphogenetic protein-2: Effect of cofactors on differentiating lineages. BMC Dev Biol. 2005;5, 1.

14. Spielmann H. et al. The embryonic stem cell test (EST), an *in vitro* embryotoxicity test using two permanent mouse cell lines: 3T3 fibroblasts and embryonic stem cells. Vitro Toxicol. 1997;119–127.

15. Genschow E. et al. The ECVAM international validation study on *in vitro* embryotoxicity tests: results of the definitive phase and evaluation of prediction models. European Centre for the Validation of Alternative Methods. ATLA-Altern Lab Anim. 2002;30, 151–176.

16. Genschow E. et al. Validation of the embryonic stem cell test in the international ECVAM validation study on three *in vitro* embryotoxicity tests. ATLA-Altern Lab Anim. 2004;32, 209–244.

17. Walker L. et al. Non-human primate and rodent embryonic stem cells are differentially sensitive to embryotoxic compounds. Toxicol Rep. 2014;2, 165-174.

18. Geng L. et al. Probing flecainide block of INa using human pluripotent stem cell-derived ventricular cardiomyocytes adapted to automated patch-clamping and 2D monolayers. Toxicol. Lett. 2018;294, 61–72.

19. da Silva Lara L. et al. *Trypanosoma cruzi* infection of human induced pluripotent stem cell-derived cardiomyocytes: an *in vitro* model for drug screening for Chagas disease. Microbes Infect. 2018;20, 312–316.

20. Sparks NRL. et al. Low Osteogenic Yield in Human Pluripotent Stem Cells Associates with Differential Neural Crest Promoter Methylation. Stem Cells. 2018;36, 349-362.

21. Madrid JV. et al. Human Pluripotent Stem Cells to Assess Developmental Toxicity in the Osteogenic Lineage. Methods Mol Biol. 2018;1797, 125-145.

22. Buesen, R. et al. Embryonic stem cell test remastered: comparison between the validated EST and the new molecular FACS-EST for assessing developmental toxicity *in vitro*. Toxicol Sci Off J Soc Toxicol. 2009;108, 389–400.

23. Spielmann, H. et al. Preliminary results of the ECVAM validation study on three *in vitro* embryotoxicity tests. ATLA Altern Lab Anim. 2001;29, 301–303.

24. Knoll M and Talbot P. Cigarette smoke inhibits oocyte cumulus complex pick-up by the oviduct *in vitro* independent of ciliary beat frequency. Reprod Toxicol. 1998;12, 57–68.

25. Knoll M. et al. Ciliary beat frequency of hamster oviducts is decreased *in vitro* by exposure to solutions of mainstream and sidestream cigarette smoke. Biol Reprod. 1995;53, 29–37.

26. Martinez IKC. et al. Video-based kinetic analysis of calcification in live osteogenic human embryonic stem cell cultures reveals the developmentally toxic effect of Snus tobacco extract. Toxicol Appl Pharmacol. 2019;363, 111-121.

27. zur Nieden NI and Baumgartner L. Assessing developmental osteotoxicity of chlorides in the embryonic stem cell. Reprod Toxicol. 2010;30, 277-283.

28. zur Nieden NI, Davis LA, Rancourt DE. Comparing three novel endpoints for developmental osteotoxicity in the embryonic stem cell test. Toxicol Appl Pharmacol. 2010;247, 91-97.

29. Seiler AEM. et al. Use of murine embryonic stem cells in embryotoxicity assays: the embryonic stem cell test. Methods Mol Biol. 2006;329, 371–395.

30. Livak KJ and Schmittgen TD Analysis of relative gene expression data using real-time quantitative PCR and the 2(-Delta Delta C(T)) Method. Methods. 2001;25, 402-408.

31. Puig-Sanvicens VA, Semino CE, zur Nieden NI. Cardiac differentiation potential of human induced pluripotent stem cells in a 3D self-assembling peptide scaffold. Differentiation. 2015;90, 101-110.

32. Seiler AEM and Spielmann H. The validated embryonic stem cell test to predict embryotoxicity *in vitro*. Nat Protoc. 2011;6, 961–978.

33. zur Nieden NI. et al. Molecular markers in embryonic stem cells. Toxicol In Vitro. 2001;15, 455-61.

34. Jones G, Riley M, and Dwyer T. Maternal smoking during pregnancy, growth, and bone mass in prepubertal children. J. Bone Miner Res. 1999;14, 146–151.

35. England LJ. et al. Adverse pregnancy outcomes in snuff users. Am J Obstet Gynecol. 2003;189, 939–943.

36. Gupta PC and Sreevidya S. Smokeless tobacco use, birth weight, and gestational age: population based, prospective cohort study of 1217 women in Mumbai, India. BMJ. 2004;328, 1538.

37. Wikström AK. et al. Effect of Swedish snuff (Snus) on preterm birth. BJOG Int J Obstet Gynaecol. 2010; 117, 1005–1010.

38. Bruneau BG. et al. Chamber-Specific Cardiac Expression of Tbx5 and Heart Defects in Holt–Oram Syndrome. Dev Biol. 1999;211, 100–108.

39. Edmondson DG. et al. Mef2 gene expression marks the cardiac and skeletal muscle lineages during mouse embryogenesis. Dev Camb Engl. 1994;120, 1251–1263.

40. Liberatore CM, Searcy-Schrick RD, and Yutzey KE. Ventricular Expression of tbx5 Inhibits Normal Heart Chamber Development. Dev Biol. 2000;223, 169–180.

41. Veronesi B and Ehrich M. Differential cytotoxic sensitivity in mouse and human cell lines exposed to organophosphate insecticides. Toxicol Appl Pharmacol. 1993;120, 240–246.

42. Sucov HM and Evans RM. Retinoic acid and retinoic acid receptors in development. Mol Neurobiol. 1995;10, 169-184.

43. Wilson JG and Warkany J. Aortic-arch and cardiac anomalies in the offspring of vitamin A deficient rats. Am J Anat. 1949;85, 113-155.

44. Cohlan SQ. Congenital anomalies in the rat produced by excessive intake of vitamin a during pregnancy. Pediatrics. 1954;13, 556.

45. Iulianella A. et al. A molecular basis for retinoic acid-induced axial truncation. Dev Biol. 1999;205, 33-48.

46. Chien CY. et al. Maternal vitamin A deficiency during pregnancy affects vascularized islet development. J Nutr Biochem. 2016;36,51-59.

47. Malik S. et al. Maternal smoking and congenital heart defects. Pediatrics. 2008;121, e810-816.

48. Talhout R. et al. Hazardous Compounds in Tobacco Smoke. Int J Environ Res Public Health. 2011;8, 613–628.

49. Golz S, Lantin C, and Mey J. Retinoic acid-dependent regulation of BMP4 and Tbx5 in the embryonic chick retina. Neuroreport. 2004;15, 2751–2755.

50. De Bono C. et al. T-box genes and retinoic acid signaling regulate the segregation of arterial and venous pole progenitor cells in the murine second heart field. Hum Mol Genet. 2018;27, 3747–3760.

CHAPTER 4

Sidestream smoke extracts from harm-reduction and conventional Camel cigarettes inhibit osteogenic differentiation via oxidative stress and differential activation of intrinsic apoptotic pathways

Lauren M. Walker, Nicole RL Sparks, Steven R. Sera, Joseph V Madrid, Ivann KC Martinez, Michael Hanna, Prue Talbot, Nicole I zur Nieden

Abstract

Tobacco smoking has been implicated in an array of health-related diseases including those that affect adult bone. However, little is known regarding the impact of conventional and harm-reduction tobacco products on bone tissue as it develops in the embryo. To assess the effects of tobacco products on developing bone *in vitro*, human embryonic stem cells were differentiated into osteoblasts and concomitantly exposed to various concentrations of either mainstream or sidestream smoke solutions from Camel (conventional) and Camel Blue (harm-reduction) cigarettes. Differentiation inhibition was determined by calcium assays on osteogenically differentiating cells and compared to the cytotoxicity of the tobacco smoke solution.

Exposure to mainstream smoke from both Camel and Camel Blue cigarettes caused no inhibition of cell viability or calcification of the osteogenic cultures. Sidestream smoke from conventional Camel cigarettes concentration-dependently elicited calcification

inhibition that was triggered by high levels of mitochondrially-generated oxidative stress, loss of mitochondrial membrane potential, and reduced ATP production. Moreover, Camel sidestream smoke induced DNA damage and caspase9-dependent apoptosis. Camel Blue exposed cells, in contrast, invoked only intermediate levels of reactive oxygen species insufficient to activate caspase3/7. In the absence of apoptotic gene activation, damage to the mitochondrial phenotype was noted in addition to completely retarded mineralization at subtoxic concentrations. Collectively, the presented findings in differentiating pluripotent stem cells imply that embryos may exhibit low bone mineral density if exposed to certain kinds of environmental smoke during development.

Introduction

A growing body of evidence has shown that cigarette smoking produces numerous adverse health effects, making cigarette use the leading cause of preventable death in the world. The most well-known of the adverse health consequences of tobacco use are cancer, cardiovascular disease, and respiratory complications. However, cigarette smoking has also been shown to have adverse effects on bone tissue. For example, smoking increases the occurrence of developing osteopathies, such as osteoporosis [1-3] and Legg-Calve-Perthes Disease [4] and has been implicated in delayed healing of fractured bones [5-6].

A recent trial suggested that nicotine replacement therapies to help women quit during pregnancy often deliver inadequate nicotine levels (as measured via nicotine metabolite content in urine) to aid in smoking cessation [7]. Consequently, smokers who become pregnant and are unsuccessful in quitting can expose their children *in utero*. This

is important since tobacco use during pregnancy may also adversely affect pregnancy outcomes and impair the health of the unborn [8-10]. Among other environmental factors, smoking while pregnant accounts for the high frequencies of congenital anomalies [11-12]. Limited research in young adults and immature animals suggests a detrimental effect of tobacco on bone during growth by suppressing bone formation [13].

Increasing concerns about the health risks associated with tobacco smoke led the tobacco industry to create "harm-reduction" products including "light" versions of their conventional cigarettes. Smoke from these products typically contain less tar, nicotine, and chemical additives than would be found in smoke from conventional products. Because users of harm-reduction products often engage in compensatory smoking, the frequency of smoking-associated cancer deaths seems equally high in those who use harm-reduction products [14]. While the beneficial impact of harm-reduction cigarettes on overall health is still being debated, it is even less clear whether the reduction of nicotine and tar content in harm-reduction products sufficiently eliminates embryotoxic effects in developing bone.

Studies to understand adverse effects on embryo health are typically performed using rodent models [15-16]. These types of studies require the routine sacrifice of animals, are often not cost effective, and may not accurately predict the outcome of human exposure. Our group has recently shown that the yield of osteoblasts from *in vitro* exposed and differentiated human embryonic stem cells (hESCs) can predict adverse effects of a chemical towards bone development [17]. The purpose of this study was to investigate the molecular mechanisms of embryotoxicity exerted on osteogenesis by cigarette smoke. Further, this study also sought to evaluate the comparative embryotoxicity of harm-

reduction cigarette smoke in contrast with conventional cigarettes. The data revealed that sidestream (SS) smoke was more inhibitory to osteogenic differentiation than mainstream (MS) smoke in both tested brands. The detrimental effect of SS smoke from conventional Camel cigarettes was due to the general cytotoxicity of the smoke solution. In contrast, smoke extracts from harm-reduction Camel Blue cigarettes showed differentiation inhibition at sub-toxic concentrations in both the MS and the SS preparations. These data provide further evidence to suggest that *in utero* tobacco exposure could have detrimental effects on human bone development and that harm-reduction products may not be less harmful than conventional products.

Methods

Cell culture

Human ESCs (H9), acquired from WiCell (WiCell Research Institute), were maintained in mTeSR® medium (Stem Cell Technologies) and kept in the undifferentiated state at 37°C in a humid 5% CO_2 environment. Pluripotent colonies were passaged every 5 days by dissociating cells with Accutase® (Innovative Cell Technologies, Inc.) and a cell scraper. Cells were replated on Matrigel (BD Biosciences) coated culture plates. Human foreskin fibroblasts (hFF) were a kind gift of Dr. Derrick Rancourt (University of Calgary) and were maintained in high glucose L-glutamine Dulbecco's modified Eagle's medium (DMEM, Corning) with 10% fetal bovine serum (FBS, Atlanta Biologicals), 1% non-essential amino acids (NEAA, Gibco), and 0.5% penicillin/streptomycin (10,000 units/10,000 units, Gibco).

Osteogenic differentiation

At confluency, pluripotent colonies were induced to undergo osteogenesis with control differentiation medium consisting of Dulbecco's modified Eagle's medium (DMEM; Gibco) containing 15% FBS (Atlanta Biologicals), 1% non-essential amino acids (NEAA; Gibco), 1:200 penicillin/streptomycin (Gibco), and 0.1 mM β-mercaptoethanol (Sigma-Aldrich) for 5 days as described [18]. Starting from the fifth day of culture, control differentiation medium was supplemented for the remaining differentiation duration with osteogenic factors: 0.1 mM β-glycerophosphate (βGP; Sigma-Aldrich), 50 μg/ml ascorbic acid (AA; Sigma-Aldrich), and $1.2x10^{-7}$ M $1,25(OH)_2$ Vitamin D_3 (VD_3; Calbiochem).

Production of smoke solution

Commercially available conventional and harm-reduction Camel cigarettes were purchased from a local retailer and used to make mainstream (MS) and sidestream (SS) smoke solutions with a method described previously in detail [19-20]. Smoke solutions were generated using a University of Kentucky smoking machine that took a 2.2 second puff of MS every minute. MS smoke solution was generated by pulling 30 puffs of MS smoke through 10 ml of DMEM culture medium. During MS smoke production, SS smoke solution was produced by collecting the smoke that burned off the end of the cigarette and pulling it through 10 ml of DMEM. SS smoke was collected continuously, while MS smoke was collected during each puff. Both MS and SS solutions were made at concentrations of 3 puff equivalents (PE). Immediately after preparation, smoke solutions were filtered through a 0.2 μm Acrodisc® PSF Syringe Filter (Pall Corporation, Port Washington, NY),

aliquoted into sterile Eppendorf tubes, and stored in a -80°C freezer until used. Desired PEs were acquired through serial dilutions, and experiments were performed using either MS or SS at indicated concentrations alongside an untreated control. Immediately after preparation, smoke solutions were filtered through a 0.2 μm Acrodisc® PSF Syringe Filter (Pall Corporation, Port Washington, NY), aliquoted into sterile Eppendorf tubes, and stored in a -80°C freezer until used. Desired PEs were acquired through serial dilutions, and experiments were performed using either MS or SS at indicated concentrations alongside an untreated control.

Osteogenic differentiation of hESCs was induced as described above, and cultures were treated with smoke solution throughout the 20-day differentiation protocol. Smoke solutions were replenished with each media change.

Antioxidant and caspase inhibitor treatment

To counteract tobacco-induced oxidative stress, three antioxidants were used concomitantly with tobacco treatment during days 5-7 of differentiation: ascorbic acid (AA; Sigma-Aldrich) [10 μM], dl-α-tocopherol acetate (vitamin E; Supelco, Sigma-Aldrich) [10 μM], and glutathione reduced ethyl ester (GSHOEt; Sigma-Aldrich) [500 μM]. The antioxidant medium was replaced with each media change.

To explore the involvement of caspases 4 and 9 in tobacco-related inhibition of osteogenic differentiation, tobacco-treated cultures were simultaneously dosed with caspase 4 inhibitor (4i; Promokine) [3 μM] or caspase 9 inhibitor (9i; R&D Systems) [3 μM] during days 5-7 of differentiation. Inhibitor-supplemented medium was replaced with

every media change.

Cell viability assay

Osteoblast and hFF survival in response to smoke solutions was determined by 3-[4,5-dimethylthiazol-2-yl]-2,5-diphenylterazolium bromide (MTT) assay. Briefly, cells were incubated with MTT (120 mg/ml) at 37°C for 3 h. After the supernatant was removed, 0.04 mol/l HCl in isopropanol was added to each well, and the optical density of the solution was read at 595 nm in an iMark™ microplate reader (Bio-Rad). As the generation of the blue product is proportional to the dehydrogenase activity, a decrease in the absorbance at 595 nm provided a direct measurement of the number of viable cells [17, 21-25].

Calcium assay

For quantification of calcium in the extracellular matrix, cells were harvested in modified radioimmunoprecipitation (RIPA) buffer [26]. Calcium deposition was determined based on calcium ions (Ca^{2+}) reacting with Arsenazo III (Genzyme) to form a purple Ca-Arsenazo III complex, which was measured at 655 nm. The concentration of total calcium in the sample was calculated based on a $CaCl_2$ standard [26]. Calcium content was normalized to the total protein content of the sample using the Lowry method [26].

Superoxide anion detection

Generation of superoxide anion was determined using a Lumimax Superoxide

Anion Detection Kit (Agilent Technologies). H9 cells were trypsinized, washed with phosphate-buffered saline (PBS), and resuspended in fresh medium to incubate for 30 minutes at 37°C. A total of 5×10^5 cells was incubated in superoxide anion assay medium including 0.1 mM luminol solution and 125 μM enhancer at room temperature for 30 min. The chemiluminescent light emissions of superoxide anion were measured with a luminometer (Lucetta™).

MitoSOX assay

Superoxide formation specially produced by mitochondria was assessed using the commercially available MitoSOX Red Mitochondrial Superoxide Indicator dye (ThermoFisher M36008). Adherent cells were washed with PBS and incubated with 2.5 μM MitoSOX in PBS for 10 min in the dark. Cells were then immediately imaged on a Nikon Ti fluorescent microscope. MitoSOX positive cells were identified using NIH ImageJ analysis software as outlined by Jensen (2013).

MitoTracker staining and mitochondrial analysis

Stress-related changes in mitochondrial morphology were visualized and quantified using the MitoTracker Deep Red FM fluorescent dye (ThermoFisher). H9 cells were trypsinized, washed with PBS, and resuspended in 200 nM MitoTracker dye prepared in fresh medium. Cells were incubated in darkness for 20 minutes at 25°C, washed with PBS, and fixed in 4% paraformaldehyde for 15 minutes at room temperature. Fixed cells were then washed three times with PBS and permeabilized with 0.1% Triton X- 100 in PBS for

15 minutes at room temperature. Cells were washed again and counterstained with 1 μg/ml 4', 6-diamidino-2-phenylindole (DAPI) in PBS for 30 minutes. Cells were washed three more times with PBS and resuspended in PBS supplemented with 2% FBS and 1 mM ethylenediaminetetraacetic acid (EDTA). Cell number was quantified and adjusted to a concentration of 5 x 10^5 cells/ml. Cells were spun onto pre-coated Shandon Single Cytoslides (ThermoFisher) using a Shandon Cytospin 3 (Shandon). For each treatment, a 100 μl volume of fixed and stained cellular suspensions was loaded into a cytospin funnel and centrifuged at 200 rpm for 5 minutes at low acceleration/deceleration settings. Slides were allowed to air-dry overnight before mounting with Fluoro-Gel (Electron Microscopy Sciences) imaging.

Z-stack images were taken for each slide using a Leica DMi8 fluorescent confocal microscope and max projected to flatten out each image. Resultant images were pre-processed in ImageJ (NIH) to prepare for mitochondrial morphological analysis. The MitoTracker Deep Red channel was first separated from the nuclear DAPI channel to allow for specific analysis of the mitochondria. Images were further processed using the Mitochondrial Network Analysis (MiNA) ImageJ plug-in to prepare images for evaluation of mitochondrial networks within individual cells. The MiNA plug-in is freely available at https://github.com/ScienceToolkit/MiNA. Using the default MiNA settings, images were subjected to a 2-pixel gaussian blur, rendering through the Enhance Local Contrast median filter, and a final processing through an unsharp mask tool to yield a "skeleton" or tracing of the mitochondrial networks in a given cell. Mitochondrial networks were evaluated using the MiNA analysis method as outlined by Valente et al., 2017. The mitochondrial

network length, number of branches, and area of mitochondrial footprint were measured from the skeletons to quantify tobacco-related changes to mitochondrial networks.

Caspase 3/7 stain

For determination of activated caspases 3/7, cells were incubated for 1 hour in a 1X caspase 3/7 reagent conjugated to carboxyfluorescein fluorochrome (Guava Technologies, US). The fluorescent signal was detected in cells where the reagent is covalently bound to the activated caspases, any unbound reagent was washed away with 1X apoptosis buffer provided by the manufacturer. Cells were observed and imaged on a Nikon Ti fluorescent microscope.

Apoptosis RT^2 profiler qPCR array

The correlation between tobacco exposure and apoptosis was examined based on expression changes of 84 apoptosis-associated genes using a Qiagen human Apoptosis RT^2 Profiler Array. For this, hESCs were differentiated into osteoblasts as described above with concomitant exposure to either solvent, non-effective, or effective doses (50% inhibition of calcification) of tobacco smoke solutions/extracts as determined from the concentration response curves shown in Fig. 4.1. RNA was isolated using the NucleoSpin RNA kit (Macherey-Nagel) and examined for RNA integrity using the Agilent 2100 Bioanalyzer. Only samples with an RNA integrity number of >8 were used for further processing. Five hundred nanograms of RNA were input into a cDNA reaction as described before [18]. qPCR reactions were set up using iQ SYBR Green Supermix (Bio-Rad) and 12.5 ng of

cDNA per array well and cycled in a Bio-Rad iQ5 qPCR machine. Data were uploaded to the Qiagen Data Analysis Center at www.SABiosciences.com/pcrarraydataanalysis.php for analysis.

Real-time quantitative PCR (qPCR)

Changes in cellular stress-related gene expression related to DNA damage, growth arrest, and apoptosis were assessed using real-time quantitative PCR (qPCR) measurements of *GADD45α*, *GADD45β*, and *GADD45γ* isoform expression. RNA was extracted from cells and subsequently purified using the NucleoSpin RNA kit (Macherey-Nagel) protocol. Isolated RNA was quantified using a NanoDrop® 1000 spectrophotometer (Thermo Scientific) at 260nm. Synthesis of cDNA was performed using 25ng of total RNA as a template and a cDNA mastermix as described before [18]. Quantitative PCR analysis utilized resultant 25ng cDNA transcripts and iQ SYBR Green Supermix (Bio-Rad) on the CFX Connect thermocycler (Bio-Rad). Reactions were programmed for 5 minutes of initial denaturing at 94°C, followed by 40 cycles of denaturing at 94°C for 45 seconds and annealing at 60°C for 45 seconds. The ΔΔCT method [29] was used to calculate n-fold expression in target gene expression by normalizing target C_T values to their respective *GAPDH* expression values. Primer sequences for human *GADD45α* were 5'-TTACTCAAGCAGTTACTCCCTACA-3' and 5'-CCTTCTTCATTTTCACCTCTTTCCA-3', for *GADD45β* they were 5'-ATGACATCGCCCTGCAAATC-3' and 5'-GTGACCAGGAGACAATGCAG-3', and for *GADD45γ* they were 5'-CGCGCTGCAGATCCATTTTA-3' and 5'-

GGGGTTCGAAATGAGGATGC-3'. Primer sequences for human *GAPDH* were 5'-GAGTCAACGGATTTGGTCGT-3' and 5'-TTGATTTTGGAGGGATCTCG-3'

Comet assay and analysis

Comet assay slides were prepared prior to cell collection by coating clean frosted microscope slides (Fisher Scientific) with 1% normal melting agarose (NMA, Sigma) in PBS. A volume of 75 µl of melted NMA was pipetted directly to the surface of each slide and immediately covered with a coverslip. The NMA layer was allowed to solidify at 25°C for 10 minutes prior to coverslip removal. Slides were stored at -20°C until use. Cells were trypsinized, washed with PBS, counted and resuspended in PBS supplemented with 2% FBS. A cell suspension of 200,000 cells per ml in 0.1% low melting point agarose (LMA, Fisher Bioreagents) was prepared immediately prior to distributing cells onto slides for the assay. NMA-coated slides were allowed to come to room temperature before coating with the LMA-cell mixture. The cell-LMA solution was pipetted directly onto each slide in a volume of 75 µL and immediately covered with a coverslip. The LMA-cell layer was allowed to solidify at 25°C for 10 minutes prior to coverslip removal. An additional 5-minute solidification period at 25°C was observed after the coverslip was removed. The slides were then placed in a slide tray and the cells were lysed in comet assay lysis buffer (1.2 M NaCl, 100 mM Na_2EDTA, 0.1% sodium lauryl sarcosinate, 0.26 M NaOH, pH >13) for 1 hour at 25°C. Next, lysis buffer was aspirated off the slides and replaced with electrophoresis solution (0.03 M NaOH, 2 mM Na_2EDTA, pH~12.3) for 20 min at 4°C. Slides were transferred to an electrophoresis box and subjected to electrophoresis for 20

min at 1V/cm and 4°C. Slides were rinsed in ddH_2O for 1 minute, then immersed in 70% ethanol for 5 minutes. Slides were air-dried overnight and stained with 1 μg/ml 4', 6-diamidino-2-phenylindole (DAPI) in PBS for 30 minutes. Slides were rinsed with PBS and air dried prior to imaging on a Nikon Ti Eclipse fluorescent microscope. Three slides per treatment group were prepared and scored visually. Fifty cells per slide were scored. Fluorouracil (5-FU; Sigma-Aldrich) treated cells were evaluated as a positive control. To ensure accuracy of comet parameter measurements, DAPI signal intensity was subjected to a color threshold in ImageJ (commands used: *Image* > *Adjust* > *Color Threshold*). Comet score was determined by the presence of a comet tail as well as the relative length of the comet tail and % of DNA in the comet tail (if present). Comet tail length was manually quantified in ImageJ by measuring the distance spanned by comet tails (if present) from the edge of the cell nucleus to the furthest end of the comet tail.

Western blotting

Prior to lysing, cells were pretreated for 30 min with 1mM sodium orthovanadate to inhibit protein tyrosine phosphatases. Cells were then lysed with RIPA buffer (pH 7.4 150 mM NaCl, 2 mM EDTA, 50 mM Tris-HCl pH 7.4, 1% NP-40, 0.5% sodium deoxycholate, 0.1% sodium dodecyl sulfate (SDS), 1 mM sodium orthovanadate, 1 mM sodium fluoride, 1 mM phenylmethylsulfonyl fluoride (PMSF), and 1:100 Halt Protease Inhibitor Cocktail (ThermoFisher) to collect whole-cell protein lysates. A modified Lowry protein assay (Bio-Rad DC™ protein assay) was used to determine protein concentration in fresh lysates. For western blot analysis, equal amounts of protein per treatment group

were loaded into a 6%-10% SDS/polyacrylamide gel and separated by electrophoresis prior to electrophoretic transfer to a polyvinylidene difluoride (PDVF) membrane. Membranes were immediately blocked in 5% bovine serum albumin (BSA) in tris-buffered saline with tween 20 (TBS-T) for 30 minutes at room temperature on an orbital shaker. Membranes were incubated with one of the following primary antibodies for 2 hours at room temperature with shaking: mouse anti-caspase 8 (CST 9746S), mouse anti-caspase 9 (CST 9508S), rabbit anti-phospho-caspase 9 (Tyr153) (abcam ab79202), rabbit anti-c-Abl (CST 2862S), rabbit anti-phospho-c-Abl (Tyr245) (CST 2868S), rabbit anti-phospho-c-Abl (Tyr412) (CST 247C7S), rabbit anti-caspase 4 (ab22687) mouse anti-actin (CST 3700S). Membranes were subsequently incubated for 1 hour at room temperature with horseradish peroxidase-conjugated anti-rabbit (CST 7074S) or anti-mouse (CST 7076S) secondary antibody was used to detect antigens of interest. Bands were visualized using chemiluminescence substrate (SuperSignal West Pico PLUS Chemiluminescent Substrate, ThermoFisher) and the Bio-Rad ChemiDoc MP System imager.

Live/Dead assay

Healthy live and apoptotic cell populations were quantified in different treatment groups using the LIVE/DEAD Viability/Cytotoxicity Kit (ThermoFisher L3224). H9 cells were trypsinized, washed with PBS, and resuspended in fresh medium containing 0.1 μM calcein AM and 8 μM ethidium homodimer-1 (EthD-1). Cells were incubated away from light for 20 minutes at 25°C, washed with PBS, and centrifuge-strained to encourage a single-cell suspension (Fisher Scientific, 08-771-23). Cells were resuspended in ice-cold

PBS supplemented with 2% FBS and immediately analyzed on a FACSCalibur Flow Cytometer (BD Biosciences). Fluorescence was detected at excitation/emission at λ = 494/517 nm and 517/617 nm. Cytometer gating was set using unstained untreated samples and adjusting forward scatter and side-scatter light. For each sample, 10,000 events were recorded.

Mitochondrial membrane potential

Changes in mitochondrial membrane potential were assessed using the commercially available JC-1 Dye (ThermoFisher T3168). Cells were trypsinized, washed with PBS, and resuspended in fresh medium containing 5 μM JC-1. Cells were incubated for 20 minutes at 25°C, washed with PBS, and centrifuge-strained to break up cells into a single-cell suspension (Fisher Scientific, 08-771-23). Cells were subsequently resuspended in ice-cold PBS supplemented with 2% FBS and immediately analyzed on a FACSCalibur Flow Cytometer (BD Biosciences). Fluorescence was detected at excitation/emission at λ = 488⁄530 nm and 488⁄585 nm. Cytometer gating was set using unstained untreated samples and adjusting forward scatter and side-scatter light. For each sample, 10,000 events were recorded.

ATP:AMP assays

ATP and AMP levels were quantified via an ATP Determination Kit (ThermoFisher A22066) and an AMP ELISA (Kamiya Biomedical Company KT-52769), respectively. For both assessments, cells were washed with PBS, trypsinized, and resuspended in PBS.

In the ATP assay, a cell suspension for each treatment group was counted and readjusted to a final concentration of 12.5×10^6 cells/ml. For each reading, 10 µl of ATP standard or sample was combined with 90 µl of the ATP reaction solution provided by the ATP Determination Kit immediately before to recording the reaction luminescence output using a Lucetta luminometer (Lonza). Relative ng amounts of ATP in each treatment group were determined from an ATP standard curve. For AMP determination, each cell suspension was adjusted to a final concentration of 1.25×10^6 cells/ml. PBS-suspended cells were prepared for ELISA analysis by freeze-thawing three times with gentle mixing between freezing followed by centrifugation at 1,000 x g for 15 minutes at 4°C. Cell lysates were assessed according to the manufacturer's ELISA protocol and final optical density was measured at 450 nm using an iMark microplate reader (Bio-Rad). Relative ng amounts of AMP were determined using a standard curve constructed from an AMP standard.

Statistical analysis

The lowest concentrations at which calcification or cell viability dropped below the untreated control were identified with one-way analysis of variance (ANOVA) followed by a paired student's t-test. Half-maximal inhibitory doses of cytotoxicity (IC_{50}) and differentiation (ID_{50}) were taken from concentration-response curves and used to classify chemical embryotoxicity via an embryotoxicity biostatistical prediction model [30]. Other assays were also assessed with one-way analysis of variance (ANOVA) followed by a paired student's t-test (GraphPad QuickCalcs). For all conducted tests, *P*-values below 0.05 were considered significant.

Results

The potency of mainstream (MS) and sidesteam (SS) smoke extracts of conventional and harm-reduction Camel cigarettes to induce differentiation defects in hESCs undergoing differentiation into osteoblasts was compared to assess the hazardous effects of smoking on developing bone tissue.

MS smoke from conventional Camel cigarettes is neither cytotoxic nor teratogenic to differentiating osteogenic cultures

First, MS smoke of conventional Camel cigarettes was tested to determine its effects on cell survival as measured by an MTT assay after 20 days of culture [25]. At that time these cultures express marker genes and proteins of osteoblasts [18]. No adverse effects on mitochondrial dehydrogenase activity were found (Fig. 4.1A). As osteoblasts emerge from hESC cultures, they begin to form nodules made of calcified extracellular matrix [18]. This process is unique to bone forming cells. This functional characteristic of bone was assayed via the quantification of calcium ions deposited into the matrix [25]. Conventional MS Camel tobacco smoke solution did not affect calcification, as assessed using Arsenazo III, a reagent for measuring calcium contents in samples [23, 26] (Fig. 4.1A). These results suggest that MS Camel smoke extract has no observable effects on viability or functional calcification of osteogenic cultures at any of the concentrations tested. The half-maximal concentrations for cytotoxicity (IC_{50} MTT hESCs and IC_{50} MTT hFF) and differentiation inhibition (ID_{50} Calcium hESCs) obtained from the concentration-response curves were then evaluated in a biostatistical model (Fig 4.1E) [30] which

revealed that MS Camel smoke extract was non-embryotoxic.

SS from conventional Camel cigarettes demonstrates harmful effects on human osteoblast differentiation

SS, the major component of secondhand smoke, was next investigated using the previously described method and concentrations. In contrast to the MS smoke solution, Camel SS smoke solution caused excessive cell death and a measurable lack of calcification at 0.3 PE (Fig. 4.1B). The biostatistical model classified Camel SS smoke extract as strongly embryotoxic (Fig. 4.1E).

Harm-reduced Camel Blue cigarette smoke extract is harmful to differentiating osteoblasts at subtoxic concentrations

To evaluate whether cigarettes that contain fewer carcinogens also cause less harm in differentiating hESCs, smoke extracts from Camel Blue cigarettes were screened using five concentrations. While cell viability was not inhibited in the tested range, calcification of the hESC-derived osteoblasts was severely inhibited at 1PE (Fig. 4.1C). The biostatistical model categorized MS Camel Blue smoke as weakly embryotoxic (Fig. 4.1E).

As with the conventional Camel smoke extract, the SS smoke from Camel Blue cigarettes was more detrimental to differentiating osteoblasts than the MS smoke. Camel Blue SS smoke ablated calcification starting at 0.1 PE, one dose lower than for the conventional Camel SS. Notably, the absence of calcification occurred in the absence of changes in cell viability up to a dose of 0.3 PE (Fig. 4.1D). While the biostatistical model

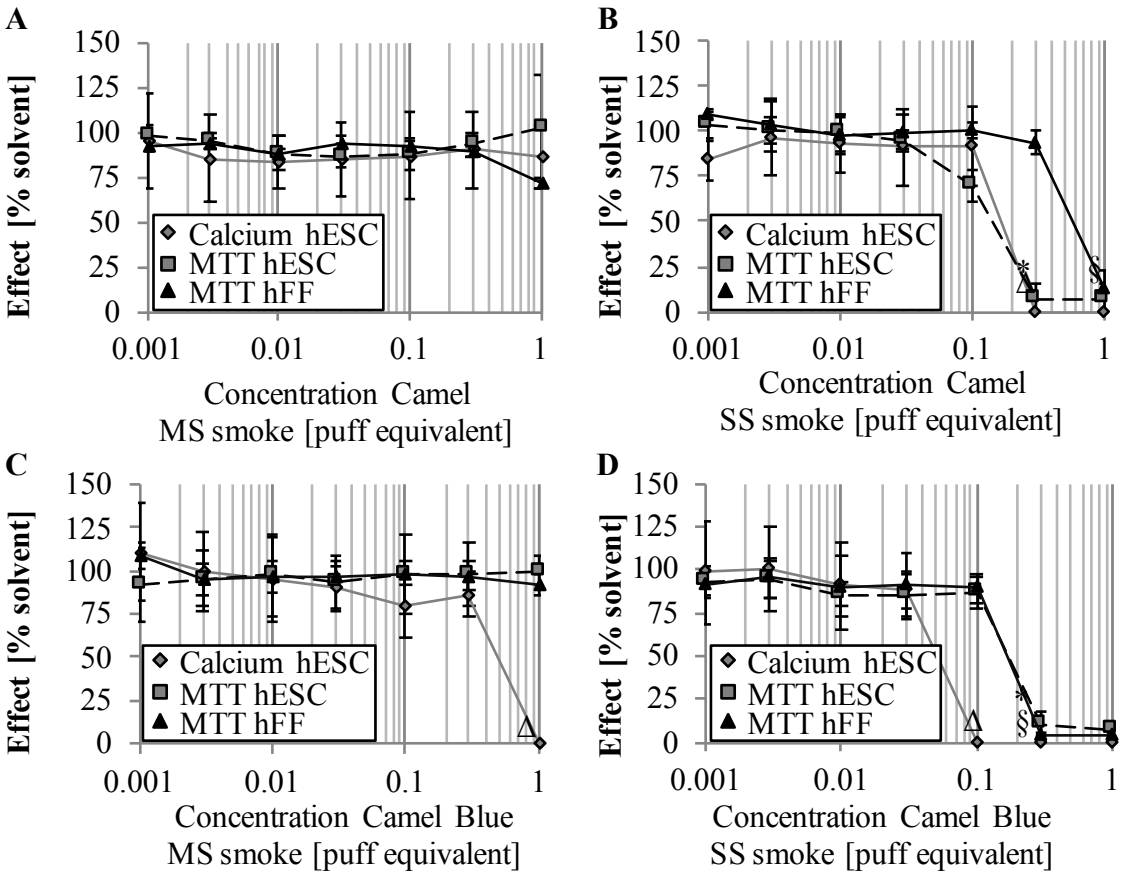

E

	IC50 hFF	IC50 H9	ID50 H9	class	categorization
Camel MS	>1	>1	>1	I	Non-embryotoxic
Camel Blue MS	>1	>1	0.51 ± 0.08	II	Weakly embryotoxic
Camel SS	0.58 ± 0.08	0.14 ± 0.03	0.17 ± 0.04	III	Strongly embryotoxic
Camel Blue SS	0.18 ± 0.03	0.16 ± 0.05	0.05 ± 0.01	III	Strongly embryotoxic

Figure 4.1. SS smoke inhibited osteogenesis and cell viability. Human ESCs were treated with different concentrations of MS and SS smoke solution concurrently with osteogenesis. Cultures were assessed for on calcium deposition and cell viability using Arsenazo III and MTT assay, respectively. (A) Camel MS smoke solution. (B) Camel SS smoke solution. (C) Camel Blue MS smoke solution. (D) Camel Blue SS smoke solution. Each graphed point is the average of three independent experiments ± standard deviation. $^{\Delta}P<0.05$ represents the lowest concentration that is significantly below the untreated control in the calcium assay, as determined by one-way ANOVA. $^{*}P<0.05$ represents the lowest concentration significantly below the untreated control in the hESC MTT assay as determined by one-way ANOVA. $^{\S}P<0.05$ represents the lowest concentration that is significantly below the untreated control in the hFF MTT assay as determined by one-way ANOVA. (E) List of IC_{50} and ID_{50} values determined from concentration-response curves for all tobacco products grouped by mainstream and sidestream smoke and embryotoxicity classifications as calculated according to Genschow et al. (2000). hFF, human foreskin fibroblast; hESC, human embryonic stem cell; MS, mainstream; MTT, mitochondrial dehydrogenase activity assay; SS, sidestream.

also categorized Camel Blue SS smoke extract as strongly embryotoxic (Fig. 1E), it is of note that the embryotoxic effect was caused at subtoxic concentrations suggesting that this particular harm-reduction product inhibited differentiation producing developmentally toxic effects independent of cytotoxicity.

Embryotoxicity of SS smoke is associated with oxidative stress

Cytotoxicity in cells and tissues is commonly ascribed to oxidative stress, which arises as a consequence of chemical or environmental insult. Classically, oxidative stress is defined as the "imbalance of reducing and oxidizing equivalents where the latter predominates" [31]. In such cases, increased production of reactive oxygen species (ROS) contributes to a loss of tissue function [32-35]. Indeed, different human teratogens have recently been described to cause oxidative stress [36-38].

Due to this existing relationship between developmental inhibition and oxidative stress, we investigated the level of superoxide anion ($\bullet O2^-$) generated upon exposure to Camel and Camel Blue smoke extracts. An effective dose, determined from the concentration-response curve as the concentration that reduced calcification to 50%, and a non-effective dose (no effect) were compared to non-treated control cultures. MS Camel and MS Camel Blue showed no statistical difference in $\bullet O2^-$ content, while the Camel SS revealed a 2.4-fold increase in the effective dose over the non-effective dose (Fig. 4.2A). In contrast, the Camel Blue SS effective dose evoked elevated $\bullet O2^-$ content in the range between 1.6- and 1.9-fold. Further evaluation of the potential source of the $\bullet O2^-$ uncovered elevated mitochondrial oxidative stress in the Camel SS, but not in Camel Blue (Fig. 4.2B).

In an effort to link oxidative stress-mediated embryotoxicity to altered gene regulation, we next performed a Qiagen RT^2 Apoptosis Profiler qPCR array (Fig. 4.2C). A clustergram generated from all de-regulated genes across all treatment groups indicated a close relationship between the solvent controls, all non-effective doses, and the effective dose of Camel Blue SS smoke solution suggesting that there was very little gene de-regulation observed (Appendix Fig. 1.4.1). In contrast, global apoptotic gene regulation was significantly different in the effective dose of Camel SS. Specifically—and as expected based on the elevated $\bullet O2^-$ levels measured in the effective doses—genes involved in ROS signaling were increasingly expressed in the effective dose of Camel SS and to a lesser extent in the effective dose of Camel Blue SS. These same genes were mainly unaltered in the non-effective doses (Fig. 4.2D, Appendix Fig. 1.4.2). Calcification in both effective doses was rescued by the addition of antioxidants during tobacco treatment, causally relating oxidative stress to the osteogenic defect (Fig. 4.2E).

Conventional Camel, but not the harm-reduction Camel Blue smoke extract elicits apoptotic gene expression and activates executioner caspases

The high $\bullet O2^-$ levels found in Camel SS effective doses cultures occurred in the presence of up-regulated caspase 8 mRNA (Fig. 4.3A) as well as higher levels of total and cleaved caspase 8 protein expression (Fig. 4.3B). Although caspase 9 mRNA was also elevated in Camel SS effective doses, Western blot could not detect increased total or cleaved Caspase 9 (Fig. 4.3B). However, when we probed with an antibody against the caspase 9 specifically phosphorylated at Y153, a well-established activation mark [39], it

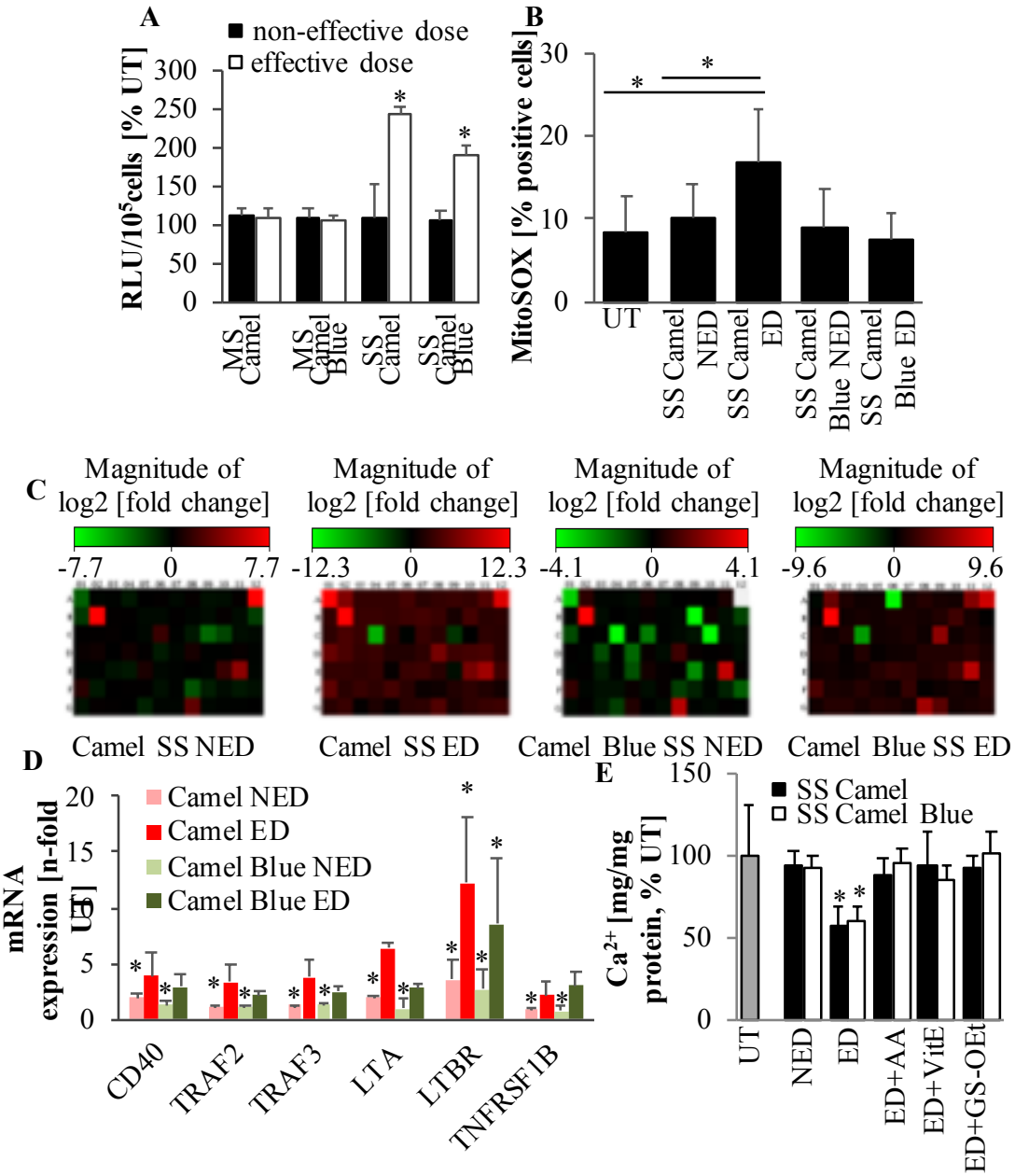
A
non-effective dose
effective dose
RLU/10^5cells [% UT]
300
250
200
150
100
50
0
MS Camel
MS Camel Blue
SS Camel
SS Camel Blue
B
MitoSOX [% positive cells]
30
20
10
0
UT
SS Camel NED
SS Camel ED
SS Camel Blue NED
SS Camel Blue ED
C
Magnitude of log2 [fold change]
-7.7 0 7.7
-12.3 0 12.3
-4.1 0 4.1
-9.6 0 9.6
Camel SS NED
Camel SS ED
Camel Blue SS NED
Camel Blue SS ED
D
mRNA expression [n-fold UT]
20
15
10
5
0
Camel NED
Camel ED
Camel Blue NED
Camel Blue ED
CD40
TRAF2
TRAF3
LTA
LTBR
TNFRSF1B
E
Ca2+ [mg/mg protein, % UT]
150
100
50
0
SS Camel
SS Camel Blue
UT
NED
ED
ED+AA
ED+VitE
ED+GS-OEt

Figure. 4.2. Differentiation inhibition caused by harm-reduction tobacco exposure occurred through generation of intermediate levels of reactive oxygen species. (A) Superoxide anion content measured upon reaction of the cells with luminol and charted as percent of the untreated cultures; n=3±SD. (B) Cells were exposed for seven days, incubated with MitoSOX, photographed and positive cells counted. Only Camel exposure elicited a significant increase specifically in mitochondrial oxidative stress. (C) Heat map of apoptotic genes de-regulated in tobacco exposed hESCs as measured with the RT^2 qPCR array for apoptosis (D) Apoptosis qPCR array revealed upregulation of genes associated with ROS signaling. E) Calcium deposit was quantified from cultures exposed for 20 days with and without concomitant addition of antioxidants. Effective doses of tobacco smoke solutions and extracts reduced calcification, which was rescued with antioxidant treatment; n=3±SD. *P<0.05, one-way ANOVA followed by student's t-test versus untreated cultures. AA, ascorbic acid; ED, effective dose; GSHOEt, glutathione reduced ethyl ester; MS, mainstream; NED, non-effective dose; RLU, relative light unit; SS, sidestream; UT, untreated; VitE, Vitamin E.

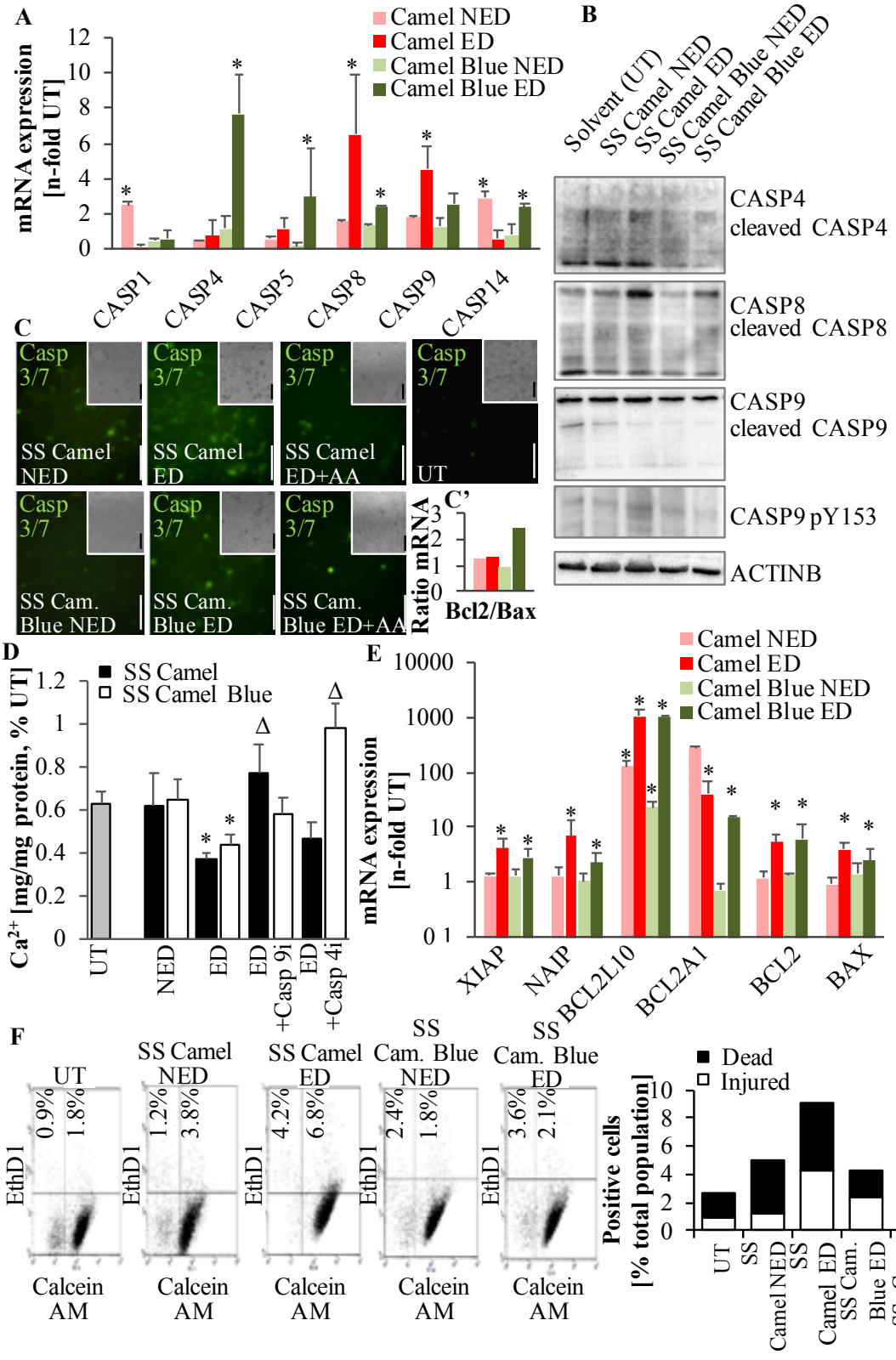
A
mRNA expression [n-fold UT]
Camel NED
Camel ED
Camel Blue NED
Camel Blue ED
CASP1
CASP4
CASP5
CASP8
CASP9
CASP14
B
Solvent (UT)
SS Camel NED
SS Camel ED
SS Camel Blue NED
SS Camel Blue ED
CASP4
cleaved CASP4
CASP8
cleaved CASP8
CASP9
cleaved CASP9
CASP9 pY153
ACTINB
C
Casp 3/7
SS Camel NED
SS Camel ED
SS Camel ED+AA
UT
SS Cam. Blue NED
SS Cam. Blue ED
SS Cam. Blue ED+AA
C'
Ratio mRNA
Bcl2/Bax
D
SS Camel
SS Camel Blue
Ca2+ [mg/mg protein, % UT]
UT
NED
ED
ED +Casp 9i
ED +Casp 4i
E
Camel NED
Camel ED
Camel Blue NED
Camel Blue ED
mRNA expression [n-fold UT]
XIAP
NAIP
BCL2L10
BCL2A1
BCL2
BAX
F
UT
SS Camel NED
SS Camel ED
SS Cam. Blue NED
SS Cam. Blue ED
EthD1
Calcein AM
0.9%
1.8%
1.2%
3.8%
4.2%
6.8%
2.4%
1.8%
3.6%
2.1%
Dead
Injured
Positive cells [% total population]
UT
SS Camel NED
SS Camel ED
SS Cam. Blue ED
SS Cam. Blue ED

Figure. 4.3. Camel Blue SS elicits a weaker apoptosis response than Camel SS. (A) RT^2 qPCR array for apoptosis identified distinct expression patterns of various caspase isoforms between Camel and Camel Blue SS smoke exposed cells. n=3±SD. **P*<0.05, One-Way ANOVA versus untreated cultures. (B) Western blots revealed the differential activation of caspases associated with extrinsic and intrinsic apoptotic pathways. (C) Accordingly, the executioner caspases 3/7 were highly activated in cells exposed to Camel, but only mildly when exposed to Camel Blue. Antioxidant treatment inhibited this activation. Insets show brightfield images of the same field of view. Bar = 100 μM. (C') The ratio of Bcl2 to Bax mRNA expression suggested an antiapoptotic response in Camel Blue SS cultures. (D) Inhibition of these caspases rescues calcification in cells treated with effective doses of tobacco products; n=5±SD. **P*<0.05, One-Way ANOVA versus untreated cultures. (E) Some proapoptotic genes were found upregulated in both Camel and Camel Blue SS cultures. n=5±SD. **P*<0.05, One-Way ANOVA versus untreated cultures. (F) LIVE/DEAD assay reveals cell death in cells exposed to conventional smoke extracts only. AA, ascorbic acid; ED, effective dose; NED, non-effective dose; SS, sidestream; UT, untreated.

was higher in Camel SS effective doses than in any other treatment group. Concomitantly, downstream executioner caspases 3 and 7 were found to be highly activated in Camel SS (Fig. 4.3C).

In contrast, the intermediate intracellular $\bullet O2^-$ levels released upon exposure to Camel Blue SS were found to occur in the absence of apoptosis. Caspase 8 activation was milder in Camel Blue SS than in Camel SS (Fig. 4.3A, B) and caspase 9 was only slightly elevated at the mRNA level (Fig. 4.3A). This lower activation of upstream caspase activation may have been responsible for marginal activation signals observed in the caspase3/7 stain (Fig. 4.3C). Conversely, caspase 4 showed higher mRNA expression in Camel Blue SS (Fig. 4.3A, 4.3C). Inhibition of caspase 9 in Camel SS effective doses and inhibition of caspase 4 in Camel Blue SS effective doses rescued calcification, providing an isoform-specific causal link between caspase activation and differentiation inhibition for both Camel products.

Changes in mRNA expression were also observed for other apoptosis-related genes (Fig. 4.3D). Significant upregulation of mRNA expression for pro-apoptotic factors *XIAP* and *BAX* were observed in both effective doses. Anti-apoptotic genes *BCL2L10*, *BCL2A1*, and *BCL2* were also upregulated in both Camel SS and Camel Blue SS effective doses. However, the anti-apoptotic genes *BCL2L10* and *BCL2A1* were highest in the SS Camel non-effective dose—potentially explaining the survival noted in those cultures. Similarly, despite the activation of multiple apoptotic genes, the ratio between *BCL2* and *BAX* was most beneficial for survival in the effect dose of SS Camel Blue (Fig. 4.3C').

While Camel SS and Camel Blue SS both cause cellular injury and pro-apoptotic

responses at the mRNA level, the type of molecular responses that may drive the cellular injury inflicted may also drive the differential molecular responses observed in cells treated with either tobacco extract. In line with this notion, a Live/Dead assay revealed Camel SS effective dose cultures to possess the highest percentage of dead cells but a similar number of injured cells as the Camel Blue SS exposed cultures (Fig. 4.3F).

Conventional Camel, but not the harm-reduction Camel Blue smoke extracts elicit a DNA damage response

The noted severity of apoptosis in the Camel SS effective dose may not only be founded in the different expression levels of pro- and anti-apoptotic genes, but could also be caused by an upregulation in genes associated with genotoxic response. Indeed, the cell cycle arrest and DNA damage genes *GADD45α, GADD45β, and GADD45γ* mRNA were significantly upregulated exclusively in cells treated with a Camel SS effective dose (Fig. 4.4A). Furthermore, mRNA for the DNA-damage response kinase *ABL1* was only upregulated in the Camel SS effective dose and was notably the highest upregulated gene observed (Fig. 4.4B). Western blot analysis confirmed greater ABL1 phosphorylation at Y412 and Y245 (Fig. 4.4C), residues that contribute to full kinase activation in the event of DNA damage and subsequent DNA repair response [40, 41]. Additional mRNA markers related to cellular stress, including *BIRC5*, *CIDEA, CIDEB*, were also examined. Rarely expressed in adult tissues, *BIRC5* (also known as survivin) is reported to control apoptosis patterns in early embryos and is implicated in normal tissue development [42, 43]. *BIRC5* mRNA levels were conspicuously upregulated for Camel SS and Camel Blue SS effective

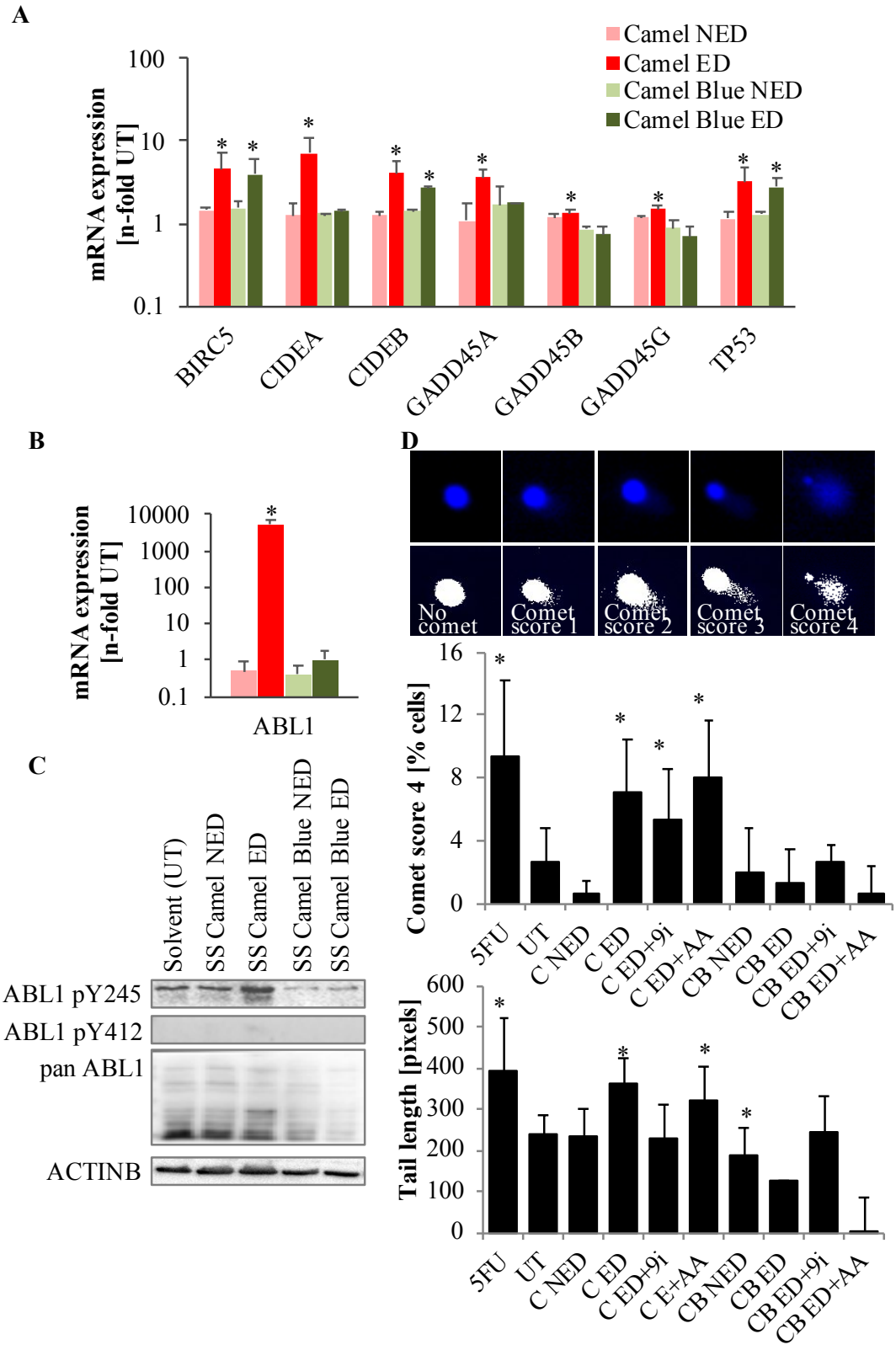
A
Camel NED
Camel ED
Camel Blue NED
Camel Blue ED
mRNA expression [n-fold UT]
100
10
1
0.1
BIRC5
CIDEA
CIDEB
GADD45A
GADD45B
GADD45G
TP53
B
mRNA expression [n-fold UT]
10000
1000
100
10
1
0.1
ABL1
C
Solvent (UT)
SS Camel NED
SS Camel ED
SS Camel Blue NED
SS Camel Blue ED
ABL1 pY245
ABL1 pY412
pan ABL1
ACTINB
D
No comet
Comet score 1
Comet score 2
Comet score 3
Comet score 4
Comet score 4 [% cells]
16
12
8
4
0
5FU
UT
C NED
C ED
C ED+9i
C ED+AA
CB NED
CB ED
CB ED+9i
CB ED+AA
Tail length [pixels]
600
500
400
300
200
100
0
5FU
UT
C NED
C ED
C ED+9i
C E+AA
CB NED
CB ED
CB ED+9i
CB ED+AA

Figure. 4.4. Reduced viability in hESCs exposed to conventional Camel extract is due to DNA damage. (A) RT^2 qPCR array for apoptosis found upregulation of genes associated with DNA damage response in Camel SS smoke exposed cells. n=3±SD. **P*<0.05, One-Way ANOVA versus untreated cultures. (B) *ABL1* mRNA expression was upregulated in the Camel SS effective dose. n=3±SD. **P*<0.05, One-Way ANOVA versus untreated cultures. (C) Western blots confirmed ABL1 activation in Camel SS effective doses at the protein level. (D) Comet assays confirm DNA damage in response to Camel exposure, which was absent in Camel Blue exposed cells and cells treated with antioxidant. n=3±SD. **P*<0.05, One-way ANOVA followed by paired student's t-test versus untreated cultures. AA, ascorbic acid; 9i, caspase 9 inhibitor; ED, effective dose; NED, non-effective dose; SS, sidestream; UT, untreated.

doses, suggesting adverse molecular misregulation by both treatments. *CIDEB* mRNA was upregulated in both Camel SS and Camel Blue SS effective doses while *CIDEA* mRNA was only upregulated in Camel SS treated cultures.

Milder intracellular $\bullet O2^-$ levels and lack of apoptotic response in Camel Blue SS effective dose treated cultures corresponded with low or non-significant changes in *GADD45α, GADD45β, GADD45γ* despite upregulation of their upstream regulator *TP53* (Fig. 4.4A). *ABL1* mRNA expression levels were also unchanged in Camel Blue SS treated cells (Fig. 4.4B). Cells exposed to the Camel Blue SS effective dose also showed lower protein levels of ABL1 both overall and in its activated phospho forms (Fig. 4.4C), suggesting the absence of a DNA damage response.

Confirmatory assessment for DNA lesions was then performed using a Comet Assay. Camel SS effective dose exposed cells demonstrated a significantly higher proportion of the severely damaged comet phenotype and larger DNA lesion tails (Fig. 4.4D). Ascorbic acid supplement of Camel SS cultures did not reduce comet severity or tail length, suggesting that antioxidant treatment was not efficient enough to prevent oxidative DNA damage during the exposure period. Supplementation with caspase 9 inhibitor did not reduce comet severity either. Given that caspase 9 activity can drive downstream induction of apoptosis-mediated DNA fragmentation, this outcome suggests that the DNA lesions detected by the Comet Assay are predominantly from DNA damage events that occur following Camel SS ED exposure but upstream of caspase 9 activation.

Camel and Camel Blue damage mitochondria with differential severity

Observed differential mRNA upregulation patterns between Camel SS and Camel

Blue SS suggest that a precise molecular interplay may be responsible for ultimate phenotypic outcomes following exposure. As follows, this result also implies that while Camel SS and Camel Blue SS actively harm differentiating osteoblasts, both products act distinctly upon cellular regulatory mechanisms related to oxidative stress. As such, mitochondrial health was also investigated as mitochondrial dysfunction is a well-documented source of oxidative stress-related genotoxicity and disease states [45]. Mitochondrial dysregulation can lead to pathologically high levels of mitochondria-originating $\bullet O2^-$ that can go on to damage the cell. Because high levels of mitochondria-specific $\bullet O2^-$ were observed in Camel SS effective dose cultures, mitochondrial health and morphological parameters were additionally evaluated to determine if mitochondrial dysfunction was also a factor in tobacco-related inhibition of osteogenic differentiation.

Generated by proton pumps in mitochondrial Complexes I, III, and IV, mitochondrial membrane potential ($\Delta\Psi m$) is used to make ATP and regarded as the essential component of oxidative phosphorylation energy storage [46]. Healthy mitochondria are characterized by stably maintained $\Delta\Psi m$ and ATP levels, while $\Delta\Psi m$ depolarization or depleted ATP are associated with pathological impacts on mitochondrial health and function. Changes in $\Delta\Psi m$ were assessed using the JC-1 Dye, which accumulates in the mitochondria and fluoresces green in the event of $\Delta\Psi m$ depolarization [46]. Mitochondrial membrane potential was significantly reduced in the Camel SS effective doses which suggested a disturbance to mitochondrial function (Fig. 4.5B). In contrast, mitochondrial membrane potential in Camel Blue SS effective doses was unchanged from the untreated group. Further, comparative analysis of cellular AMP and

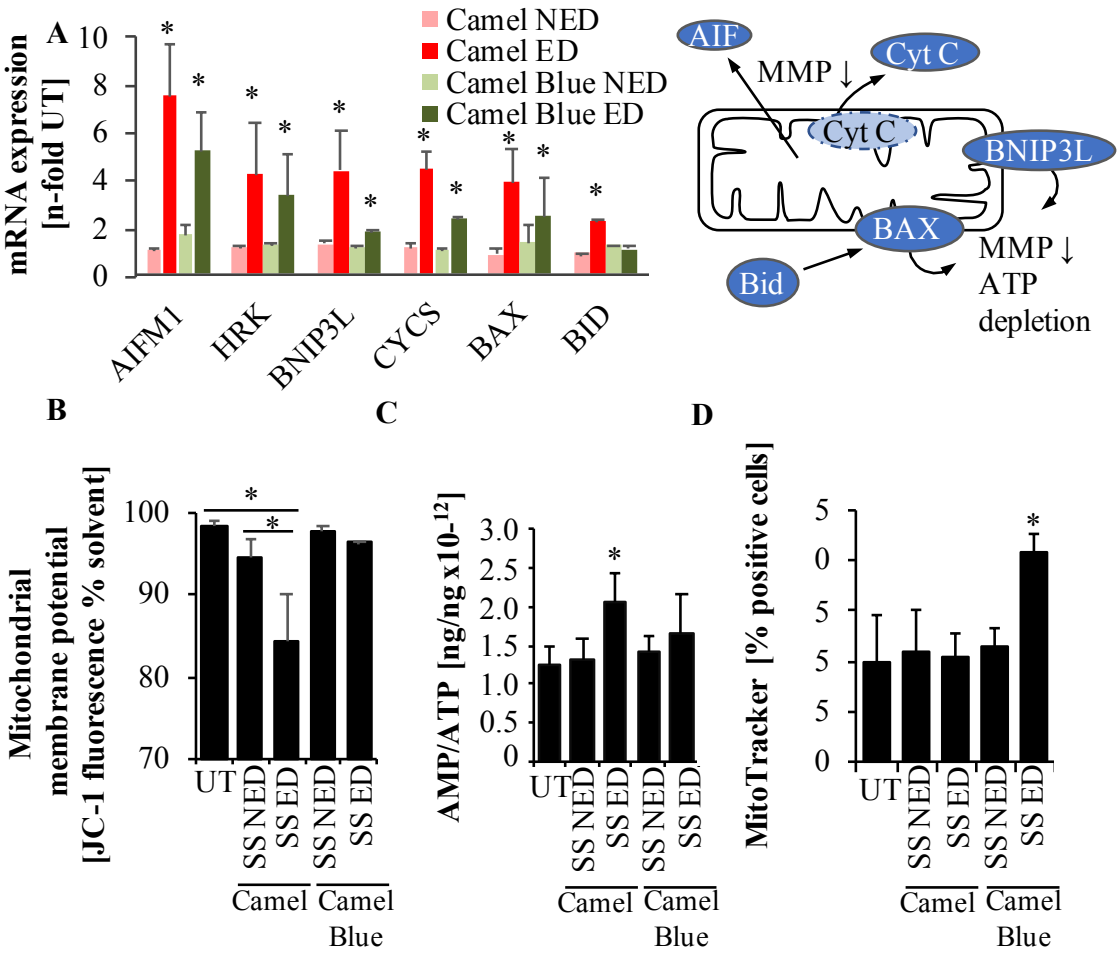

Figure. 4.5. Deterioration of mitochondrial health in exposed hESCs. (A) qPCR array analysis revealed upregulation of genes associated with integral mitochondrial apoptosis in both Camel SS and Camel Blue ED. **P*<0.05, One-way ANOVA followed by paired student's t-test versus untreated cultures. (B) Mitochondrial membrane potential measurements revealed a reduced membrane potential in Camel exposed cells as a sign for execution of the intrinsic apoptotic pathway. **P*<0.05, One-way ANOVA followed by paired student's t-test versus untreated or NED cultures (C) AMP-to-ATP ratio was increased in Camel SS ED, suggesting mitochondrial dysfunction. **P*<0.05, One-way ANOVA followed by paired student's t-test versus untreated cultures (D) Mitotracker dye analysis revealed increased mitochondrial signal in the Camel Blue SS effective dose. **P*<0.05, One-way ANOVA followed by paired student's t-test versus untreated cultures. ED, effective dose; NED, non-effective dose; SS, sidestream; UT, untreated.

ATP levels revealed the AMP/ATP ratio to be increased in the Camel SS effective dose. This outcome signifies a potential underproduction of ATP and further evidence of mitochondrial dysfunction in Camel SS treated cells (Fig. 4.5C).

To additionally explore molecular changes in connection with observed mitochondrial dysfunction, the expression of genes associated with mitochondrial intrinsic apoptosis was assessed. *BAX, BID,* and *BNIP3* and *CYCS* were upregulated by the Camel SS effective dose, while a mild upregulation was observed in the Camel Blue SS effective dose (Fig. 4.5A). Given that the corresponding first three proteins are involved in permeabilization of the mitochondrial outer membrane to prepare for cytochrome C release [47-50], it follows that mitochondrial membrane potential was depolarized in Camel SS cultures versus Camel Blue SS cultures. Together, these results suggest a strong mitochondrial-driven apoptotic response in Camel SS cultures. However, the similar *HRK* and *AIFM1* expression patterns between both Camel and Camel Blue SS indicate a potential issue with mitochondrial function in the Camel Blue SS as well.

Thus, to assess mitochondrial behavior was further a quantitative measurement of mitochondrial number following tobacco exposure was conducted. Under normal conditions, mitochondria perpetually fuse and divide to maintain a balanced mitochondrial population and overall morphology [51 52]. Mitochondrial number in Camel SS and Camel Blue SS effective doses did not deviate from mitochondrial numbers in the untreated. Cells treated with Camel Blue SS, conversely, featured a significant increase in total mitochondrial “bright spots” (Fig. 4.5D). These spots may be indicative of mitochondrial congregation as a result of increased fusion activity. Collectively, these outcomes infer that

Camel SS and Camel Blue SS elicited differential responses in mitochondrial behavior.

Next, altered mitochondrial networks were investigated by measuring mitochondrial network branch lengths, branch number per network, and mitochondrial footprint. Camel SS showed reduced network interconnection (Fig. 6A), as well as a significant increase in mitochondrial branch length, and decrease in overall mitochondrial footprint (Fig. 4.6B). Concurrent treatment of Camel SS effective doses with an inhibitor to caspase 9, but not caspase 4, restored network morphology (Fig. 4.6A) and rescued mitochondrial footprint (Fig. 4.6B).

Camel Blue SS exposed cells, in contrast, featured variable branch lengths within mitochondrial networks that were not significantly different from the untreated cultures (Fig. 4.6B), although trends towards decreased branch lengths were detectable. Instead, cells exposed to Camel Blue SS demonstrated more highly branched networks and a significantly reduced mitochondrial footprint. Simultaneous treatment of Camel Blue SS effective doses with caspase 9 inhibitor yielded abnormal mitochondrial network morphology comprised of shorter fragmented networks mixed with some filamentous, interconnected networks (Fig. 4.6A). Caspase 9 inhibitor treatment did not significantly rescue mean branch length or mitochondrial footprint (Fig. 4.6B), suggesting a lack of intrinsic mitochondrial apoptosis response. Treatment with caspase 4 inhibitor did, however, restore interconnected mitochondrial network morphology (Fig. 4.6A), rescued mitochondrial footprint (Fig. 4.6B), and decreased the number of branches per network (Fig. 4.6B), suggesting caspase 4 involvement in these mitochondrial behaviors.

Cellular redox status also appeared to partly influence mitochondrial network

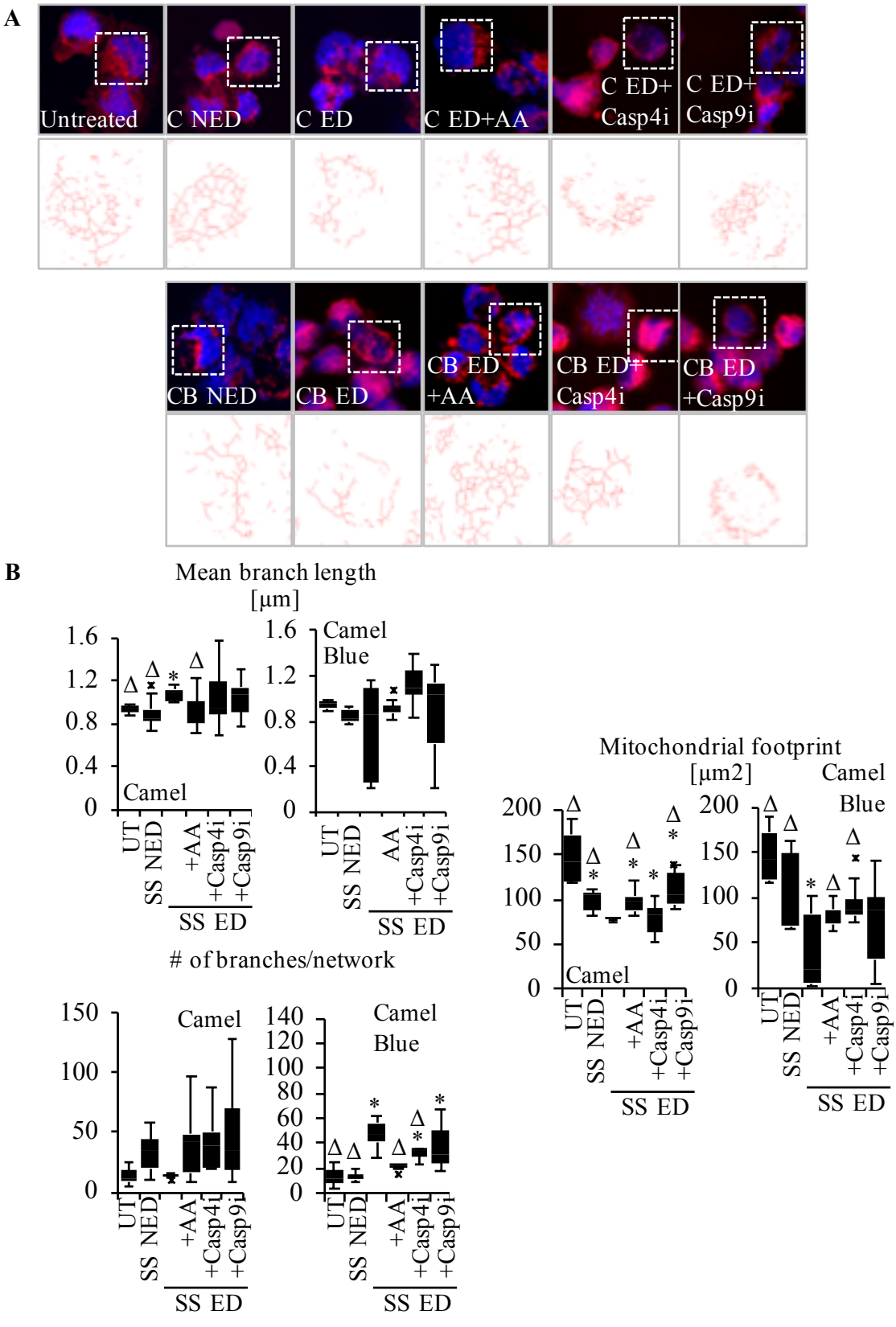
A
Untreated
C NED
C ED
C ED+AA
C ED+ Casp4i
C ED+ Casp9i
CB NED
CB ED
CB ED +AA
CB ED+ Casp4i
CB ED +Casp9i
B
Mean branch length [µm]
Camel
Camel Blue
UT
SS NED
+AA
+Casp4i
+Casp9i
AA
SS ED
# of branches/network
Mitochondrial footprint [µm2]

Figure 4.6. Tobacco smoke exposure elicits changes in mitochondrial networks. (A) MitoTracker and MiNA visualization of mitochondrial networks. (B) Changes to mitochondrial networks were assessed via mean branch length, mitochondrial footprint, and branches per network. *P<0.05, One-way ANOVA followed by paired student's t-test versus untreated cultures, $^{\Delta}P$<0.05, One-Way ANOVA followed by paired student's t-test versus ED. C, Camel; CB, Camel Blue Casp9i, caspase 9 inhibitor; Casp4i caspase 4 inhibitor; ED, effective dose; NED, non-effective dose; SS, sidestream; UT, untreated.

morphology in both Camel SS and Camel Blue SS effective doses. Concurrent treatment with antioxidant ascorbic acid rescued branch length and slightly restored mitochondrial footprint in Camel SS cultures (Fig. 4.6B). Camel Blue SS effective doses with ascorbic acid reestablished interconnected mitochondrial network morphology (Fig. 4.6A) and modestly restored the mean branch length range (Fig. 4.6B), supporting an influential relationship between cellular redox conditions and mitochondrial morphology.

Discussion

Due to the shortage of information on teratogenic effects of tobacco smoke on the developing skeleton, hESCs directed through an osteogenic lineage were used to assess the potency of tobacco products to inhibit calcification in differentiating osteogenic cultures. Based on this endpoint, differential embryotoxicity was observed in cultures treated with cigarette smoke solutions from MS and SS smoke of Camel and Camel Blue cigarettes.

Previous studies found that SS smoke from conventional cigarettes was more potent than MS smoke, in very diverse endpoints such as free radical species levels, angiogenesis, oviductal function, adverse IVF outcome, sperm motility, and attachment ability of peri-implantation embryonic cells [56-63] With regard to differentiating osteoblasts, this current study finds that conventional MS smoke did not hinder the viability of developing osteoblasts or their differentiation. SS smoke, conversely, consistently showed detrimental effects on osteogenesis and inhibited both calcification and the survival of the osteogenic cultures, adding another item to the growing list of biological events that SS smoke inhibits more than MS smoke.

Since SS smoke is a main component of environmental tobacco exposures, our data

is also relevant to pregnant women who may not themselves smoke but expose their fetuses to tobacco smoke when they enter a smoking environment. Even in countries with extensive tobacco control policies, this is still a relevant concern. For example, in New York City, which has a comprehensive tobacco control policy, almost 50% of nonsmoking pregnant women had elevated cotinine levels suggesting that their bodies and thus their fetuses were exposed to secondhand or thirdhand smoke [64]. As follows, it is likely that exposure levels would be exacerbated in countries that do not control tobacco use in public places. Therefore, our data may inform policy makers about yet another adverse health outcome of secondhand smoke exposure.

Almost 20 years ago, a prospective mortality study performed by Thun and Heath (1997) revealed an increase rather than a decrease in smoking associated health risks over a 20-year period after the introduction of low nicotine low tar cigarettes, suggesting that harm-reduction products were not truly reducing risk of injury. Indeed, the first *in vitro* data gathered showed that harm-reduction products are just as capable of attributing harm as conventional products are [62], in agreement with the findings in the 1997 study. In a subsequent *in vitro* study, Lin and colleagues showed that the ability of hESCs to attach to a substratum was severely impaired by exposure to harm-reduction products, while conventional products had milder outcomes [66]. Although this was the first study to evaluate the health of unspecialized pluripotent stem cells in response to tobacco, it did not allow any conclusions as to the potential impairment of differentiation events. Simply extending these findings to differentiating cells may not be straightforward, since undifferentiated cells exhibit altered metabolic, transcriptional and epigenetic states than

differentiated cells [44, 67, 68], which could potentially dictate their responses to toxicants. Thus, in the current study, harm-reduction cigarettes were compared to conventional cigarettes to determine if these products also confer reduced harm on differentiating osteogenic cells. Similar to the previous findings, our data show that harm-reduction products are more embryotoxic than conventional products to differentiating osteoblasts, as exposure demonstrated differentiation inhibition in developing osteoblasts at sub-cytotoxic concentrations.

The fact that harm-reduction products inhibited osteogenesis *in vitro* more than conventional products may be explained by the alteration in chemical composition associated with the process of lowering tar and nicotine content. During this process, other constituents found in the complex chemical blend of cigarette smoke such as nitrate, nitrogen oxide, and tobacco-specific nitrosamines may be enriched [69]. Individually, these chemicals can cause adverse health effects in mammalian cells [70-73]. Not only can concentrations of such chemicals be higher in harm-reduction cigarettes because of the processing required to reduce content of other carcinogens, but smokers also compensate for the amount of delivered nicotine by smoking more cigarettes or by inhaling deeper while smoking [14]. For these reasons it is likely that concentrations of such harmful chemicals are even higher in mothers who have difficulty quitting smoking while pregnant and that the harmful effects of those chemicals are compounded in their unborn fetuses.

While it may be assumed that such chemicals individually trigger signaling cascades that are detrimental to development, another potential mechanism of action is that they induce mild oxidative stress. As we show here, the embryotoxicity of tobacco

products, primarily the harm-reduction kind, seems defined by their ability to create ROS at levels that are insufficient to kill the cells. As recently put forth by Hansen and Harris (2013), teratogenesis is defined by dysmorphogenetic events that may be preceding excessive cell death. While cytotoxicity focuses on the accumulation of ROS, the impediment of antioxidant capacities, and consequent cell death, teratogenesis may be the result of untimely regulation of critical cellular signaling rather than the result of early cell death. Our results outlined here offer support for this notion in that while Camel SS and Camel Blue SS effective doses both demonstrated reduced osteogenesis and upregulation of pro-apoptotic gene expression, Camel Blue SS effective cultures specifically failed to achieve complete caspase cascade activation and cell death as seen in Camel SS effective doses. It follows, then, that additional molecular or cellular players may be involved in the differential outcomes mediated by different tobacco products.

Our results also indicated that altered redox states as directed by exposure to either Camel or Camel Blue plays an influential role in observed embryotoxic outcomes. Antioxidant rescue of calcification suggests that elevated ROS levels may mediate some of the observed embryotoxic outcomes in Camel and Camel Blue ED cultures. Disruption of normal tissue redox balances has also been reported to interfere with normal biological processes that can lead to pathological outcomes including DNA damage [75, 76, 82]. Given that evidence of DNA damage was exclusively observed in cultures exposed to Camel SS effective doses, our results suggest that elevated ROS causes a DNA damage-mediated mode of action for embryotoxicity outcomes following Camel but not Camel Blue exposure. This notion was further supported by exclusive antioxidant-mediated

reduction of DNA damage cell populations in Camel SS effective doses. Given that DNA damage is well-reported to activate caspase 9-mediated apoptosis [77-79], it follows that concurrent *CASP9* mRNA upregulation and posttranslational activation of caspase 9 protein in Camel SS effective dose cultures support a biochemical basis for intrinsic apoptotic responses observed exclusively with Camel exposure.

During the intrinsic apoptosis process, caspase 9 has been reported to regulate the collapse of mitochondrial membrane potential, causing further mitochondrial disruption [80, 81]. Aberrant mitochondrial behavior is well-associated with stress responses and a variety of pathologies [53, 54] and also reported to follow mitochondrial membrane depolarization and precede mitophagy and apoptosis [82, 83]. In accordance with elevated caspase 9 activity, our study found concurrent functional and morphophological mitochondrial changes exclusively in Camel effective dose cultures that were reversed when caspase 9 was inhibited. These data provided further support for the notion that ROS-mediated DNA damage elicited the caspase 9-driven cytotoxic responses that may be responsible for osteogenic inhibition following SS Camel exposure (Fig. 4.7). In contrast, mitochondrial morphological changes observed in the absence of altered mitochondrial function or DNA damage in Camel Blue effective dose cultures hint at divergent modes of embryotoxic action for conventional versus harm-reduction tobacco products.

In contrast with Camel ED cultures, Camel Blue ED cells demonstrated upregulation of caspase 4 mRNA and protein in the absence of caspase 9 activation. Notably, caspase 4 has been proposed to function as an endoplasmic reticulum (ER)-stress specific caspase [84, 85]. Furthermore, the ER and mitochondria have an important cross-

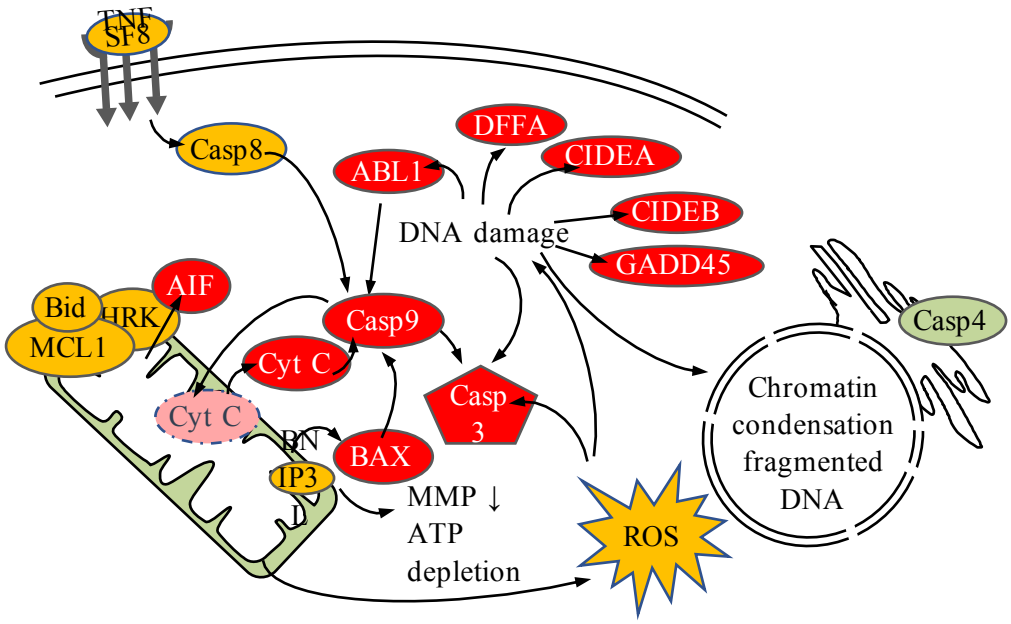

Figure 4.7. Working model of conventional tobacco-induced embryotoxic effects on osteogenesis.

talk relationship that may be of further relevance in the context of development [87-91]. Because treatment with caspase 4 inhibitor rescued mitochondrial network morphology, it is possible that ER stress is also involved in the differential molecular response of cells exposed to the Camel Blue effective dose. Notably, disruption to normal cross-talk between the mitochondria and ER has been implicated in early brain development [90, 91] as well as metabolic and degenerative diseases [87,88]. Moreover, ER stress can interfere with protein folding processes [92], which may be detrimental to osteogenic differentiation as new sets of proteins required for differentiation progression may be made incorrectly or not at all. Secretion of critical regulatory proteins by osteoblasts could also be adversely impacted in this context. Follow up studies, however, are required to confirm ER stress and dysfunction in Camel Blue exposed cultures.

Conclusion

International experts on tobacco policies recently urged the World Health Organization to embrace harm-reduction products to promote better health [93]. However, based on our data dealing with *in vitro* osteogenesis, SS smoke from some harm-reduction products may not be any safer than SS smoke from conventional products. Our data in combination with other studies on harm-reduction products suggest that women should abstain from smoking completely rather than switch to these products.

References

1. Brook JS, Balka EB, Zhang C. The smoking patterns of women in their forties: their relationship to later osteoporosis. Psychol Rep. 2012;110:351-362.

2. Iqbal J, Sun L, Cao J, Yuen T, Lu P, Bab I, Leu NA, Srinivasan S, Wagage S, Hunter CA, Nebert DW, Zaidi M, Avadhani NG. Smoke carcinogens cause bone loss through the aryl hydrocarbon receptor and induction of Cyp1 enzymes. Proc Natl Acad Sci USA 2013;110:11115-11120.

3. Ayo-Yusuf OA and Olutola BG. Epidemiological association between osteoporosis and combined smoking and use of snuff among South African women. Niger J Clin Pract. 2014;17(2):174-177.

4. Daniel AB, Shah H, Kamath A, Guddettu V, Joseph B. Environmental tobacco and wood smoke increase the risk of Legg-Calvé-Perthes disease. Clin Orthop Relat Res. 2012;470(9):2369-2375.

5. Sloan A, Hussain I, Maqsood M, Eremin O, El-Sheemy M. The effects of smoking on fracture healing. Surgeon. 2010;8:111-116.

6. Moghaddam-Alvandi A, Zimmermann G, Hammer K, Bruckner T, Grützner PA, von Recum J. Cigarette smoking influences the clinical and occupational outcome of patients with tibial shaft fractures. Injury. 2013;44(11): 1670-1671.

7. Bowker KA, Lewis S, Coleman T, Vaz LR, Cooper S. Comparison of cotinine levels in pregnant women while smoking and when using nicotine replacement therapy. Nicotine Tob Res. 2014;16:895-898.

8. U.S. Department of Health and Human Services. The Health Consequences of Involuntary Exposure to Tobacco Smoke: A Report of the Surgeon General. Secondhand Smoke What It Means to You. U.S. Department of Health and Human Services, Centers for Disease Control and Prevention, Coordinating Center for Health Promotion, National Center for Chronic Disease Prevention and Health Promotion, Office on Smoking and Health, 2006.

9. DiFranza JR and Aligne CA, Weitzman M. Prenatal and postnatal environmental tobacco smoke exposure and children's health. Pediatrics. 2004;113:1007-1015.

10. Soares SR and Melo MA. Cigarette smoking and reproductive function. Curr Opin Obstet Gynecol. 2008;20:281-291.

11. Karatza AA, Varvarigou A, and Beratis NG. Growth up to 2 years in relationship to maternal smoking during pregnancy. Clin Pediatr (Phila). 2003;42:533-541.

12. Karatza AA, Giannakopoulos I, Dassios TG, Belavgenis G, Mantagos SP, Varvarigou AA. Periconceptional tobacco smoking and isolated congenital heart defects in the neonatal period. Int J Cardiol. 2011;148:295-299.

13. Riesenfeld A. Growth-depressing effects of alcohol and nicotine in two strains of rats. Acta Anat. 2005;122:18-24.

14. Burns DM and Benowitz NL. Public health implications of changes in cigarette design and marketing. In: US Department of Health and Human Services monograph 13, Risks associated with smoking cigarettes with low machine-measured yields of tar and nicotine. 2001;1-12.

15. Balansky RB, D'Agostini F, Zanacchi P, De Flora S. Protection by N-acetylcysteine of the histopathological and cytogenetical damage produced by exposure of rats to cigarette smoke. Cancer Lett. 1992;64(2):123-131.

16. Givi ME, Blokhuis BR, Da Silva CA, Adcock I, Garssen J, Folkerts G, Redegeld FA, Mortaz E. Cigarette smoke suppresses the surface expression of c-kit and FcεRI on mast cells. Mediators Inflamm. 2013;2013:813091.

17. Sparks NRL, Martinez IKC, and zur Nieden NI. Lineage tracing and replicate analysis reveals low osteogenic yield in human induced pluripotent stem cells correlated with differential Twist1 expression. Stem Cells. Under review.

18. Sparks, NRL. et al. Low Osteogenic Yield in Human Pluripotent Stem Cells Associates with Differential Neural Crest Promoter Methylation. Stem Cells. 2018; 36:349–362.

19. Knoll M, Shaoulian R, Magers T, Talbot P. Ciliary beat frequency of hamster oviducts is decreased *in vitro* by exposure to solutions of mainstream and sidestream cigarette smoke. Biol Reprod. 1995;53:29-37.

20. Knoll M and Talbot P. Cigarette smoke inhibits oocyte cumulus complex pick-up by the oviduct *in vitro* independent of ciliary beat frequency. Reprod Toxicol. 1998;12:57-68.

21. Martinez IKC, Sparks NRL, Madrid JV, Affeldt H 3rd, Vera MKM, Bhanu B, Zur

Nieden NI. Video-based kinetic analysis of calcification in live osteogenic human embryonic stem cell cultures reveals the developmentally toxic effect of Snus tobacco extract. Toxicol Appl Pharmacol. 2019;363:111–121.

22. zur Nieden NI and Baumgartner L. Assessing developmental osteotoxicity of chlorides in the embryonic stem cell. Reprod. Toxicol. 2010;30:277-283.

23. zur Nieden NI, Davis LA, and Rancourt DE. Comparing three novel endpoints for developmental osteotoxicity in the embryonic stem cell test. Toxicol Appl Pharmacol. 2010;247:91-97.

24. Walker L, Baumgartner L, Keller K, Ast J, zur Nieden NI. Non-human primate and rodent embryonic stem cells are differentially sensitive to embryotoxic compounds. Toxicol Rep. 2014;2:165-174.

25. Madrid JV, Sera SR, Sparks NRL, zur Nieden NI. Human Pluripotent Stem Cells to Assess Developmental Toxicity in the Osteogenic Lineage. Methods Mol Biol. 2018;1797:125-145.

26. Davis LA, Dienelt A, and zur Nieden NI. Absorption-based assays for the analysis of osteogenic and chondrogenic yield. Methods Mol Biol. 2011;690:255-272.

27. Jensen C. Quantitative Analysis of Histological Staining and Flurescence Using ImageJ. Anat Rec (Hoboken). 2013; 296(3):378-81.

28. Valente AJ, Maddalena LA, Robb EL, Moradi F, Stuart JA. A simple ImageJ macro tool for analyzing mitochondrial network morphology in mammalian cell culture. Acta Histochem. 2017;119:315–326.

29. Livak KJ and Schmittgen TD Analysis of relative gene expression data using real-time quantitative PCR and the 2(-Delta Delta C(T)) Method. Methods. 2001;25, 402-408.

30. Genschow, E, Spielmann H, Scholz G, Seiler A, Brown N, Piersma A, Brady M, Clemann N, Huuskonen H, Paillard F, Bremer S, Becker K. The ECVAM international validation study on *in vitro* embryotoxicity tests: results of the definitive phase and evaluation of prediction models. European Centre for the Validation of Alternative Methods. Altern Lab Anim. 2002;30:151–176.

31. Sies H. Oxidative stress. London, UK: Academic Press; 1985.

32. Weinbrenner T, Cladellas M, Isabel Covas M, Fitó M, Tomás M, Sentí M, Bruguera J, Marrugat J. High oxidative stress in patients with stable coronary heart disease. Atherosclerosis. 2003;168: 99–106.

33. Abramson JL, Hooper WC, Jones DP, Ashfaq S, Rhodes SD, Weintraub WS, Harrison DG, Quyyumi AA, Vaccarino V. Association between novel oxidative stress markers and C-reactive protein among adults without clinical coronary heart disease. Atherosclerosis. 2005;178:115-121.

34. Kaneto H, Katakami N, Kawamori D, Miyatsuka T, Sakamoto K, Matsuoka TA, Matsuhisa M, Yamasaki Y. Involvement of oxidative stress in the pathogenesis of diabetes. Antioxid Redox Signal. 2007;9:355–66.

35. Mena S, Ortega A, Estrela JM. Oxidative stress in environmental-induced carcinogenesis. Mutat Res. 2009;674:36–44.

36. Dennery PA. Effects of oxidative stress on embryonic development. Birth Defects Research C Embryo Today. 2007;81:155–162.

37. Hansen JM. Oxidative stress as a mechanism of teratogenesis. Birth Defects Res C Embryo Today. 2006;78:293–307.

38. Kovacic P and Somanathan R. Mechanism of teratogenesis: electron transfer, reactive oxygen species, and antioxidants. Birth Defects Res C Embryo Today. 2006;78:308–325.

39. Raina D, Pandey P, Ahmad R, Bharti A, Ren J, Kharbanda S, Weichselbaum R, Kufe D. c-Abl tyrosine kinase regulates caspase-9 autocleavage in the apoptotic response to DNA damage. J Biol Chem. 2005; 280:11147–11151.

40. Brasher BB and Etten RAV. c-Abl Has High Intrinsic Tyrosine Kinase Activity That Is Stimulated by Mutation of the Src Homology 3 Domain and by Autophosphorylation at Two Distinct Regulatory Tyrosines. J. Biol. Chem. 2000;275:35631–35637.

41. Pluk H, Dorey K, Superti-Furga G. Autoinhibition of c-Abl. Cell. 2002;108:247-59.

42. Kawamura K, Fukuda J, Shimizu Y, Kodama H, Tanaka T. Survivin contributes to the anti-apoptotic activities of transforming growth factor alpha in mouse blastocysts through phosphatidylinositol 3'-kinase pathway. Biol Reprod. 2005;73:1094-101.

43. Delvaeye M, De Vriese A, Zwerts F, Betz I, Moons M, Autiero M, Conway EM. Role of the 2 zebrafish survivin genes in vasculo-angiogenesis, neurogenesis, cardiogenesis and hematopoiesis. BMC Developmental Biology. 2009;9:25.

44. Liu Y, Shin S, Zeng X, Zhan M, Gonzalez R, Mueller FJ, Schwartz CM, Xue H, Li H, Baker SC, Chudin E, Barker DL, McDaniel TK, et al. Genome wide profiling of human embryonic stem cells (hESCs), their derivatives and embryonal carcinoma cells to develop base profiles of U.S. Federal government approved hESC lines. BMC Dev Biol. 2006;6: 20.

45. Kim B and Song YS. Mitochondrial dynamics altered by oxidative stress in cancer. Free Radic Res. 2016;50(10):1065-1070.

46. Ly JD, Grubb DR, Lawen A. The mitochondrial membrane potential (Δψm) in apoptosis; an update. Apoptosis. 2003;8:115–128.

47. Shamas-Din A, Kale J, Leber B, and Andrews DW. Mechanisms of Action of Bcl-2 Family Proteins. Cold Spring Harb Perspect Biol. 2013; 5: a008714.

48. Shelton SN, Shawgo ME, Robertson JD. Cleavage of Bid by executioner caspases mediates feed forward amplification of mitochondrial outer membrane permeabilization during genotoxic stress-induced apoptosis in Jurkat cells. J Biol Chem. 2009;284:11247-55.

49. Kubli DA, Ycaza JE, Gustafsson AB. Bnip3 mediates mitochondrial dysfunction and cell death through Bax and Bak. Biochem J. 2007;405:407-15.

50. D'Alessio M, De Nicola M, Coppola S, Gualandi G, Pugliese L, Cerella C, Cristofanon S, Civitareale P, Ciriolo MR, Bergamaschi A, Magrini A, Ghibelli L. Oxidative Bax dimerization promotes its translocation to mitochondria independently of apoptosis. FASEB J. 2005;19:1504-6.

51. Chan DC. Mitochondrial fusion and fission in mammals. Annu Rev Cell Dev Biol. 2006;22:79-99.

52. Suen DF, Norris KL, Youle RJ. Mitochondrial dynamics and apoptosis. Genes Dev. 2008;22:1577-90.

53. Yu T, Shey-Shing S, Robotham JL, Yoon Y. Mitochondrial fission mediates high glucose-induced cell death through elevated production of reactive oxygen species.

Cardiovasc Res. 2008;79:341-51.

54. Makino A, Scott BT, Dillmann WH. Mitochondrial fragmentation and superoxide anion production in coronary endothelial cells from a mouse model of type 1 diabetes. Diabetologia. 2010;53:1783-94.

55. Rosati E, Sabatini R, Rampino G, De Falco F, Di Ianni M, Falzetti F, Fettucciari K, Bartoli A, Screpanti I, Marconi P. Novel targets for endoplasmic reticulum stress-induced apoptosis in B-CLL. Blood. 2010;116:2713-23.

56. Gieseke C and Talbot P. Cigarette smoke inhibits hamster oocyte pickup by increasing adhesion between the oocyte cumulus complex and oviductal cilia. Biol Reprod. 2005;73: 443-451.

57. Lin S, Tran V, Talbot P. Comparison of toxicity of smoke from traditional and harm-reduction cigarettes using mouse embryonic stem cells as a novel model for preimplantation development. Hum Reprod. 2009;24:386-397.

58. Melkonian G, Le C, Zheng W, Talbot P, Martins-Green M. Normal patterns of angiogenesis and extracellular matrix deposition in chick chorioallantoic membranes are disrupted by mainstream and sidestream cigarette smoke. Toxicol Appl Pharmacol. 2000;163:26-37.

59. Melkonian G, Cheung L, Marr R, Tong C, Talbot P. Mainstream and sidestream cigarette smoke inhibit growth and angiogenesis in the day 5 chick chorioallantoic membrane. Toxicol Sci. 2002;68:237-248.

60. Neal MS, Hughes EG, Holloway AC, Foster WG. Sidestream smoking is equally as damaging as mainstream smoking on IVF outcomes. Hum Reprod. 2005;20: 2531-2535.

61. Polyzos A, Schmid TE, Piña-Guzmán B, Quintanilla-Vega B, Marchetti F. Differential sensitivity of male germ cells to mainstream and sidestream tobacco smoke in the mouse. Toxicol Appl Pharmacol. 2009;237:298-305.

62. Riveles K, Tran V, Roza R, Kwan D, Talbot P. Smoke from traditional commercial, harm-reduction, and research brand cigarettes impairs oviductal functioning in hamsters (*Merocricetus auratus*) *in vitro*. Human Reprod. 2007;22:346-355.

63. Valavanidis A and Haralambous E. A comparative study by electron paramagnetic

resonance of free radical species in the mainstream and sidestream smoke of cigarettes with conventional acetate filters and 'bio-filters'. Redox Rep. 2001;6: 161-171.

64. Hawkins SS, Dacey C, Gennaro S, Keshinover T, Gross S, Gibeau A, Lulloff A, Aldous KM. Secondhand Smoke Exposure Among Nonsmoking Pregnant Women in New York City. Nicotine Tob Res. 2014;16:1079-1084.

65. Thun MJ and Heath CW. Changes in mortality from smoking in two American Cancer Society prospective studies since 1959. Prev Med. 1997;26(4):422-426.

66. Lin S, Fonteno S, Weng JH, Talbot P. Comparison of the toxicity of smoke from conventional and harm-reduction cigarettes using human embryonic stem cells. Toxicol Sci. 2010;118:202-212.

67. Bibikova M, Chudin E, Wu B, Zhou L, Garcia EW, Liu Y, Shin S, Plaia TW, Auerbach JM, Arking DE, Gonzalez R, Crook J, Davidson B, et al. Human embryonic stem cells have a unique epigenetic signature. Genome Res. 2006;16(9):1075-1083.

68. Han S, Auger C, Thomas SC, Beites CL, Appanna VD. Mitochondrial biogenesis and energy production in differentiating murine stem cells: a functional metabolic study. Cell Reprogram. 2014;16: 4-90.

69. Hoffmann D and Hoffmann I. The changing cigarette, 1950-1995. J Toxicol Environ Health. 1997;50:307-364.

70. Nayak BN, Ray M, Persaud TV. Maternal and fetal chromosomal aberrations in mice following prenatal exposure to subembryotoxic doses of lead nitrate. Acta Anat (Basel). 1995;135: 185-188.

71. Fujinaga M, Baden JM, Mazze RI. Susceptible period of nitrous oxide teratogenicity in Sprague-Dawley rats. Teratology. 1989;40: 439-444.

72. Sasaki S, Sata F, Katoh S, Saijo Y, Nakajima S, Washino N, Konishi K, Ban S, Ishizuka M, Kishi R. Adverse birth outcomes associated with maternal smoking and polymorphisms in the N-Nitrosamine-metabolizing enzyme genes NQO1 and CYP2E1. Am J Epidemiol. 2008;67:719-726.

73. Zeman C, Beltz L, Linda M, Maddux J, Depken D, Orr J, Theran P. New questions

and insights into nitrate/nitrite and human health effects: a retrospective cohort study of private well users' immunological and wellness status. J Environ Health. 2011;74:8-18.

74. Hansen JM and Harris C. Redox control of teratogenesis. Reprod Toxicol. 2013;35: 165-179.

75. Lepka K, Berndt C, Hartung HP, Aktas O. Redox Events As Modulators of Pathology and Therapy of Neuroinflammatory Diseases. Front Cell Dev Biol. 2016;4:63.

76. Burgoyne JR, Mongue-Din H, Eaton P, Shah AM. Redox signaling in cardiac physiology and pathology. Circ Res. 2012;111:1091-106.

77. Sharma P, Bhushan Jha A, Shanker Dubey R, Pessarakli M. Reactive Oxygen Species, Oxidative Damage, and Antioxidative Defense Mechanism in Plants under Stressful Conditions. Am J Bot. 2012;2012:1-26.

78. D'Sa-Eipper C, Leonard JR, Putcha G, Zheng TS, Flavell RA, Rakic P, Kuida K, Roth KA. DNA damage-induced neural precursor cell apoptosis requires p53 and caspase 9 but neither Bax nor caspase 3. Development. 2001;128(1):137-46.

79. Ochs K and Kaina B. Apoptosis induced by DNA damage O6-methylguanine is Bcl-2 and caspase-9/3 regulated and Fas/caspase-8 independent. Cancer Res. 2000;60(20):5815-24

80. Chen M, Guerrero AD, Huang L, Shabier Z, Pan M, Tan TH, Wang J. Caspase-9-induced mitochondrial disruption through cleavage of anti-apoptotic BCL-2 family members. J Biol Chem. 2007;282(46):33888-95

81. Eeva J, Nuutinen U, Ropponen A, Mättö M, Eray M, Pellinen R, Wahlfors J, Pelkonen J. The involvement of mitochondria and the caspase-9 activation pathway in rituximab-induced apoptosis in FL cells. Apoptosis. 2009;14(5):687-98

82. Elmore SP, Qian T, Grissom SF, Lemasters JJ. The mitochondrial permeability transition initiates autophagy in rat hepatocytes. FASEB J. 2001;15:2286-7.

83. Edwards JL, Quattrini A, Lentz SI, Figueroa-Romero C, Cerri F, Backus C, Hong Y, Feldman EL. Diabetes regulates mitochondrial biogenesis and fission in mouse neurons. Diabetologia. 2010;53:160–169.

84. Hitomi J, Katayama T, Eguchi Y, Kudo T, Taniguchi M, Koyama Y, Manabe T, Yamagishi S, Bando Y, Imaizumi K, Tsujimoto Y, Tohyama M. Involvement of caspase-4 in endoplasmic reticulum stress-induced apoptosis and Abeta-induced cell death. J Cell Biol. 2004;165:347-56.

85. Kim SJ, Zhang Z, Hitomi E, Lee YC, Mukherjee AB. Endoplasmic reticulum stress-induced caspase-4 activation mediates apoptosis and neurodegeneration in INCL. Hum Mol Genet. 2006;15(11):1826-34.

86. Giacomello M and Pellegrini L. The coming of age of the mitochondria-ER contact: a matter of thickness. Cell Death Differ. 2016;23:1417-27.

87. Filadi R, Theurey P, Pizzo P. The endoplasmic reticulum-mitochondria coupling in health and disease: Molecules, functions and significance. Cell Calcium. 2017;62:1-15.

88. Theurey P, Tubbs E, Vial G, Jacquemetton J, Bendridi N, Chauvin MA, Alam MR, Le Romancer M, Vidal H, Rieusset J. Mitochondria-associate endoplasmic reticulum membranes allow adaptation of mitochondrial metabolism to glucose availability in the liver. J Mol Cell Biol. 2016;8(2):129-43.

89. Marchi S, Patergnani S, Pinton P. The endoplasmic reticulum-mitochondria connection: one touch, multiple functions. Biochim Biophys Acta. 2014;1837:461-9.

90. Angebault C, Fauconnier J, Patergnani S, Rieusset J, Danese A, Affortit CA, Jagodzinska J, Mégy C, Quiles M, Cazevieille C, Korchagina J, Bonnet-Wersinger D, Milea D, et al. ER-mitochondria cross-talk is regulated by the Ca2+ sensor NCS1 and is impaired in Wolfram syndrome. Sci Signal. 2018;11(553) pii: eaaaq1380.

91. Cagalinec M, Liiv M, Hodurova Z, Hickey MA, Vaarmann A, Mandel M, Zeb A, Choubey V, Kuum M, Safiulina D, Vasar E, Veksler V, Kaasik A. Role of Mitochondrial Dynamics in Neuronal Development: Mechanism for Wolfram Syndrome. PLoS Biol. 2016;14(7):e1002511.

92. Oslowski CM and Urano F. Measuring ER stress and the unfolded protein response using mammalian tissue culture system. Methods Enzymol. 2011;490:71-92.

93. Torjesen I. Tobacco control policies should embrace harm-reduction products, nicotine experts say. BMJ. 2014;48:g3604.

CHAPTER 5

Snus smokeless tobacco extract inhibits osteogenic differentiation through manipulation of redox signaling pathways and biochemical survival networks

Lauren M. Walker, Nicole RL Sparks, Steven R. Sera, Jolie Carreon, Edward Dominguez, Ivann KC Martinez, Avani Vaghela, Tiffany S Satoorian, Nicole I zur Nieden

Abstract

In recent years, concerns surrounding tobacco-related health disparities have shifted from conventional cigarette smoking to other forms of tobacco use. Harm-reduction tobacco products (HRTPs) are marketed as less harmful to users than conventional cigarettes. As such, pregnant women struggling with nicotine addiction may turn to HRTPs as a perceived safer alternative. Contrarily, some epidemiological and *in vivo* studies implicate HRTPs in adverse pregnancy outcomes though studies on molecular etiology of HRTP-mediated embryotoxicity have yet to be reported. Here, we demonstrate that Snus exposure, one type of HRTP, directly targets osteogenesis through modulation of redox signaling proteins and survival signaling networks.

Developing mouse embryos exposed *in utero* to Snus smokeless tobacco extract during early gestation demonstrated reduced overall length, skull length, and skull mineralization. To explore molecular and biochemical changes *in vitro*, human embryonic stem cells were differentiated into osteoblasts to model early osteogenesis. Concurrent

Snus exposure revealed reduced osteoblast differentiation at sub-cytotoxic Snus doses concomitant with increased cellular reactive oxygen species and the absence of active apoptosis. Notably, osteogenic inhibition of osteogenesis occurred only when differentiating cells were exposed to Snus extract during the first week of differentiation. Mechanistic analysis found hyperphosphorylation and reduced nuclear levels of FOXO1/3a redox signaling transcription factors. Knockdown of FOXO1/3a significantly reduced osteogenic output, suggesting a role for FOXO1/3a misregulation in inhibitory impacts of Snus. Upstream of FOXO1/3a, survival kinase AKT1 was found to be upregulated. Global proteomic analysis of AKT signaling pathway targets found that Snus exposure also manipulated important aspects of the AKT signaling network with further implications for inhibited protein synthesis. Collectively, our data suggest that Snus can interrupt key biochemical events during early osteogenesis that inhibit proper osteoblast development.

Introduction

In light of biomedical studies demonstrating a myriad of adverse health impacts connected to cigarette smoking [1, 2], the tobacco industry has endeavored to create new products aimed to reduce tobacco-related harm to users [3, 4]. These so-called "harm-reduction" tobacco products (HRTPs) are characterized as products that have been modified via altered manufacturing processes to remove some of the harmful chemicals associated with tobacco use and/or present a method of tobacco use that reduces user chemical exposure [5].

Smokeless tobacco, one such HRTP, is considered to minimize some of the harmful chemical exposures associated with conventional cigarette use. Smokeless tobacco includes snuff, dip, chew and Snus products that are sniffed, dipped (that is, placed in the mouth and sucked on), or chewed by users [6]. In the absence of combustion, smokeless tobacco use reduces exposure to chemicals produced by pyrolysis and incomplete combustion reactions such as polycyclic aromatic hydrocarbons (PAHs) like naphthalene and benzo[a]pyrene [6, 7]. Within this category, Snus products (also referred to as oral moist snuff in Sweden) are unique in that raw cured tobacco is heat-treated for 24-36 hours to kill bacteria [8]. This production method is maintained to inhibit microbial metabolism of tobacco nitrites into harmful tobacco-specific nitrosamines (TSNAs) [9].

Public perception of smokeless tobacco products generally holds smokeless tobacco products as safer than smoking a conventional cigarette [10-13]. Studies examining health risks of Snus smokeless tobacco compared to conventional cigarettes have also found some evidence for modestly reduced user risk for cardiovascular disease, mortality, as well as lung, oral, and gastric cancer [8]. With regard to developmental and pregnancy risks, however, less information is readily available for risks posed by Snus use. Some epidemiological studies suggest that Snus use during pregnancy is likely to inhibit normal development and encourage adverse pregnancy outcomes by way of preterm delivery, reduced birth weight, neurological effects, and preeclampsia [14, 15]. *In vivo* studies examining the impact of smokeless tobacco on embryonic development have reported embryo growth retardation and reduced bone ossification in rats and mice [16, 17], though it is unclear what type of smokeless tobacco was used for these studies. To

date, a mechanistic investigation of Snus-mediated embryotoxicity has yet to be reported. Here, we present an investigation of Snus-driven developmental toxicity as well as an investigation into the molecular basis for Snus-related embryotoxicity outcomes for the first time.

Methods

Animals

Animal experiments were conducted in accordance with guidelines for care and use of laboratory animals [18] and approved by the Institutional Animal Care and Use Committee at the University of California, Riverside (AUP#20180064). Ten female and 10 male mice on a mixed 129/Sv plus C57BL/6 (Charles River Laboratories) background were bred for one generation to produce enough females for experimental purposes. Animals were housed in specific pathogen free (SPF) conditions with a 12/12-hour light-dark cycle, controlled temperature conditions (23 ± 2°C), and relative humidity of 50 ± 10%. Mice had *ad libitum* access to food and water.

Animal exposures and tissue collection

Timed matings with virgin females were performed for Snus extract and negative control PBS exposure. Pregnant females were exposed via intravenous tail vein injection to 100 µl of 10% Snus extract or PBS on days E6.5 and E8.5 of pregnancy. Snus exposure dose was determined according to an analysis of nicotine in Snus content (data not shown) that determined a Snus dose with a nicotine level within range of nicotine levels found in

the blood of human tobacco users. Maternal weight was measured every other day starting on E0.5 of pregnancy and concluding on E17.5 when dams were euthanized. Mice were euthanized by carbon dioxide inhalation, in accordance with NIH guidelines. On E17.5, pups, placentas, and maternal organs were collected, washed in PBS, and weighed. Pups and placentas were also imaged for dimensional measurements. Pups were prepared for and subjected to Alizarin Red and Alcian Blue staining of the embryonic mouse skeleton and cartilage tissues, respectively, as previously described [19].

Liver histopathology preparation

Dam livers were fixed overnight in 10% neutral buffered formalin. Fixed livers were processed using ascending concentrations of 70-100% isopropyl alcohol to dehydrate the tissues. Processed livers were embedded in optimal cutting temperature compound (OCT compound) and sectioned into 5 μm sections using a cryostat. Sections were subsequently mounted and stained with hematoxylin and eosin (H&E) stain. Stained liver sections were imaged on a Leica dissection microscope for histological analysis.

Human embryonic stem cell culture

H9 human embryonic stem cell (hESC) (WiCell Research Institute) cultures were maintained in an undifferentiated state through maintenance culture in mTeSR® culture medium (Stem Cell Technologies) in incubator conditions set to 37°C, 5% CO_2, and 95% relative humidity. hESC colonies were passaged every 5 days using Accutase® (Innovative Cell Technologies, Inc.) and a cell scraper to gently dissociate colonies without overly

dissociating cells. hESCs were then plated on culture plates coated with Matrigel (BD Biosciences).

Human embryonic stem cell osteogenic differentiation

Osteogenic differentiation using hESCs was performed as described previously by Sparks et al., 2018. Pluripotent hESCs were grown to approximately 70% confluency mTeSR® culture medium (Stem Cell Technologies) prior to osteogenic differentiation induction. Osteogenic induction commenced with application of control differentiation medium comprised of Dulbecco's modified Eagle's medium (DMEM; Gibco) plus 15% FBS (Atlanta Biologicals), 1% non-essential amino acids (NEAA; Gibco), 1:200 penicillin/streptomycin (Gibco), and 0.1mM β-mercaptoethanol (Sigma-Aldrich). Differentiating cells were cultured in control differentiation medium for 5 days. On the fifth day of culture, control differentiation medium was supplemented with osteogenic induction factors: 0.1 mM β-glycerophosphate (βGP; Sigma-Aldrich), 50 µg/ml ascorbic acid (AA; Sigma-Aldrich), and $1.2x10^{-7}$ M $1,25(OH)_2$ Vitamin D_3 (VD_3; Calbiochem).

Human foreskin fibroblast cell culture

Human foreskin fibroblasts (hFFs) were a gift of Dr. Derrick Rancourt (University of Calgary). hFFs cultures were in high glucose L-glutamine Dulbecco's modified Eagle's medium (DMEM, Corning) with 10% fetal bovine serum (FBS, Atlanta Biologicals), 1% non-essential amino acids (NEAA, Gibco), and 0.5% penicillin/streptomycin (10,000 units/10,000 units, Gibco).

Mouse embryonic stem cell culture

D3 mouse embryonic stem cells (mESCs) (ATCC) were maintained in culture medium consisting of Dulbecco's modified Eagle's medium (DMEM; Gibco) supplemented with 15% FBS (Atlanta Biologicals), 1% non-essential amino acids (NEAA; Gibco), 1:200 penicillin/streptomycin (Gibco), 0.1mM β-mercaptoethanol (Sigma-Aldrich), and 1000 U/ml Leukemia Inhibitory Factor (LIF) (EMD Millipore). mESCs were kept in an incubator set to 37°C, 5% CO_2, and 95% relative humidity and passaged every 48 hours using 0.25% trypsin-EDTA (Invitrogen) as a dissociation agent.

Mouse embryonic stem cell osteogenic differentiation

Osteogenic differentiation using hESCs was performed as described previously [23]. Using 0.25% trypsin-EDTA (Invitrogen), mESCs were made into a single cell suspension of 3.75×10^4 cells/ml in control differentiation medium consisting of 15% FBS (Atlanta Biologicals), 1% non-essential amino acids (NEAA; Gibco), 1:200 penicillin/streptomycin (Gibco), and 0.1mM β-mercaptoethanol (Sigma-Aldrich). Drops of 20 μL of cell suspension were applied to the underside of a Petri dish cover. Drop plates were kept in an incubator at 37°C, 5% CO_2, and 95% relative humidity for 3 days to allow for passive embryoid body formation. On the third day of culture, embryoid bodies were collected and transferred to non-adherent culture dishes filled with control differentiation medium. Embryoid bodies were allowed to continue growing and differentiating until day 5 of differentiation. On day 5, embryoid bodies were collected and dissociated into a single cell suspension using 0.25% trypsin-EDTA. Cells were then seeded at 50,000 cells/cm^2 in

culture dishes filled with control differentiation medium supplemented with osteogenic induction factors 10 mM β-glycerophosphate (βGP; Sigma-Aldrich) and 25 μg/L ascorbic acid (AA; Sigma-Aldrich), and 5×10^{-8} M $1,25(OH)_2$ Vitamin D_3 (VD_3; Calbiochem).

Creation of shFOXO1/3a mouse embryonic stem cell cell line

A pSuperior-*FOXO1/3a* plasmid [20] was linearized using HindIII restriction enzyme, gel purified, and transfected into mESCs with Effectene using 1 μg of plasmid. Clones were chosen following 72 hours of puromycin selection. Successful plasmid integration was confirmed via PCR for the puromycin gene (forward primer 5′-TGCAAGAACTCTTCCTCACG-3′, reverse primer 5′-AGGCCTTCCATCTGTTGCT-3′) with a 65°C annealing temperature protocol. Approximate percentage of FOXO1/3a knockdown was also confirmed via western blot.

Production of Snus smokeless tobacco extract

For cell culture applications, a 10% (w/v) stock extract of Snus tobacco was made by incubating 10 grams of Camel Snus in 85 ml of DMEM with 15% FBS overnight at 4°C. The extract was then centrifuged 450×*g* for 10 minutes at room temperature and again at 13,000 ×g for 1 hour. Extract supernatant was pH adjusted to 7.4, brought to a final volume of 100 ml with DMEM with 15% FBS, and filter sterilized. Snus tobacco extract intended for *in vivo* exposures was made following the same protocol using sterile PBS supplemented with 15% FBS in lieu of DMEM.

In vitro Snus exposures

hESC and mESC cultures were treated with Snus tobacco extract throughout the entire 20-day osteogenic differentiation protocol with the exception of the timed exposure experiment.

During the timed window Snus exposure experiment, cells were treated with Snus tobacco extract during a prescribed window of differentiation: days 0-20, days 0-3, days 3-5, days 5-7, or days 7-20. Snus tobacco extract was screened at five different concentrations to generate a concentration-response curve and determine half-maximal inhibition of differentiation (ID_{50}) and cell viability (IC_{50}) concentrations. Culture medium containing Snus extract was replenished with each media change.

Cell viability assay

Cell survival for differentiating osteoblasts and hFFs was assessed via the -[4,5-dimethylthiazol-2-yl]-2,5-diphenylterazolium bromide (MTT) assay. Cells were incubated with MTT for 3 hours at 37°C. Culture media was then removed and 0.04 mol/L HCl in isopropanol was added to each well. Optical density was measured at 595 nm in an iMark™ microplate reader (Bio-Rad). A decrease in absorbance at 595 nm was interpreted as a measurement of reduction in viable cell populations as the previously described [21-23].

Calcium assay

Cells were lysed in a modified radioimmunoprecipitation (RIPA) buffer [24]. Extracellular matrix calcification was quantified based on the interaction of calcium ions

(Ca^{2+}) in cell lysates with Arsenazo III (Genzyme) to form a purple Ca-Arsenazo III complex. The concentration of total calcium in the sample was calculated based on solution absorbance at 655 nm and a $CaCl_2$ standard [24]. A modified Lowry protein assay (Bio-Rad DC™ protein assay) was used to normalize total calcium content to total protein content in each sample as described by Davis et al., 2011.

Live/Dead assay

The LIVE/DEAD Viability/Cytotoxicity Kit (ThermoFisher L3224) was used to quantify healthy live, apoptotic, and necrotic cell populations in untreated and Snus-exposed cultures. Cells were dissociated into a single cell suspension using 0.25% trypsin-EDTA (Invitrogen), washed with PBS, and resuspended in fresh medium containing 0.1 μM calcein AM and 8 μM ethidium homodimer-1 (EthD-1) assay stains. Cells were then incubated in the dark for 20 minutes at 25°C. Freshly stained cells were washed with PBS and strained using strain-cap centrifuge tubes (FisherScientific, 08-771-23) to dissociate any remaining cell aggregates into a single cell suspension. Cells were resuspended in ice-cold PBS with 2% FBS and promptly analyzed using a FACScalibur Flow Cytometer (BD Biosciences). Fluorescence was detected at excitation/emission at λ = 494/517 nm and 517/617 nm. Cytometer gating was set using unstained untreated samples and adjusting forward scatter and side-scatter light. For each sample, 10,000 events were recorded.

Caspase 3/7 stain

Executioner caspase 3 and 7 activation was visually assessed via staining with a

caspase 3/7 reagent conjugated to carboxyfluorescein fluorochrome (Guava Technologies). Live cells were incubated for 1 hour in a solution of 1X caspase 3/7 reagent to allow for covalent binding of reagent to activated caspases. Excess, unbound reagent was washed away with 1X apoptosis buffer provided by the kit manufacturer. Stained cultures were imaged using a Nikon Ti fluorescent microscope.

Superoxide anion detection

A Lumimax Superoxide Anion Detection Kit (Agilent Technologies) was used to measure endogenous superoxide anion levels. Cells were rendered into a single cell suspension using 0.25% trypsin-EDTA (Invitrogen), washed with PBS, and resuspended in fresh culture medium. Cells were then incubated at 37°C for 30 minutes. This was followed by second incubation of 5×10^5 cells in 190 µL of superoxide anion (SOA) assay medium with 5 µL of 4.0 mM luminol solution and 5 µL of 5.0 mM enhancer medium for 30 minutes at 25°C. Endogenous superoxide anion species were detected as chemiluminescent light emissions measured on a luminometer (Lucetta™).

Hydrogen peroxide detection

Endogenous hydrogen peroxide was measured using dihydrorhodamine 123 (DHR123; Invitrogen, D23806), a hydrogen peroxide indicator that fluoresces green proportional to hydrogen peroxide levels [25-26]. Cells were washed with PBS and incubated wtih 1µM of DHR123 in PBS for 30 min at 37°C. Cells were then washed twice with PBS and collected in 500µl of ice-cold PBS for flow analysis using a Beckman Coulter

flow cytometer. Detection was set at excitation/emission at λ = 485/535 nm and unstained control samples were used to set appropriate gating according to forward and side scatter light. A total of 10,000 events per sample were recorded.

8-isoprostane assay

8-isoprostane levels were measured using an ELISA assay kit from Cayman Chemical (516351). Medium from cell cultures was collected and assayed immediately to avoid storage-induced sample degradation. For each sample, 50 µl of sample was combined with 50 µl of 8-Isoprostane acetylcholinesterase (AChE) Tracer, and 50 µl of 8-Isoprostane ELISA Antiserum prior to incubation for 18 hours at 4°C. The ELISA assay plate then washed five times with kit wash buffer. Each sample well received 200 µl of Ellman's Reagent and incubated for 90 minutes to facilitate detection. Absorbance was measured at 405 nm in 2-minute intervals until the blank-subtracted wells reached a minimum of 0.3 absorbance units. Sample absorbance results were compared to a 8-point standard curve. Assay results were normalized to cellular protein content as determined via modified Lowry protein assay (Bio-Rad DC™ protein assay).

Superoxide dismutase enzymatic activity assay

Superoxide dismutase activity was measured using an assay kit from Cayman Chemical (706002). Cells were washed with PBS, harvested in 300 µl of RIPA buffer, and stored at -20°C until assayed. For each sample, 10 µl of lysate was combined with 200 µl of radical detector. Enzymatic activity was initiated with the addition of 20 µl of xanthine

oxidase. The solutions were incubated for 20 min at 25°C and absorbance was measured at 450 nm. Sample absorbance results were compared to a 7-point superoxide dismutase activity standard curve to calculate sample enzyme activity. A modified Lowry protein assay (Bio-Rad DC™ protein assay) was subsequently performed to normalize superoxide dismutase activity for each sample to respective total protein content.

Antioxidant treatment

Three antioxidants were used to counter Snus-induced oxidative stress: ascorbic acid (AA; Sigma-Aldrich) [10 μM], dl-α-tocopherol acetate (vitamin E; Supelco, Sigma-Aldrich) [10 μM], and glutathione reduced ethyl ester (GSHOEt; Sigma-Aldrich) [500 μM]. Oxidants were added to medium concomitantly with Snus exposure during days 5-7 of differentiation. Antioxidant-containing medium was replaced with every media change.

Catalase enzymatic activity assay

Catalase activity was measured using an assay kit from Cayman Chemical (707002). Cells were washed with PBS, harvested in 300 μl of RIPA buffer, and stored at -20°C until assayed. For each sample, 20 μl of sample, 30 μl of methanol, and 20 μl of hydrogen peroxide substrate were combined to initiate the reaction. Sample solutions were incubated for 20 minutes at 25°C then subsequently the reactions were terminated with the addition of 30 μl of potassium hydroxide. Purpald, a chromogen, was added to colorimetrically measure catalase formaldehyde product formation. Finally, 10 μl of catalase potassium periodate was added to each sample. After a 5-minute incubation at

25°C, sample solution absorbance was measured at 540 nm. Sample absorbance outcomes were compared to a 7-point catalase formaldehyde standard curve. A modified Lowry protein assay (Bio-Rad DC™ protein assay) was also performed to normalize catalase activity for each sample to respective total protein content.

Glutathione peroxidase enzymatic activity assay

Glutathione peroxidase activity was measuring using an assay kit from Cayman Chemical (703102). Cells were washed with PBS, harvested in 300 µl of RIPA buffer, and stored at -20°C until assayed. For each sample, 20 µl of sample, 50 µl of assay buffer, 50 µl of co-substrate mixture, and 50 µl of NADPH were combined. Cumene hydroperoxide was added at a volume of 20 µl to initiate the reactions. Absorbance was read at 340 nm initially and once every 10-minutes for a total of 5 minutes.

Sample absorbance outcomes were compared to a 6-point glutathione peroxidase activity standard curve. A modified Lowry protein assay (Bio-Rad DC™ protein assay) was performed to normalize glutathione peroxidase activity for each sample to respective total protein content.

Hydrogen peroxide treatment

To assess the effects of ROS alone on osteogenic differentiation, cells were treated with 0.5 µM hydrogen peroxide. Hydrogen peroxide was added to cell culture medium during specified windows of osteogenic differentiation: days 0-3, days 3-5, days 3-7, days 5-7, and days 7-20.

Real-time quantitative (qPCR)

Changes in *FOXO1* and *FOXO3A* mRNA gene expression were assessed using real-time quantitative PCR (qPCR) analysis. cDNA was synthesized using 25ng of total RNA as a template and a cDNA mastermix: 5x reaction buffer, 1.25µl 10mM dNTPs, 1.25µl 400U/µl RNase inhibitor, 0.1µl 200 U/µl reverse transcriptase, 0.1µl 3µg/µl random primer, and 1.5µl DEPC H_2O. A total volume of 25µl per cDNA reaction was used. iQ SYBR Green Supermix (Bio-Rad) was used to measure relative expression on the CFX Connect thermocycler system (Bio-Rad). Reactions were programmed for 5 minutes of initial denaturing at 94°C, followed by 40 cycles of denaturing at 94°C for 45 seconds and annealing at 60°C for 45 seconds. The ΔΔCT method was used to calculate n-fold expression in target gene expression by normalizing target Ct values to their respective *GAPDH* expression values. and 5'-GGGGTTCGAAATGAGGATGC-3'. Primer sequences for Primer sequences for human *FOXO1* were 5'- TAGCATAAACCTGGGCCCAA-3' and 5'- ACCCAGCTTGCCCATTACTCT-3', *FOXO3A* were 5'- CGCACCAATTCTAACGCCAG-3' and 5'- CTGCCATATCAGTCAGCCGT-3', human *GAPDH* were 5'-ACAGTCAGCCGCATCTTCTT-3' and 5'-ACGACCAAATCCGTTGACTC-3'.

Whole cell protein lysis and western blotting

Cells were pretreated for 30 minutes with 1mM sodium orthovanadate to inhibit protein tyrosine phosphatases. Cells were subsequently lysed with protein RIPA buffer (pH 7.4 150 mM NaCl, 2 mM EDTA, 50 mM Tris-HCl pH 7.4, 1% NP-40, 0.5% sodium

deoxycholate, 0.1% sodium dodecyl sulfate (SDS), 1mM sodium orthovanadate, 1mM sodium fluoride, 1mM phenylmethylsulfonyl fluoride (PMSF), 1:100 Halt Protease Inhibitor Cocktail (ThermoFisher). Protein concentration was measured via a modified Lowry protein assay (Bio-Rad DC™ protein assay). Equal amounts of protein per sample were loaded into a 6%-10% SDS/polyacrylamide gel. Proteins were separated by electrophoresis then electrophoretically transferred to a polyvinylidene difluoride (PDVF) membrane. Membranes were blocked in 5% milk or 5% bovine serum albumin (BSA) (for phospho proteins) in tris-buffered saline with tween 20 (TBS-T) for 30 minutes at 25°C on an orbital shaker. Membranes were incubated with one of the following antibodies for 2 hours at 25°C on an orbital shaker: rabbit anti-FOXO3a (abcam, ab70315), rabbit anti-FOXO1 (abcam, ab61760), rabbit anti-FOXO3 (S253) (CST, 9466), rabbit anti-FOXO1 (S256) (CST, 9461), rabbit anti-phospho AKT (S473) (CST, 4060), rabbit anti-AKT (abcam, ab8805), rabbit anti-phospho AMPKα (T172) (CST, 50081S), rabbit anti-AMPKα (abcam, ab32047), rabbit anti-phospho ERK1/2 (T202/Y204) (CST, 9101), rabbit anti-ERK1/2 (CST, 4695S), rabbit anti-phospho JNK1/2 (T185/Y185) (abcam, ab4821), rabbit anti-JNK1/2 (abcam, ab112501), mouse anti-TBP (abcam, ab51841), mouse anti-beta actin (CST, 3700) and mouse anti-tubulin (CST, 2146). Membranes were then incubated for 1 hour at 25°C with horseradish peroxidase-conjugated anti-rabbit (CST 7074S) or anti-mouse (CST 7076S) secondary antibody. Bands were visualized using chemiluminescence substrate (SuperSignal West Pico PLUS Chemiluminescent Substrate, ThermoFisher) and the Bio-Rad ChemiDoc MP System imager.

Phospho-AKT protein array

Snus-induced disruption of the AKT and related signaling pathways was assessed according to phosphorylation changes at 72 distinct protein phosphorylation sites using an AKT Pathway Phospho Antibody Array (PAA137; Full Moon BioSystems) and Antibody Array Assay Kit (KAS02; Full Moon Biosystems). Whole cell protein lysates were collected as described above with additional mechanical lysis as outlined by the assay kit protocol. Protein lysates were purified and RIPA buffer exchanged for array kit labeling buffer using exchange columns provided by the assay kit. Protein concentration in each sample was measured by modified Lowry protein assay (Bio-Rad DC™ protein assay) and 150 µg of protein for each sample was biotin-labeled. Array slides were blocked in kit blocking buffer for 45 minutes at 25°C on an orbital shaker before subjection to thorough rinses in Milli-Q grade water. Biotin-labeled protein lysates were subsequently coupled to array slides by incubating protein lysates and array slides in kit coupling buffer for 2 hours at 25°C. Array slides were thoroughly rinsed in in Milli-Q grade water and incubated in kit detection buffer with 1:1000 0.5 mg/ml Cy3-streptavidin (ThermoFisher) for 20 minutes at 25°C. Cy3-streptavidin was introduced to slide to allow streptavidin to bind biotin-labeled proteins and thus fluorescently label biotin-labeled proteins that have been captured on the slide. Slides were rinsed well with Milli-Q grade water and air-dried via centrifugation at 1300 x *g* for 10 minutes. Slides were scanned for imaging and collection using a GenePix® Microarray Scanner. For each sample, mean fluorescence intensity for each protein was normalized to respective mean actin signal to allow for comparison between slides. Normalized signal intensities were used to perform visual heatmap analysis

and clustering to using the limma [27], dplyr [28], and gplots [29] packages in RStudio 0.99.903 [30]. Normalized signal intensities were also subjected to log2 transformation for statistical analysis of protein and phosphorylation fold changes between treatment groups. Fold changes of greater than

AKT inhibitor treatment

AKT inhibitor (AbMole, M4988) was used to explore the specific impact of AKT1 and AKT2 isoforms on osteogenic differentiation. AKT inhibitor (58 nM AKT1; 210 nM AKT2) was added to culture medium on days 5-7 of differentiation, with fresh inhibitor replaced every 24 hours.

JNK activator treatment

JNK1/2 activator treatment was used to investigate the influence of supplemented JNK activity with concurrent Snus exposure. JNK activator (0.01 μM; AbMole, M5145) was added to culture medium on days 5-7 of differentiation, with fresh inhibitor replaced every 24 hours.

Dual-energy X-ray absorptiometry (DXA) Analysis

Skull bone mineral density and bone mineral content measurements for 13-month-old mice PBS or Snus exposed mice were acquired from DXA using the UltraFocus^{DXA} (Faxtiron®). Mouse *in utero* exposures were performed as described above.

Statistical analysis

One-way analysis of variance (ANOVA) statistical testing followed by Moses Test of Extreme Reactions and Mann-Whitney U tests were used to determine statistical differences in *in vivo* experimental parameters. One-way analysis of variance (ANOVA) statistical testing followed by a paired student's t-test was used to identify the lowest concentrations at which *in vitro* calcification or cell viability dropped below that of the untreated control. Differences between exposure outcomes mediated by half-maximal inhibitory doses for differentiation (ID_{50}) and cell viability (IC_{50}) were assessed with a one-way ANOVA followed by an appropriate post hoc test (GraphPad QuickCalcs). For all assessments, *P*-values below 0.05 were considered significant.

Results

In utero exposure to Snus extract does not elicit maternal toxicity or excessive cytotoxicity in exposed pups

Before evaluating the effects of *in utero* exposure on embryonic development, dams were assessed for signs of maternal toxicity that could influence adverse outcomes in pups. Parameters were selected based on their classic use in *in vivo* teratology assessments [31]. Normal progression of pregnancies was measured by semi-daily evaluation of maternal weight gain from E0.5 through termination of the pregnancy at E17.5. PBS- and Snus-exposed dams demonstrated similar trends in weight gain, with no noted significant deviations (Fig. 5.1A). Similarly, no difference in total pregnancy weight gain was observed between PBS- and Snus- exposed dams (Fig. 5.1B). Gross necropsy of maternal

organs (not shown) did not indicate signs of maternal toxicity in Snus-exposed dams. Maternal organ masses respective to body weight were not significantly different between PBS- and Snus-exposed mice (Fig. 5.1D, 1E, 1F, 1G). Histopathological assessment of dam livers did not find any evidence of maternal liver toxicity (Fig. 5.1D).

Litter and pup parameters were also assessed for evidence of cytotoxic effects on the exposed embryos. Late-stage embryo loss or resorptions were quantified at E17.5. No significant differences in resorptions were found between PBS- and Snus-exposed dams (Fig. 5.1C). Litter sizes were not significantly different between PBS- and Snus-exposed pups, though some Snus-exposed dams did produce smaller litter sizes than those observed in PBS dams (Fig. 5.1H). Pup and placental masses were not significantly changed between PBS- and Snus-exposed litters (Fig. 5.1I, J). Gross necropsy of fetal placentas (not shown) did not show evidence of placental injury. The ratio of placental mass to respective pup mass was not significantly different either (Fig. 5.1K). Collectively, these data suggest that *in utero* Snus extract exposure did not elicit cytotoxic effects on maternal, placental, or fetal tissues.

Normal pup morphological development and skull mineralization is disrupted by Snus in utero

PBS- and Snus-exposed pups were visually and quantitatively assessed for changes in overall and skeletal morphology. Gross morphological evaluation (Fig. 5.2A) did not find any striking alterations in Snus-exposed offspring compared to the PBS group. Snus-exposed mice did, however, demonstrate quantitative differences in overall morphology.

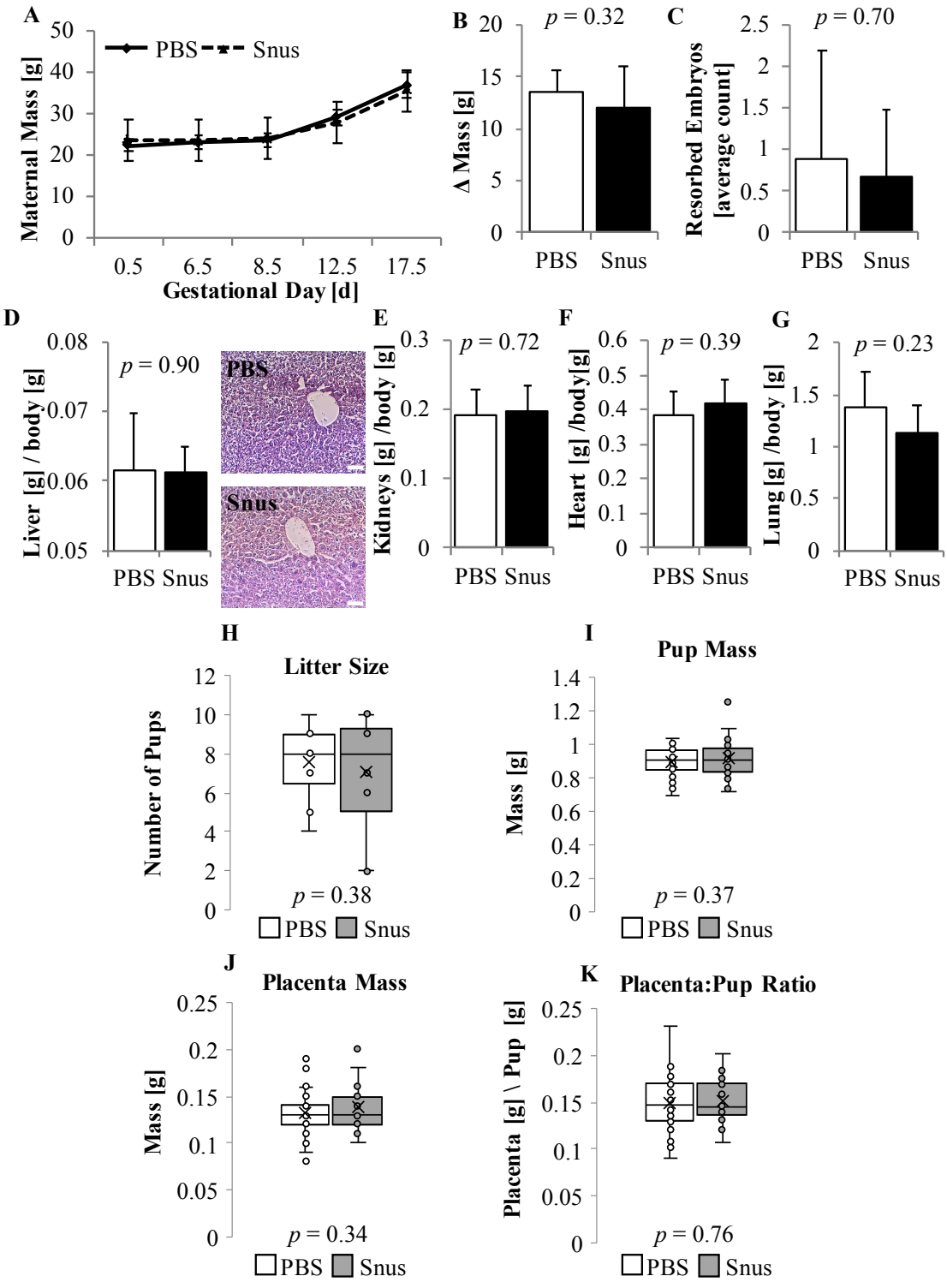
A
Maternal Mass [g]
PBS
Snus
Gestational Day [d]
B
Δ Mass [g]
p = 0.32
C
Resorbed Embryos [average count]
p = 0.70
D
Liver [g] / body [g]
p = 0.90
PBS
Snus
E
Kidneys [g] /body [g]
p = 0.72
F
Heart [g] /body[g]
p = 0.39
G
Lung [g] /body [g]
p = 0.23
H
Litter Size
Number of Pups
p = 0.38
I
Pup Mass
Mass [g]
p = 0.37
J
Placenta Mass
Mass [g]
p = 0.34
K
Placenta:Pup Ratio
Placenta [g] \ Pup [g]
p = 0.76

Figure. 5.1. *In utero* Snus exposure did not impart maternal toxicity or reduce pup viability. *In vivo* pregnancies were monitored for signs of maternal toxicity or cytotoxic effects on pups. A) Gestational weight gain patterns did not significantly deviate between PBS- and Snus- exposed dams. $^{\Delta}p<0.05$ represents a significant shift in maternal mass on E0.5 for PBS-exposed dams. $p^{*}<0.05$ represents a significant shift in maternal mass on E0.5 for Snus-exposed dams. *P*-values were determined using One-way ANOVA. B) PBS- and Snus-exposed dams gained similar amounts of weight over the course of pregnancy. C) No difference was observed in the average incidence of late stage resorptions (embryo loss) in PBS and Snus exposed litters. D-G) Maternal organ masses were also evaluated for signs of maternal toxicity. Liver, kidney, heart, and lung masses were not significantly different for Snus-exposed dams. Moreover, liver sections from livers of Snus-exposed dams did not show any signs of pathology. Bar = 0.5 mm. H) Some Snus-exposed dams produced litters with fewer pups, though no significant distance in overall litter size was found. I-K) Pup and placental masses as well as placental-to-pup mass ratio were not significantly different between PBS and Snus exposed litters. PBS dams n = 10. Snus dams n = 10. PBS pups n = 119. Snus pups n = 101.

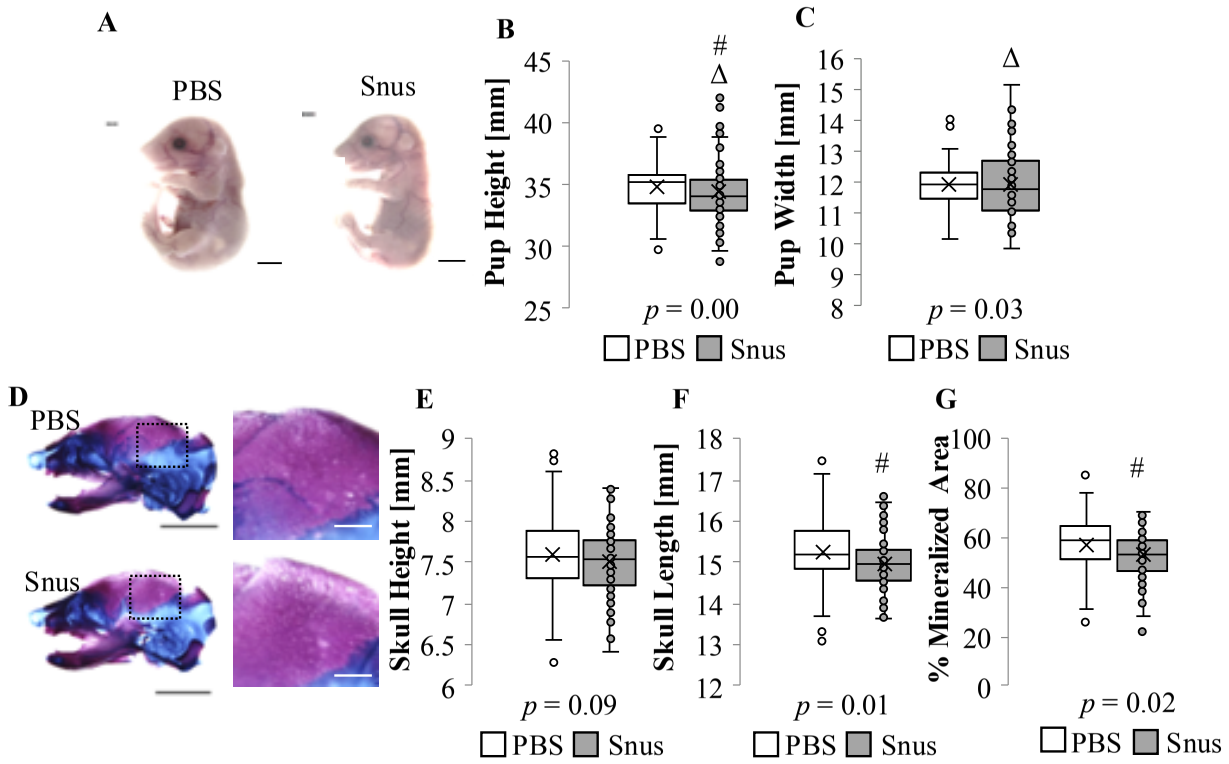

Figure. 5.2. *In utero* Snus exposure interferes with normal pup morphology. A) Gross morphological assessments did not note any visual differences between PBS- and Snus-exposed litters. Bar = 5 mm. B) Pup height was significantly reduced in Snus-exposed litters. C) Pup width varied significantly. D) Snus-exposed pups featured consistent porosity in the parietal bone of the skull. Bar = 5 mm. E-F) While no difference in skull height was observed between PBS and Snus exposed litters, skull length was significantly reduced in Snus litters. G) Percentage of total mineralized skull area was also significantly reduced in Snus exposed pups. $^{\#}p<0.05$ represents a significant deviation as measured by the Mann-Whitney U Test. $^{\Delta}p<0.05$ represents a significant deviation as measured by the Moses Test of Extreme Reaction. PBS pups n = 119. Snus pups n = 101.

Pup height (crown-to-rump) varied significantly between Snus and PBS mice (Fig. 5.2B) while pup width (across the widest part of the pup) was significantly increased compared to PBS-exposed mice (Fig. 5.2C). Skull length was also affected by Snus exposure, with a significant reduction in length compared to PBS-exposed pups (Fig. 5.2F). No difference was observed in skull height between both groups (Fig. 5.2E).

Histochemical staining of pup skeletons revealed a pattern of increased porosity in the parietal bone of the skull (Fig. 5.2D) for Snus-exposed pups. Further, the total percentage of mineralized skull area was found to be significantly reduced in Snus-exposed pups, compared to PBS-exposed offspring (Fig. 5.2G). Evaluation of Snus-exposed pups at approximately 1 year of age suggested long-term persistence of impaired bone function (Appendix Fig. 1.5.1).

Human osteoblast differentiation is negatively impacted by Snus at sub-cytotoxic doses

The capacity of Snus extract to induce differentiation defects and cytotoxicity was also assessed in human embryonic stem cells (hESCs) undergoing osteogenic differentiation. Cell survival and osteogenic output were measured on day 20 of differentiation, when hESC-derived osteogenic cultures express osteoblast markers [32]. While dose-dependent reductions in cell viability and osteogenesis were both observed (Fig. 5.3A), osteogenic inhibition occurred in both non-cytotoxic and cytotoxic doses. This duality suggests that at mid-range doses Snus extract inhibited osteogenesis without concurrently inducing cell death. Dose-dependent reductions in cell viability were also observed in hFFs exposed to Snus extract (Fig. 5.3A). Half-maximal concentrations for

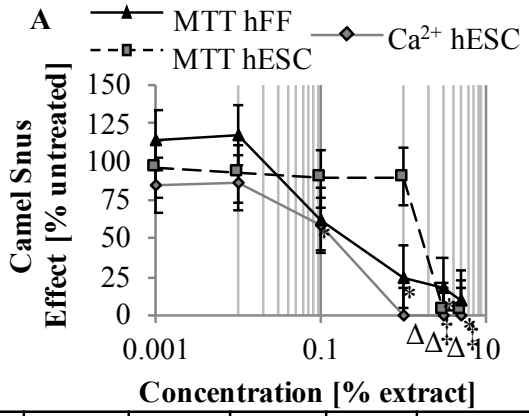

	IC50 HFF	IC50 H9	ID50 H9	class	categorization
Snus	0.29 ± 0.36	1.70 ± 0.41	0.15 ± 0.12	III	Strongly embryotoxic

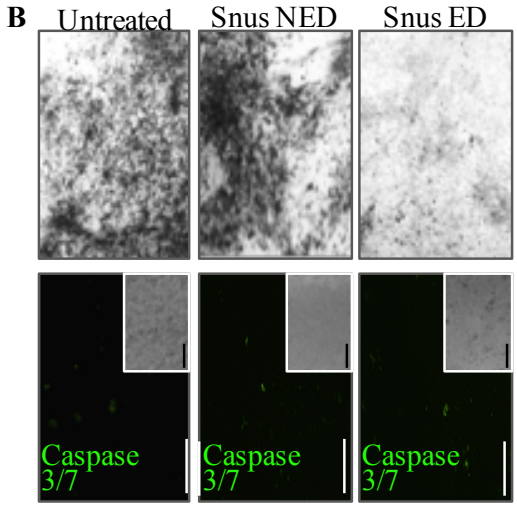

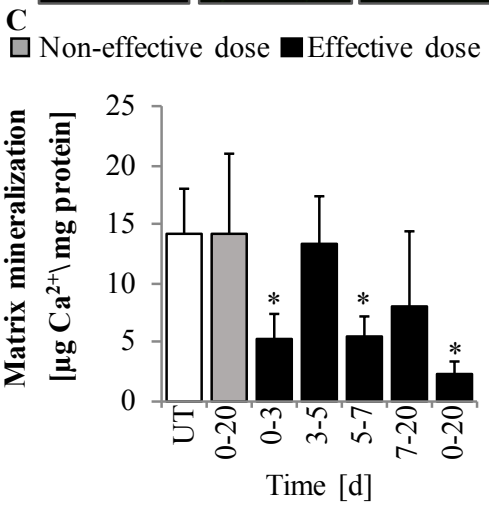

Figure 5.3. Snus inhibits *in vitro* osteogenic differentiation at sub-cytotoxic doses. Human ESCs were treated with different concentrations of Snus extract as they were differentiated into osteoblasts. Cultures were evaluated for differentiation inhibition and cell viability via calcium and MTT assays, respectively. A) Snus exposure reduced osteogenesis and cell viability in a dose-dependent manner. Differentiation inhibition was observed in the absence of cytotoxicity. Using the EST biostatistical model, Snus was classified as strongly embryotoxic. B) Snus exposure failed to activate executioner caspases 3 and 7, suggesting the absence of active apoptosis concurrent with an osteogenic defect. Bar = 100 μm. C) Snus seems to impart a time-dependent effect on differentiation inhibition—suggesting additional mechanisms are responsible for observed inhibition of Snus-dependent osteotoxicity. Snus inhibition of osteogenesis was most potent during early differentiation periods, as later time point exposures did not negatively impact osteogenesis. $^{*, ‡, Δ}P<0.05$ represents the lowest concentration of Snus exposure that features significant reduction in given parameter as compared to the untreated control, as determined by One-Way ANOVA. hFF, human foreskin fibroblast; hESC, human embryonic stem cell; NED, non-effective dose; ED, effective dose.

cytotoxicity (IC_{50}MTT hESCs, IC_{50} hFF MTT) and differentiation inhibition (ID_{50} hESCs) were obtained from concentration-response curves. Half-maximal concentration input into the embryonic stem cell test (EST) biostatistical model [33] classified Snus as strongly embryotoxic (Fig. 5.3A).

Snus effective (ED) and non-effective (NED) doses were also determined from the dose-response curve. The effective dose was defined as the dose that reduced calcification to 50% (0.1% Snus extract), while the non-effective dose was the lowest Snus dose that did not elicit any reduction in calcification (0.001% Snus extract) (Fig. 5.3A). An active apoptosis response was absent in both Snus NED and ED treatment groups, as indicated by a lack of active executioner caspase 3 and 7 species (Fig. 5.3B). This result followed trends observed in the initial dose-response curve and suggested that mechanisms specific to osteogenic differentiation were disturbed upon Snus exposure. Further investigation revealed that Snus-mediated disruption of osteogenesis was dependent on time-of-exposure during the differentiation process (Fig. 5.3C). Targeted early exposures during days 0-3 or days 5-7 of differentiation significantly reduced osteogenic outcomes on day 20 of differentiation exclusively. Notably, late stage Snus exposure during days 7-20 of differentiation did not significantly inhibit osteogenic differentiation.

Snus-mediated embryotoxicity occurs concurrently with induction of oxidative stress conditions

Disease pathogenesis and teratogenic outcomes have been previously ascribed to excessive ROS generation [34-39] that causes a state of imbalance between reducing and

oxidizing cellular counterparts known as oxidative stress [40]. To investigate if Snus exposure encouraged oxidative stress conditions, several ROS species and markers of oxidative stress were evaluated. Cellular levels of two ROS species, superoxide anion ($\bullet O2^-$) and hydrogen peroxide (H_2O_2), were significantly increased in Snus ED cultures (Fig. 5.4A). Levels of 8-isoprostane, a well-established biomarker of oxidative stress and oxidative lipid damage [41-43], were also significantly increased in Snus ED cultures (Fig. 5.4A).

Assessments to investigate causality between ROS and poor osteogenic outcomes found evidence for ROS-mediated inhibition of osteogenesis. Dosing differentiating osteoblasts with hydrogen peroxide alone during defined windows of osteogenesis significantly reduced osteogenic output in all tested time points (Fig. 5.4C). Co-treatment of Snus effective dose cultures with antioxidants rescued mineralization in cultures co-treated with ascorbic acid or glutathione reduced ethyl ester (Fig. 5.4B). Vitamin E did not significantly rescue osteogenic output. Together, these data suggest that elevated ROS contributes to Snus-mediated osteogenic inhibition.

Follow up analysis evaluated the activity of endogenous antioxidant enzymes responsible for the degradation of superoxide anion and hydrogen peroxide ROS species. Superoxide dismutase enzyme species convert superoxide anion into hydrogen peroxide and oxygen (O_2) molecules. Hydrogen peroxide can be subsequently processed by glutathione peroxidase and catalase enzymes into water and O_2 [44]. Superoxide dismutase and catalase activity was significantly reduced in Snus ED cultures (Fig. 5.4D), suggesting Snus-facilitated inhibition of normal activity for these enzymes. Glutathione peroxidase

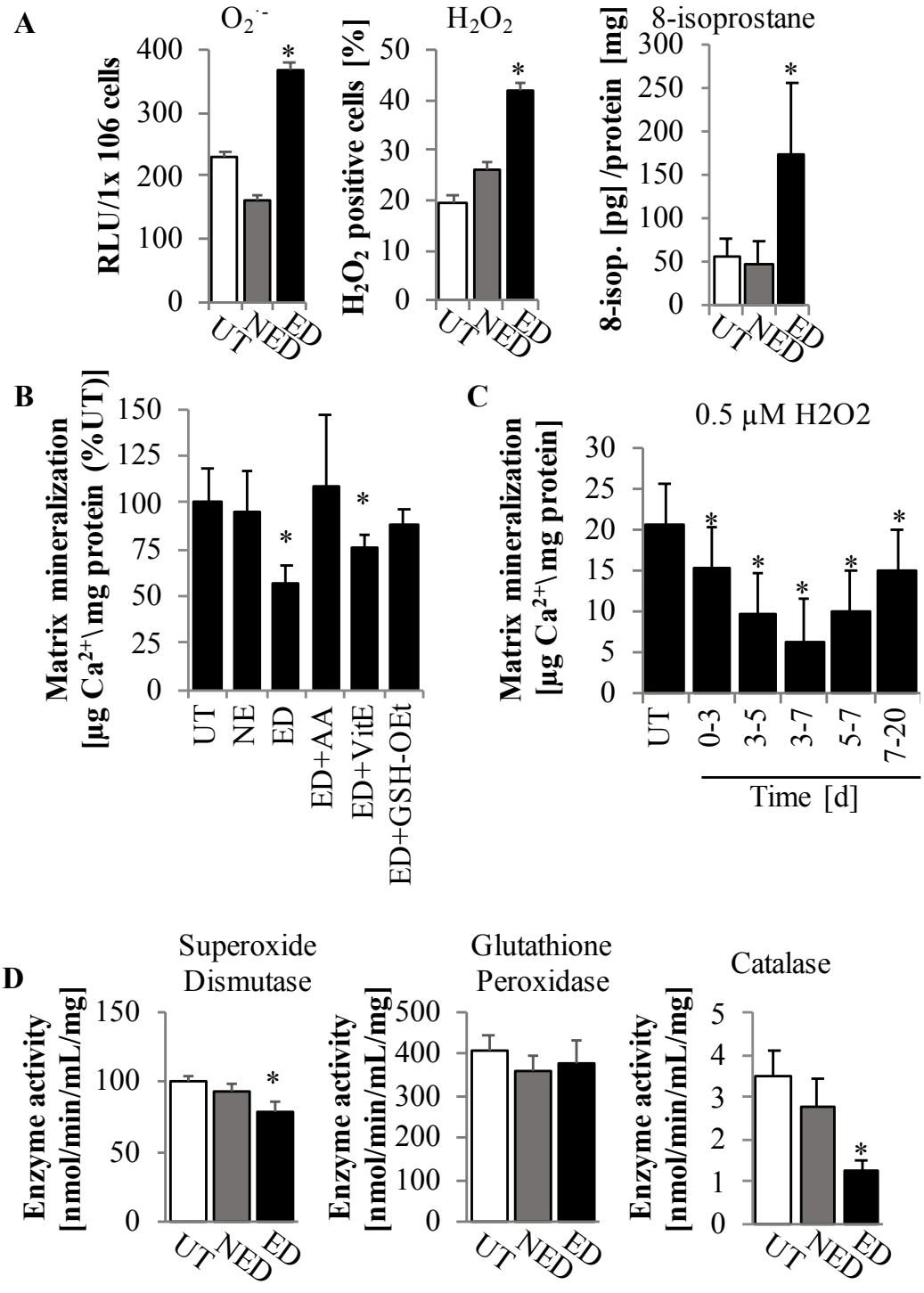
A
$O_2^{\cdot-}$
RLU/1x 106 cells
400
300
200
100
0
UT
NED
ED
H_2O_2
H_2O_2 positive cells [%]
50
40
30
20
10
0
8-isoprostane
8-isop. [pg] /protein [mg]
300
250
200
150
100
50
0
B
Matrix mineralization
[µg Ca^{2+}\mg protein (%UT)]
150
125
100
75
50
25
0
UT
NE
ED
ED+AA
ED+VitE
ED+GSH-OEt
C
0.5 µM H2O2
Matrix mineralization
[µg Ca^{2+}\mg protein]
30
25
20
15
10
5
0
UT
0-3
3-5
3-7
5-7
7-20
Time [d]
D
Superoxide Dismutase
Glutathione Peroxidase
Catalase
Enzyme activity
[nmol/min/mL/mg]
150
100
50
0
500
400
300
200
100
0
5
4
3
2
1
0
UT
NED
ED

Figure 5.4. Snus exposure elicits oxidative stress. A) Superoxide anion, hydrogen peroxide, and 8-isoprostane content was significantly increased in Snus-exposed ED cultures. Superoxide anion content was measured via luminol-based reaction and reported as RLU output per a defined number of cells. Hydrogen peroxide content was measured using dihydrorhodamine 123. 8-isoprostane was measured via ELISA. n=3±SD. B) Concurrent treatment of Snus ED cultures with antioxidants ascorbic acid and glutathione reduced ethyl ester rescued osteogenic output. C) Exposing differentiating osteoblasts to hydrogen peroxide alone inhibited differentiation at any stage of osteogenesis. D) Endogenous antioxidant enzyme activity for SOD and catalase species were significantly reduced in Snus ED. GPx activity was not significantly affected by Snus exposure. n=3±SD. $^{*}P<0.05$ represents a significant deviation for a given measured parameter compared to the untreated control, as determined by One-Way ANOVA. AA, ascorbic acid; VitE, vitamin E; GSH-OEt, glutathione reduced ethyl ester; RLU, relative light unit; H_2O_2, hydrogen peroxide; UT, untreated; NED, non-effective dose; ED, effective dose; $O_2^{\cdot -}$, superoxide anion.

activity, however, was not significantly altered between either of the groups (Fig. 5.4D).

Overall, these results infer that Snus exposure induces molecular or biochemical changes that reduce antioxidant enzyme activity and increase ROS levels that could alter cellular behavior and differentiation outcomes.

Snus exposure reduces nuclear levels of key redox transcription factors FOXO1 and FOXO3A

The forkhead box, class O (FOXO) family of transcription factors are well-reported mediators of oxidative stress defense and cellular stress response [45, 46]. Given that FOXO activates transcription of MnSOD and catalase mRNA expression, *FOXO1* and *FOXO3a* mRNA expression and protein content were investigated in Snus-exposed hESC cultures. Reduced mRNA expression was observed for both *FOXO1* and *FOXO3a* with increasing Snus dose (Fig. 5.5A). Western blot and densitometry analysis revealed that Snus ED reduced nuclear levels of both FOXO1 and FOXO3A (Fig. 5.5B), though a more dramatic reduction was observed for FOXO3A. To investigate if reduced FOXO1 and FOXO3A levels during differentiation alone could impact osteogenic outcomes, FOXO1/3a knockdown mESCs were differentiated into osteoblasts against wild-type D3 mESCs. Generally, differentiations with wild-type cells produced more robust osteogenic output compared to differentiated shFOXO1/3a cells (Fig. 5.5C), suggesting an influential role for FOXO1 and/or FOXO3a during normal osteogenic differentiation. When concurrently exposed to Snus, both wild-type and shFOXO1/3a cultures showed similar responses in that Snus ED significantly reduced osteogenic output compared (Fig. 5.5C).

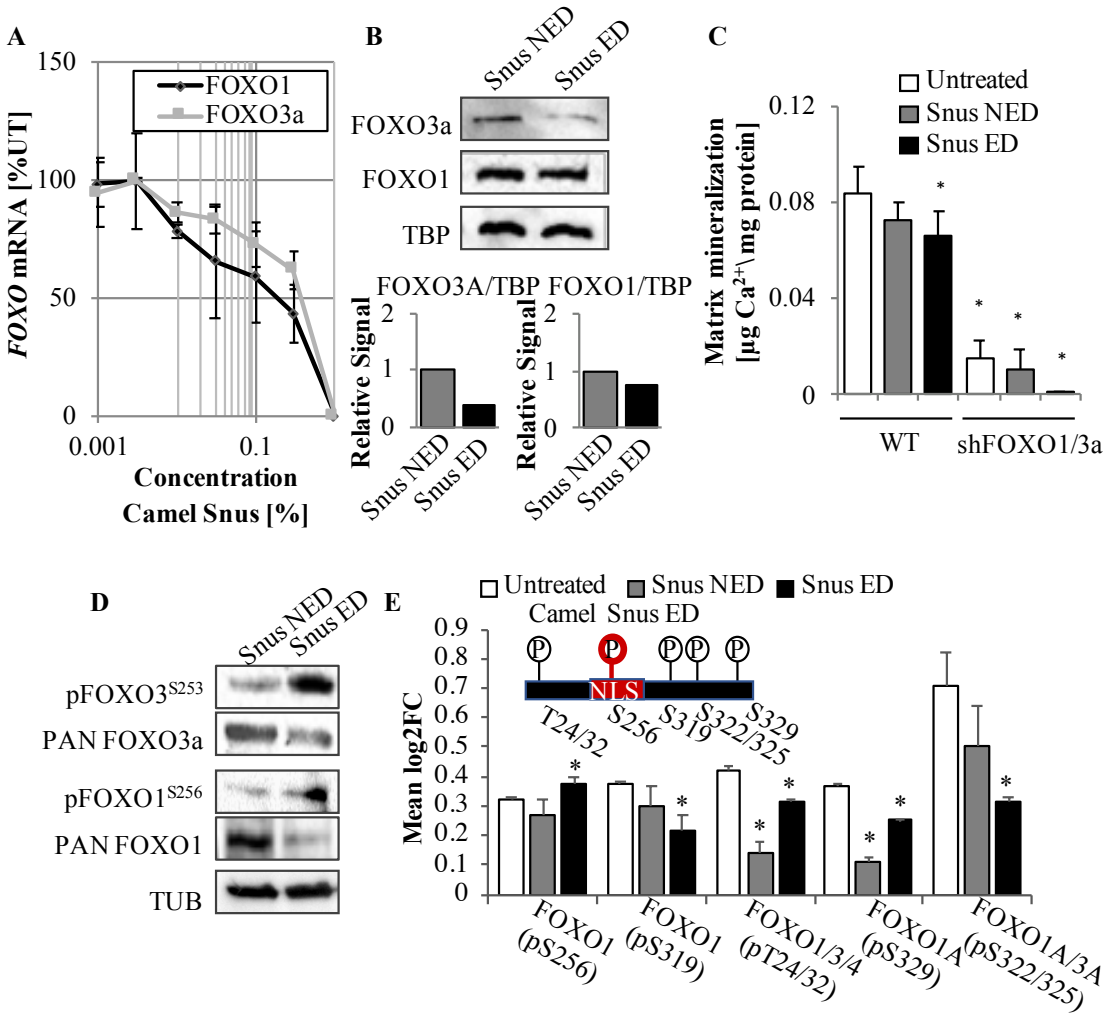
A
150
100
50
0
0.001
0.1
FOXO1
FOXO3a
FOXO mRNA [%UT]
Concentration
Camel Snus [%]
B
Snus NED
Snus ED
FOXO3a
FOXO1
TBP
FOXO3A/TBP FOXO1/TBP
Relative Signal
2
1
0
Snus NED
Snus ED
C
Untreated
Snus NED
Snus ED
Matrix mineralization
[µg Ca2+\ mg protein]
0.12
0.08
0.04
0
WT
shFOXO1/3a
D
Snus NED
Snus ED
pFOXO3S253
PAN FOXO3a
pFOXO1S256
PAN FOXO1
TUB
E
Untreated
Snus NED
Snus ED
Camel Snus ED
P
NLS
T24/32
S256
S319
S322/325
S329
Mean log2FC
0.9
0.8
0.7
0.6
0.5
0.4
0.3
0.2
0.1
0
FOXO1 (pS256)
FOXO1 (pS319)
FOXO1/3/4 (pT24/32)
FOXO1A (pS329)
FOXO1A/3A (pS322/325)

Figure 5.5. Snus exposure alters nuclear localization of FOXO1 and FOXO3a transcription factors via phosphorylation at S253 and S256 residues in osteogenic hESC cultures. A) Snus exposure reduced *FOXO1* and *FOXO3a* mRNA expression in a dose-dependent manner. B) Nuclear levels of FOXO1 and FOXO3a are reduced in Snus ED cultures. C) Knockdown of FOXO1 and FOXO3a reduces osteogenic output. This reduction is enhanced with the addition of Snus ED. $^{*}P<0.05$ represents a significant deviation for a given measured parameter compared to the untreated wild-type control, as determined by One-Way ANOVA. $^{\Delta}P<0.05$ represents a significant deviation for a given measured parameter compared to the untreated shFOXO1/3a control, as determined by One-Way ANOVA. D) FOXO1 and FOXO3a featured enhanced phosphorylation of S253 and S256, respectively, in Snus ED. These phosphorylation events are responsible for reduced DNA binding of FOXO1 and FOXO3a as mediated by AKT activity. E) Additional anti-nuclear FOXO1 and FOXO3a phosphorylation events were assessed via protein array. AKT-mediated T24/32 phosphorylation and CK1-driven p322/325 phosphorylation were non-significantly reduced in Snus ED. Significant reductions in FOXO1 phosphorylation at AKT-mediated S319 and DYRK1-mediated S329 were significantly reduced in Snus ED. $^{*}P<0.05$ represents a significant deviation in log2 fold change as compared to the untreated control, as determined by One-Way ANOVA. UT, untreated; NLS, nuclear localization signal; NED, non-effective dose; ED, effective dose; TUB, Tubulin; WT. wild-type.

Changes in cellular redox state have also been reported to influence posttranslational modification patterns in FOXOs that can direct FOXO subcellular localization and activity [47]. AKT-mediated phosphorylation at nuclear exclusion sites S253 and S256 were evaluated for FOXO1 and FOXO3A, respectively, via western blot (Fig. 5.5D). Increased phosphorylation was observed at each residue in Snus ED cultures, indicating that Snus exposure targets FOXO1 and FOXO3a isoforms for nuclear exclusion through AKT. Additional AKT FOXO1 and FOXO3a phosphorylation sites were investigated via protein array (Fig. 5.5E). AKT-mediated phosphorylation at FOXO1/3a T24/32 residues and FOXO1 S319 were reduced in Snus ED cultures. Nuclear exclusion phosphorylation events driven by CK1 on FOXO1/3a S322/325 and DYRK1 on FOXO1 S329 were also reduced. Given that phosphorylation at S256/3 also obscures the FOXO1/3a nuclear localization signal region of FOXO1/3a, observed reductions in other FOXO1/3a phosphorylation patterns suggest that AKT phosphorylation at S256/253 may the critically misregulated phosphorylation marker in the context of Snus-exposure.

Collectively, these results suggest that Snus exposure misregulates FOXO1 and FOXO3a at the transcriptional and post-translational level. Snus extract appears to stimulate nuclear exclusion of FOXO1 and FOXO3a by modulating specific phosphorylation by AKT that redirects FOXO subcellular localization. Downstream, this misregulation of FOXO1 and FOXO3a could cause poor osteogenic outcomes.

Snus exposure exerts differential effects on key players of PI3K/AKT signaling pathway

Global misregulation of the AKT signaling pathway by Snus exposure was

investigated using a commercially available phospho protein array that featured key signaling partners and targets involved in AKT signal propagation and crosstalk. Array analysis revealed unique differences in posttranslational phosphorylation modifications between untreated, non-effective, and effective doses (Fig. 5.6A, B). Comparing non-effective and effective doses alone identified 18 unique deviations in AKT-signaling related protein profiles in Snus ED cultures (Fig. 5.6C).

Snus ED cultures demonstrated unique phosphorylation patterns that suggested increased IRS1/PI3K signaling events (Fig. 5.6D). Levels of inactivated $pIRS1^{S312}$ [48] were significantly reduced in Snus ED cultures, implying an increase in active IRS1 proteins upstream of PI3K activation. Snus exposure also significantly increased levels of activated pPI3K regulatory subunit $p85\alpha/\gamma^{Y467/Y199}$ protein, supporting implications of increased activation of PI3K signaling activities as well [49]. In addition, triple phosphorylated $pPTEN^{S380/T382/T383}$ was significantly reduced in Snus ED exposed cells. Given that PTEN activity reverses PI3K signaling, this result also suggests Snus-mediated increases in PI3K signaling activity. Together, these data provide support for Snus-mediated alterations of signaling events upstream of AKT that may lead to aberrant AKT activation.

Our results also indicated a potential for differential regulation of downstream IRS1/PI3K targets. Conspicuously, levels of phosphorylated PI3K downstream kinase $pPDK1^{S241}$ were significantly reduced in Snus ED cells inferring downstream interference with the propagation of the PI3K signaling cascade through the PDK1 signaling arm (Fig. 5.6D). PDK1 is a well-reported key player in mediating translational machinery through

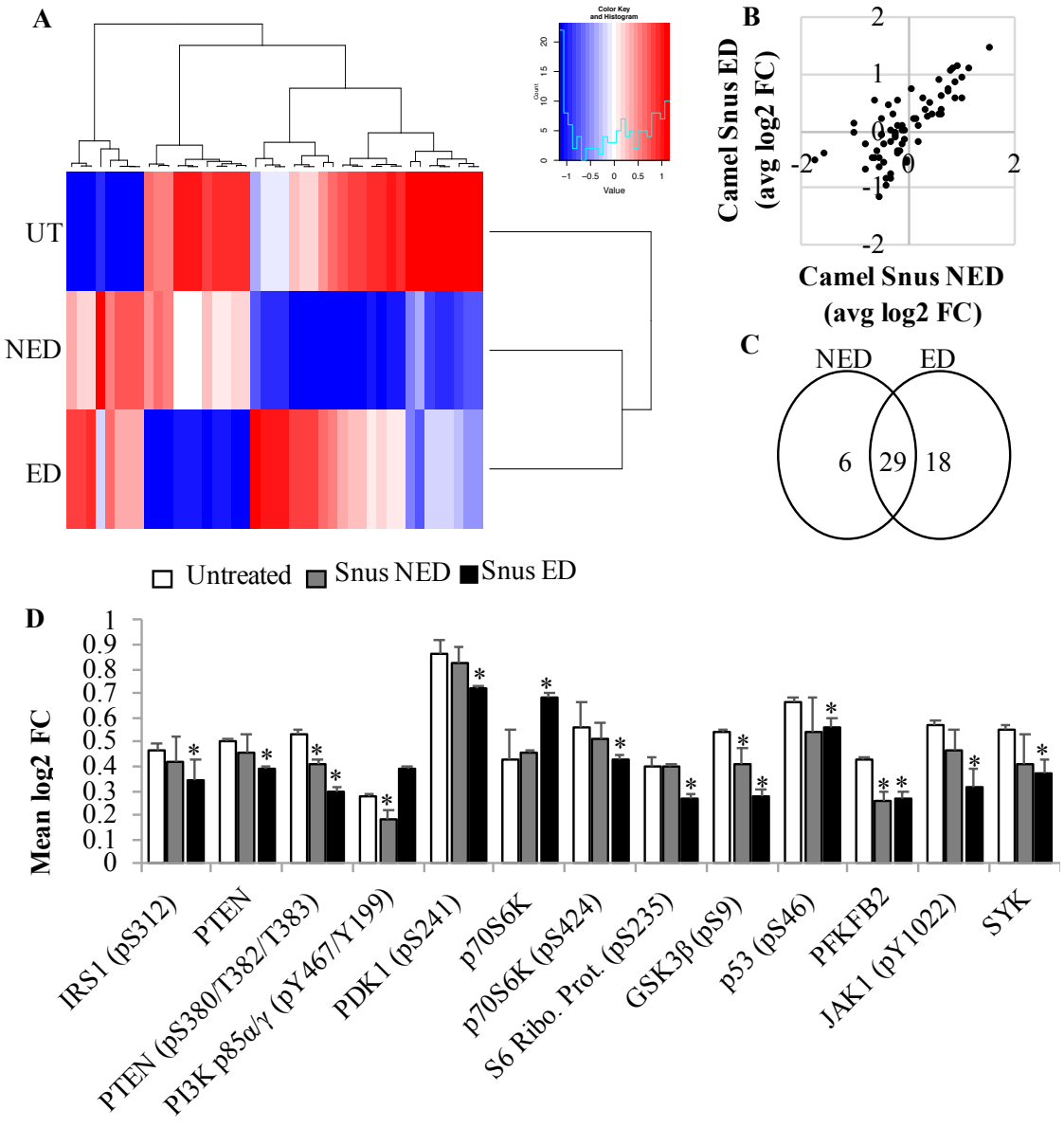
A
Color Key and Histogram
Count
Value
UT
NED
ED
B
Camel Snus ED (avg log2 FC)
Camel Snus NED (avg log2 FC)
C
NED
ED
6
29
18
Untreated
Snus NED
Snus ED
D
Mean log2 FC
IRS1 (pS312)
PTEN
PTEN (pS380/T382/T383)
PI3K p85α/γ (pY467/Y199)
PDK1 (pS241)
p70S6K
p70S6K (pS424)
S6 Ribo. Prot. (pS235)
GSK3β (pS9)
p53 (pS46)
PFKFB2
JAK1 (pY1022)
SYK

Figure 5.6. Snus exposure disrupts key players in the AKT signaling pathway. A) Heatmap visualization showing differential phosphorylation patterns for various protein targets involved in AKT signaling as revealed by AKT signaling protein array. B) Comparative analysis of pathway target protein phosphorylation and content patterns found 29 common elements between Snus NED and ED. Six elements were exclusively featured in the NED, while 18 elements included exclusively in the Snus ED group. C) AKT1 and AKT2 isoforms were differentially regulated in Snus ED exposed cultures. Snus ED exposure significantly upregulated AKT1 activation and significantly reduced AKT2 activation. D) An AKT signaling phospho protein array identified several key players within the IRS1/PI3K/AKT signaling pathway to be uniquely misregulated upon Snus ED exposure. $^{*}P<0.05$ represents a significant deviation in log2 transformed signal fold change as compared to the untreated control, as determined by One-Way ANOVA. NED, non-effective dose; ED, effective dose.

downstream phosphorylation of S6RP [51, 52] at S235/236 and subsequent activation of S6RP. S6RP phosphorylation increases translation of mRNA transcripts with 5' UTR that contain an oligopyrimidine tract [53]. In line with the observed PDK1 phosphorylation pattern, $pS6RP^{S235}$ (S6 Ribo. Prot.) was also significantly reduced in Snus ED cultures.

Collectively, these data suggest that Snus exposure disrupts normal signaling patterns within different arms of the IRS1/PI3K signaling pathway that elicit adverse effects on normal cellular functions.

Snus-mediated AKT signaling disruption is AKT isoform-specific and associated with negative consequences for osteogenic differentiation outcomes

Evaluation of the AKT signaling phospho protein results also found differential activation of AKT1 and AKT2 in Snus ED cultures compared to the untreated control (Fig. 5.7A). Activated $pAKT1^{S473}$ was significantly increased in Snus ED cultures. Conversely, Snus ED exposure also significantly reduced activated $pAKT2^{S474}$ levels. Pre-activated $pAKT1^{T450}$ [54] was also significantly upregulated in Snus ED. PI3K has been reported to activate AKT1 in a PDK1-independent manner and AKT2 in a PDK2-dependent manner [55], suggesting an etiology for the differential AKT isoform activation observed here.

Western blot analysis was performed to verify $pAKT1^{S473}$ upregulation and also assess the activation status of other major signaling kinases involved in cellular differentiation, stress response, and FOXO regulation (Fig. 5.7B). Increased levels of $pAKT1^{S473}$ were confirmed in Snus ED alongside reduced activation of ERK1/2 and JNK1/2 kinases. Levels of active AMPK did not differ between Snus NE and ED groups.

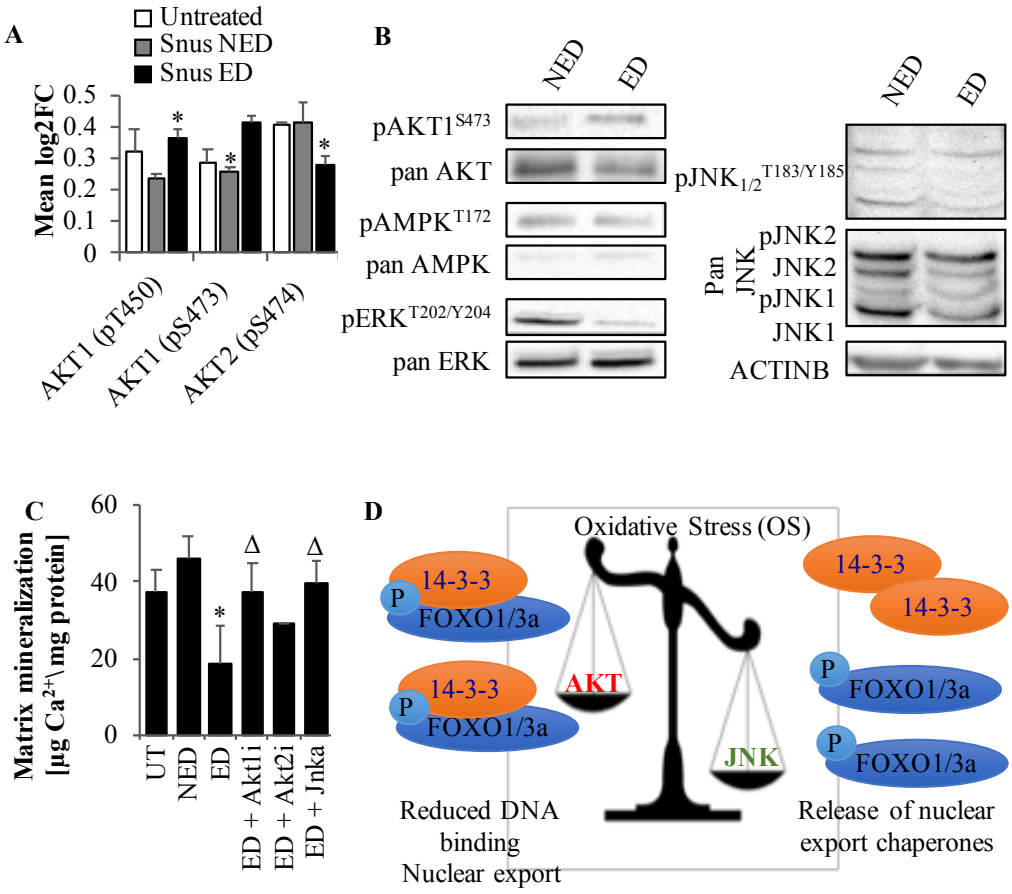
A
Untreated
Snus NED
Snus ED
Mean log2FC
0.5
0.4
0.3
0.2
0.1
0
*
*
*
AKT1 (pT450)
AKT1 (pS473)
AKT2 (pS474)
B
NED
ED
pAKT1S473
pan AKT
pAMPKT172
pan AMPK
pERKT202/Y204
pan ERK
NED
ED
pJNK1/2T183/Y185
Pan JNK
pJNK2
JNK2
pJNK1
JNK1
ACTINB
C
Matrix mineralization [µg Ca2+\mg protein]
60
40
20
0
*
Δ
Δ
UT
NED
ED
ED + Akt1i
ED + Akt2i
ED + Jnka
D
Oxidative Stress (OS)
14-3-3
P
FOXO1/3a
14-3-3
P
FOXO1/3a
AKT
JNK
14-3-3
14-3-3
P
FOXO1/3a
P
FOXO1/3a
Reduced DNA binding
Nuclear export
Release of nuclear export chaperones

Figure 5.7. Snus disruption of AKT signaling pathway may negatively impact osteogenesis by augmenting the antagonistic relationship between JNK and AKT. A) AKT signaling phospho protein array found AKT1 and AKT2 isoforms to be differentially regulated in Snus ED exposed cultures. Snus ED significantly upregulated AKT1 activation and significantly reduced AKT2 activation. $P<0.05$ represents a significant reduction in log2 fold change as compared to the untreated control, as determined by One-Way ANOVA B) Western blot analysis confirmed increased phosphorylation of AKT1 at S473 and also revealed differential activation of JNK1 and JNK2 isoforms. JNK1 activation was reduced in Snus ED, but remained unchanged for JNK2. ERK activation was reduced in Snus ED cultures. C) Treatment of Snus ED cultures with AKT1 inhibitor and JNK1/2 activator rescued osteogenesis. $^{*}P<0.05$ represents a significant reduction in osteogenesis compared to the untreated control, as determined by One-Way ANOVA. $^{\Delta}P<0.05$ represents an increase in osteogenesis compared to Snus ED, as determined by One-Way ANOVA. D) AKT and JNK exert opposite effects on FOXO subcellular localization. FOXO phosphorylation by AKT encourages reduced nuclear binding and increased nuclear export of FOXO via 14-3-3 protein interactions. JNK, conversely, can reverse this process by facilitating the release of FOXOs from 14-3-3 proteins. Thus, Snus upregulation of AKT1 in combination with reduced JNK1 activity may ultimately encourage a cellular environment that bars FOXO from the nucleus and may have implications for normal osteogenic development. UT, untreated; NED, non-effective dose; ED, effective dose.

With regard to FOXO regulation, active ERK1/2 is associated with targeting FOXO species for poly-ubiquitination and degradation [56], [57]. Considering the reduction in active pERK1/2$^{T202/Y204}$ levels, it is unlikely that reductions in nuclear FOXO1 and FOXO3a may also be attributed to ERK activity. Downregulation of ERK1/2 could, however, have other negative impacts on normal cellular differentiation [58]. Patterns of pJNK1/2$^{T183/Y185}$ activation demonstrated reduced pJNK1^{Y185} levels in Snus ED. As active JNK has been shown to antagonize AKT-directed nuclear exclusion of FOXO3a [59], reduced activation of JNK1 may cause a balance shift in direction of FOXO localization towards nuclear exclusion. JNK achieves this by phosphorylating of 14-3-3 proteins that escort and/or sequester FOXO out of the nucleus, causing 14-3-3 to release FOXO. Subsequent phosphatase removal of AKT phosphorylation modifications on FOXO can subsequently allow for full restoration of nuclear FOXO [60].

To investigate the impact of excessive AKT on osteogenesis, Snus ED cultures were concurrently treated with an inhibitor to block AKT1 or AKT2 activity or an activator of JNK1/2. Both inhibition of AKT1 and activation of JNK1/2 exclusively rescued osteogenic output in Snus ED cultures (Fig. 5.7C). Collectively, these results support the notion of a two-fold impact of biochemical misregulation as mediated by Snus exposure (Fig. 5.7D). First, AKT1 activity is upregulated targeting FOXO1 and FOXO3a species for nuclear exclusion mediated by phosphorylation events that create binding sites for 14-3-3 nuclear exclusion proteins [61]. Second, simultaneously reduced levels of active JNK creates an environment where cytoplasmically sequestered FOXO1/3a predominates within cells and effectively inhibits normal osteogenesis.

Discussion

Here we have shown for the first time, a comprehensive analysis of the embryotoxic impact of Snus exposure on the developing skeleton using a combination of *in vivo* exposures and developing osteoblasts produced by differentiating human embryonic stem cells into a osteogenic lineage. Using these approaches revealed that Snus inhibited normal skeletal development by mediating several molecular and biochemical changes in developing osteoblasts in the absence of outright cytotoxicity.

Previously reported *in vivo* studies have shown connections between smokeless tobacco exposure and adverse osteogenic outcomes, including reduced ossification in fetal bones including the skull and long bone tissues [16, 17] and reduced bone nodule formation [62]. These studies, however, did not investigate the molecular or biochemical events responsible for these outcomes. Our study found similar detrimental effects on skull mineralization and morphological development in *in utero* Snus-exposed offspring and differentiating osteoblasts *in vitro* while extending our investigation into mechanistic analyses to reveal Snus-mediated molecular changes that may be responsible for adverse osteogenic outcomes.

Induction of oxidative stress conditions in developing tissues is a well-reported mechanism of chemically-mediated teratogenicity [38, 39]. Here, we provide evidence that Snus embryotoxicity is mediated at least in part by generation of sub-cytotoxic levels of ROS. Redox driven teratogenesis is characterized by alterations to intracellular biochemical events that are critical to normal cell function and development. Such changes, in turn, can cause dysmorphogenetic outcomes in developing cells in the absence of

outright cell death. Our findings support this concept in that Snus doses showing reduced osteoblast mineralization did not possess active pro-apoptotic activation of executioner caspases despite increased levels of ROS. Furthermore, antioxidant treatment rescued osteogenesis, suggesting that excessive ROS likely plays a role in Snus-reduced osteogenic outcomes by manipulating cellular redox sensitive regulatory components or signaling pathways.

Environmental toxicant interference with key signaling pathways has also been reported to have a myriad of adverse effects on early development in a variety of contexts [63-66]. Precise activation or inhibition of particular signaling players at key points in the development of differentiating tissues can derail correct cell fate decisions. Results from this study support such a mode of action for Snus-driven inhibition of normal osteogenesis. Snus exposure upregulated activation of key players in the IRS1/PI3K/AKT signaling pathway, which showed downstream inhibitory actions on normal FOXO1 and FOXO3A subcellular localization. Further, this effect seems to be exacerbated by reduced activation of JNK1. Considering that our data also show FOXO1 and FOXO3A to be required for robust osteogenic differentiation, it is possible that osteogenic reduction by Snus is mediated downstream of AKT signaling through developmentally-relevant inhibition of FOXO1/3A function.

As FOXO1/3a proteins mediate oxidative stress defense, Snus-driven inhibition of FOXO1/3A may be responsible for observed increases in ROS and reduced superoxide dismutase and catalase antioxidant enzyme activity. While elevated ROS alone has been previously associated with antagonism of signaling pathways, bone loss pathology, and

inhibited osteogenesis [67-69], several researchers have also reported that reduced FOXO activity in osteoblasts elicits similar outcomes in adult bone tissue [70, 71]. While our results support Snus-driven inhibition of FOXO1/3A oxidative stress defense that subsequently encourages increased developmentally-harmful levels of ROS, it is unclear if FOXO1/3a proteins also influence embryonic osteogenesis, specifically. Thus, further study is required to dissect the precise relationship between FOXO1/3a and key events during developmental osteogenesis.

It is also worth noting that misregulation of other developmentally-relevant components of the IRS1/PI3K/AKT pathway suggest an additional avenue for adverse osteogenic outcomes following Snus exposure. Given that differentiating cells regularly require new sets of proteins to facilitate cell fate decisions and changes [75], reduced S6RP activity as reported here could also be detrimental for developing osteoblasts. The complexity of Snus-altered interplay between members of the IRS1/PI3K/AKT signaling pathway demonstrate a need for further study.

Further exploration of Snus-driven osteogenic inhibition is required to more clearly discern which of these disruptive events contributes most to observed adverse osteogenic outcomes.

Conclusion

Smokeless tobacco—both in general and with specific regard to Snus—has been hailed as a potential means to reduce mortality and pathology burden from tobacco-related diseases [76], [77]. With particular regard to developmental health, however, our data show

that Snus smokeless tobacco may not reduce harm to health of the developing embryo. In the context of previous studies on smokeless tobacco use and adverse pregnancy outcomes, our results indicate that women who are pregnant or planning to become pregnant should opt for complete cessation of tobacco for a healthy pregnancy.

References

1. Centers for Disease Control and Prevention (CDC). Smoking-attributable mortality, years of potential life lost, and productivity losses--United States, 2000-2004. MMWR Morb. Mortal. Wkly. Rep. 2008;57(45): 1226–1228.

2. Samet JM. Tobacco smoking: the leading cause of preventable disease worldwide. Thorac Surg Clin. 2013;23(2): 103–112.

3. Shiffman S, Gitchell JG, Warner KE, Slade J, Henningfield JE, Pinney JM. Tobacco harm reduction: conceptual structure and nomenclature for analysis and research. Nicotine Tob Res. 2002;4 Suppl 2:S113-29.

4. Slade J. Innovative nicotine delivery devices from tobacco companies. in Nicotine and public health. R. Ferrence, J. Slade, R. Room, and M. Pope, Eds. Washington DC: American Public Health Association, 2000, 209–28.

5. Institute of Medicine (US) Committee to Assess the Science. Base for Tobacco Harm. Stratton K and Shetty P. Principles of Harm Reduction. National Academies Press (US), 2001.

6. Institute of Medicine (US) Committee to Assess the Science. Base for Tobacco Harm. Products for Tobacco Exposure Reduction. National Academies Press (US), 2001.

7. Centers for Disease Control and Prevention (US). National Center for Chronic Disease Prevention and Health Promotion (US) and Office on Smoking and Health (US). Chemistry and Toxicology. of Cigarette Smoke and Biomarkers of Exposure and Harm. Centers for Disease Control and Prevention (US), 2010.

8. Foulds J, Ramstrom L, Burke M, Fagerström K. Effect of smokeless tobacco (Snus) on smoking and public health in Sweden. Tob Control. 2003;12(4): 349–359.

9. Nilsson R. A qualitative and quantitative risk assessment of snuff dipping. Regul Toxicol Pharmacol. 1998;28(1): 1–16.

10. Liu ST, Nemeth JM, Klein EG, Ferketich AK, Kwan MP, Wewers ME. Risk perceptions of smokeless tobacco among adolescent and adult users and nonusers. J Health Commun. 2015;20(5): 599–606.

11. Zhu S-H, Gamst A, Lee M, Cummins S, Yin L, Zoref L. The use and perception of electronic cigarettes and Snus among the U.S. population. PLoS ONE. 2013;8(10): e79332.

12. Choi K and Forster J. Awareness, perceptions and use of Snus among young adults from the upper Midwest region of the USA. Tob Control. 2013;22(6): 412–417.

13. Øverland S, Hetland J, and Aarø LE. Relative harm of Snus and cigarettes: what do Norwegian adolescents say? Tob Control. 2008;17(6): 422–425.

14. Frøisland DH. Nicotine withdrawal syndrome in a newborn baby after maternal use of oral applied moist tobacco (Snus), should result in greater awareness to the use of Snus among pregnant women. Acta Paediatr. 2017;106(9): 1531.

15. England LJ, Levine RJ, Mills JL, Klebanoff MA, Yu KF, Cnattingius S. Adverse pregnancy outcomes in snuff users. Am J Obstet Gynecol. 2003;189(4): 939–943.

16. Paulson RB, Shanfeld J, Mullet D, Cole J, Paulson JO. Prenatal smokeless tobacco effects on the rat fetus. J Craniofac Genet Dev Biol. 1994;14(1): 16–25.

17. Paulson R, Shanfeld J, Sachs L, Price T, Paulson J. Effect of smokeless tobacco on the development of the CD-1 mouse fetus. Teratology. 1989;40(5): 483–494.

18. National Research Council (US) Committee for the Update of the Guide for the Care and Use of Laboratory Animals. Guide for the Care and Use of Laboratory Animals, 8th ed. Washington (DC): National Academies Press (US), 2011.

19. Rigueur D and Lyons KM. Whole-Mount Skeletal Staining. Methods Mol Biol. 2014;1130113–121.

20. de Keizer PLJ, Packer LM, Szypowska AA, Riedl-Polderman PE, van den Broek NJF, de Bruin A, Dansen TB, Marais R, Brenkman AB, Burgering BMT. Activation of FOXO transcription factors by oncogenic BRAF promotes p21cip1-dependent senescence. Cancer Res. 2010;70(21): 8526–8536.

21. zur Nieden NI and Baumgartner L. Assessing developmental osteotoxicity of chlorides in the embryonic stem cell test. Reprod Toxicol. 2010;30(2): 277–283.

22. Martinez IKC, Sparks NRL, Madrid JV, Affeldt H 3rd, Vera MKM, Bhanu B, Zur Nieden NI. Video-based kinetic analysis of calcification in live osteogenic human

embryonic stem cell cultures reveals the developmentally toxic effect of Snus tobacco extract. Toxicol Appl Pharmacol. 2019;363111–121.

23. Walker L, Baumgartner L, Keller KC, Ast J, Trettner S, zur Nieden NI. Non-human primate and rodent embryonic stem cells are differentially sensitive to embryotoxic compounds. Toxicol Rep. 2015;2165–174.

24. Davis L, Dienelt A, zur Nieden NI. Absorption-Based Assays for the Analysis of Osteogenic and Chondrogenic Yield. in Embryonic Stem Cell Therapy for Osteo-Degenerative Diseases. NI zur Nieden, Ed. Humana Press, 2011, 255–272.

25. Qin Y, Lu M, Gong X. Dihydrorhodamine 123 is superior to 2,7-dichlorodihydrofluorescein diacetate and dihydrorhodamine 6G in detecting intracellular hydrogen peroxide in tumor cells. Cell Biol Int. 2008;32(2): 224–228.

26. Royall JA and Ischiropoulos H. Evaluation of 2',7'-dichlorofluorescin and dihydrorhodamine 123 as fluorescent probes for intracellular H2O2 in cultured endothelial cells. Arch Biochem Biophys. 1993;302(2): 348–355.

27. Ritchie ME, Phipson B, Wu D, Hu Y, Law CW, Shi W, Smyth GK. limma powers differential expression analyses for RNA-sequencing and microarray studies. Nucleic Acids Res. 2015;43(7): e47.

28. Wickham H and Francois R. dplyr: A Grammar of Data Manipulation. 2016. [Online]. Available: https://CRAN.R-project.org/package=dplyr.

29. Gregory R, Bolker B, Bonebakker L, Gentleman R, Huber, W, Liaw A, Lumley T, Maechler M, Magnusson A, Moeller S, Schwartz M, Venables B. gplots: Various R Programming Tools for Plotting Data. 2016. [Online]. Available: https://CRAN.R-project.org/package=gplots.

30. R Core Team. R: A Language and Environment for Statistical Computing. Vienna, Austria: R Foundation for Statistical Computing, 2016.

31. Chernoff N, Rogers JM, Kavlock RJ. An overview of maternal toxicity and prenatal development: considerations for developmental toxicity hazard assessments. Toxicology. 1989;59(2): 111–125.

32. Madrid JV, Sera S, Sparks NRL, zur Nieden NI. Human Pluripotent Stem Cells to Assess Developmental Toxicity in the Osteogenic Lineage. Methods Mol Biol. 2018;1797125–145.

33. Genschow E, Spielmann H, Scholz G, Seiler A, Brown N, Piersma A, Brady M, Clemann N, Huuskonen H, Paillard F, Bremer S, Becker K. The ECVAM international validation study on *in vitro* embryotoxicity tests: results of the definitive phase and evaluation of prediction models. European Centre for the Validation of Alternative Methods. Altern Lab Anim. 2002;30(2): 151–176.

34. Weinbrenner T, Cladellas M, Isabel Covas M, Fitó M, Tomás M, Sentí M, Bruguera J, Marrugat J. High oxidative stress in patients with stable coronary heart disease. Atherosclerosis. 2003;168(1): 99–106.

35. Dennery PA. Effects of oxidative stress on embryonic development. Birth Defects Res C Embryo Today: Reviews. 2007;81(3): 155–162.

36. Kaneto H, Katakami N, Kawamori D, Miyatsuka T, Sakamoto K, Matsuoka TA, Matsuhisa M, Yamasaki Y. Involvement of oxidative stress in the pathogenesis of diabetes. Antioxid. Redox Signal. 2007;9(3): 355–366.

37. Mena S, Ortega A, Estrela JM. Oxidative stress in environmental-induced carcinogenesis. Mutat. Res. 2009;674(1–2): 36–44.

38. Hansen JM and Harris C. Redox control of teratogenesis. Reprod Toxicol. 2013;35165–179.

39. Kovacic P and Somanathan R. Mechanism of teratogenesis: electron transfer, reactive oxygen species, and antioxidants. Birth Defects Res C Embryo Today. 2006;78(4): 308–325.

40. Sies H, Ed. Oxidative Stress. London: Academic Press, 1985.

41. Halliwell B and Whiteman M. Measuring reactive species and oxidative damage *in vivo* and in cell culture: how should you do it and what do the results mean? Br J Pharmacol. 2004;142(2): 231–255.

42. Dalle-Donne I, Rossi R, Colombo R, Giustarini D, Milzani A. Biomarkers of oxidative damage in human disease. Clin Chem. 2006;52(4): 601–623.

43. Morrow JD and Roberts LJ. The isoprostanes: their role as an index of oxidant stress status in human pulmonary disease. Am J Respir Crit Care Med. 2002;166(12 Pt 2): S25-30.

44. Birben E, Sahiner UM, Sackesen C, Erzurum S, Kalayci O. Oxidative Stress and Antioxidant Defense. World Allergy Organ J. 2012;5(1): 9–19.

45. Calnan DR and Brunet A. The FOXO code. Oncogene. 2008;27(16): 2276–2288.

46. Kops G, Dansen TB, Polderman PE, Saarloos I, Wirtz KW, Coffer PJ, Huang TT, Bos JL, Medema RH, Burgering BM. Forkhead transcription factor FOXO3a protects quiescent cells from oxidative stress. Nature. 2002;419(6904): 316–321.

47. Klotz L, Sánchez-Ramos C, Prieto-Arroyo I, Urbánek P, Steinbrenner H, Monsalve M. Redox regulation of FOXO transcription factors. Redox Biol. 2015;651–72.

48. Moloney AM, Griffin RJ, Timmons S, O'Connor R, Ravid R, O'Neill C. Defects in IGF-1 receptor, insulin receptor and IRS-1/2 in Alzheimer's disease indicate possible resistance to IGF-1 and insulin signalling. Neurobiol Aging. 2010;31(2): 224–243.

49. Vivanco I and Sawyers CL. The phosphatidylinositol 3-Kinase–AKT pathway in human cancer. Nat Rev Cancer. 2002;2(7): 489.

50. Rodig SJ, Meraz MA, White JM, Lampe PA, Riley JK, Arthur CD, King KL, Sheehan KC, Yin L, Pennica D, Johnson EM Jr, Schreiber RD. Disruption of the Jak1 gene demonstrates obligatory and nonredundant roles of the Jaks in cytokine-induced biologic responses. Cell. 1998;93(3): 373–383.

51. Williams MR, Arthur JS, Balendran A, van der Kaay J, Poli V, Cohen P, Alessi DR. The role of 3-phosphoinositide-dependent protein kinase 1 in activating AGC kinases defined in embryonic stem cells. Current Biology. 2000;10(8): 439–448.

52. Nagashima K, Shumway SD, Sathyanarayanan S, Chen AH, Dolinski B, Xu Y, Keilhack H, Nguyen T, Wiznerowicz M, Li L, Lutterbach BA, Chi A, Paweletz C, et al. Genetic and pharmacological inhibition of PDK1 in cancer cells: characterization of a selective allosteric kinase inhibitor. J Biol Chem. 2011;286(8): 6433–6448.

53. Peterson RT and Schreiber SL. Translation control: connecting mitogens and the ribosome. Curr Biol. 1998;8(7): R248-250.

54. Chan TO, Rittenhouse SE, Tsichlis PN. AKT/PKB and other D3 phosphoinositide-regulated kinases: kinase activation by phosphoinositide-dependent phosphorylation. Annu Rev Biochem. 1999;68965–1014.

55. Tsuchiya A, Kanno T, Nishizaki T. PI3 kinase directly phosphorylates Akt1/2 at Ser473/474 in the insulin signal transduction pathway. J Endocrinol. 2014;220(1): 49–59.

56. Yang W, Dolloff NG, El-Deiry WS. ERK and MDM2 prey on FOXO3a. Nat Cell Biol. 2008;10(2): 125–126.

57. Yang JY, Zong CS, Xia W, Yamaguchi H, Ding Q, Xie X, Lang JY, Lai CC, Chang CJ, Huang WC, Huang H, Kuo HP, Lee DF, et al. ERK promotes tumorigenesis by inhibiting FOXO3a via MDM2-mediated degradation. Nat Cell Biol. 2008;10(2): 138–148.

58. Sun Y, Liu WZ, Liu T, Feng X, Yang N, Zhou HF. Signaling pathway of MAPK/ERK in cell proliferation, differentiation, migration, senescence and apoptosis. J. Recept. Signal Transduct. Res. 2015;35(6): 600–604.

59. Sunayama J, Tsuruta F, Masuyama N, Gotoh Y. JNK antagonizes Akt-mediated survival signals by phosphorylating 14-3-3. J Cell Biol. 2005;170(2): 295–304.

60. Singh A, cYe M, Bucur O, Zhu S, Tanya Santos M, Rabinovitz I, Wei W, Gao D, Hahn WC, Khosravi-Far R. Protein phosphatase 2A reactivates FOXO3a through a dynamic interplay with 14-3-3 and AKT. Mol Biol Cell. 2010;21(6): 1140–1152.

61. Daitoku H, Sakamaki J, Fukamizu A. Regulation of FOXO transcription factors by acetylation and protein–protein interactions. BBA-Mol Cel Res. 2011;1813(11): 1954–1960.

62. Henderson JS and Johnson RB. The effects of smokeless tobacco extract on bone nodule formation and mineralization by chick osteoblasts *in vitro*. Arch. Oral Biol. 1995;40(7): 615–621.

63. Knobloch J, Schmitz I, Götz K, Schulze-Osthoff K, Rüther U. Thalidomide induces limb anomalies by PTEN stabilization, Akt suppression, and stimulation of caspase-dependent cell death. Mol. Cell. Biol. 2008;28(2): 529–538.

64. Eberhart JK and Harris RA. Understanding variability in ethanol teratogenicity. PNAS. 2013;110(14): 5285–5286.

65. Mirkes PE, Wilson KL, Cornel LM. Teratogen-induced activation of ERK, JNK, and p38 MAP kinases in early postimplantation murine embryos. Teratology. 2000;62(1): 14–25.

66. Wu Y, Viana M, Thirumangalathu S, Loeken MR. AMP-activated protein kinase mediates effects of oxidative stress on embryo gene expression in a mouse model of diabetic embryopathy. Diabetologia. 2012;55(1): 245–254.

67. Almeida M, Han L, Martin-Millan M, Plotkin LI, Stewart SA, Roberson PK, Kousteni S, O'Brien CA, Bellido T, Parfitt AM, Weinstein RS, Jilka RL, Manolagas SC. Skeletal involution by age-associated oxidative stress and its acceleration by loss of sex steroids. J. Biol. Chem. 2007;282(37): 27285–27297.

68. Almeida M, Ambrogini E, Han L, Manolagas SC, Jilka RL. Increased lipid oxidation causes oxidative stress, increased peroxisome proliferator-activated receptor-gamma expression, and diminished pro-osteogenic Wnt signaling in the skeleton. J. Biol. Chem. 2009;284(40): 27438–27448.

69. Manolagas SC. From estrogen-centric to aging and oxidative stress: a revised perspective of the pathogenesis of osteoporosis. Endocr. Rev. 2010;31(3): 266–300.

70. Rached M-T, Kode A, Xu L, Yoshikawa Y, Paik JH, Depinho RA, Kousteni S. FOXO1 is a positive regulator of bone formation by favoring protein synthesis and resistance to oxidative stress in osteoblasts. Cell Metab. 2010;11(2): 147–160.

71. Ambrogini E, Almeida M, Martin-Millan M, Paik JH, Depinho RA, Han L, Goellner J, Weinstein RS, Jilka RL, O'Brien CA, Manolagas SC. FOXO-mediated defense against oxidative stress in osteoblasts is indispensable for skeletal homeostasis in mice. Cell Metab. 2010;11(2): 136.

72. Benhar M, Engelberg D, Levitzki A. ROS, stress-activated kinases and stress signaling in cancer. EMBO reports. 2002;3(5): 420–425.

73. Zhang Z, Teruya K, Eto H, Shirahata S. Fucoidan Extract Induces Apoptosis in MCF-7 Cells via a Mechanism Involving the ROS-Dependent JNK Activation and Mitochondria-Mediated Pathways. PLoS ONE. 2011;6(11): e27441.

74. Yoshizumi M, Abe J, Haendeler J, Huang Q, Berk BC. Src and Cas Mediate JNK Activation but Not ERK1/2 and p38 Kinases by Reactive Oxygen Species. J. Biol. Chem. 2000;275(16): 11706–11712.

75. Buszczak M, Signer R, Morrison SJ. Cellular differences in protein synthesis regulate tissue homeostasis. Cell. 2014;159(2): 242–251.

76. Gartner C and Hall W. Harm reduction policies for tobacco users. Int J Drug Policy. 2010;21(2): 129–130.

77. Kozlowski LT. Effect of Smokeless Tobacco Product Marketing and Use on Population Harm from Tobacco Use: Policy Perspective for Tobacco-Risk Reduction. American Journal of Preventive Medicine 2007;33(6, Supplement): S379–S386.

78. Sparks, NRL, Martinez IKC, Soto CH, Zur Nieden NI. Low Osteogenic Yield in Human Pluripotent Stem Cells Associates with Differential Neural Crest Promoter Methylation. Stem Cells. 2018; 36:349–362.

CONCLUSION

To reduce the burden of birth defects both domestically and abroad, the role of environmental toxicants in developmental and reproductive disruption must be addressed. To this end, traditional animal models have been useful but are burdened by low throughput, high expense, and the risk of false negative assessments. *In vitro* cell-based assays provide one means to addressing these concerns. In particular, the embryonic stem cell test (EST) protocol provides an avenue for faster and less costly evaluations. By coupling this approach with human pluripotent stem cells (hPSCs), as this thesis has shown, the EST approach can be made more sensitive (than a mouse-based counterpart) and provide assessments that are more biologically relevant to humans.

hPSCs are a powerful tool for both embryotoxicity screens and modeling mechanisms of developmental toxicity. This thesis has shown for the first time a full comparison of the mouse embryonic stem cell-based EST (mEST) to a human pluripotent stem cell-based EST (hEST). Conclusively, the tested hEST yielded accurate embryotoxicity classifications while performing more sensitively than the standard mEST. Moreover, the hEST was able to accurately classify "real-world" embryotoxicants in the form of two tobacco products. While it is unlikely that *in vitro* approaches will completely replace traditional models in the near future, hPSC-based *in vitro* assessments provide a faster, less costly means to generating data relevant to human health and investigating the potential embryotoxicity of a chemical or chemical mixture (as is the case with tobacco products).

The hEST model is also an effective approach to investigating molecular and biochemical mechanisms of chemical embryotoxicity. Here, this thesis has presented the investigative and comparative analysis of conventional cigarette and harm-reduction tobacco product (HRTP) embryotoxicity. While both types of products inhibited normal osteogenic output in differentiating osteoblasts, conventional cigarettes were found to impart this outcome by eliciting mitochondrially-mediated apoptosis and DNA damage. Molecular and investigation of the HRTPs, however, suggested that harm-reduction cigarettes and Snus smokeless tobacco operate predominantly through differentiation inhibition mechanisms—instead of outright cytotoxicity mechanisms—to prevent normal osteogenesis. In particular, biochemical assessment of Snus-induced molecular changes was found to be mediated through specific alterations to developmentally relevant signaling pathways.

Through their special production processes, HRTPs are manufactured to expose users to chemical mixtures that are distinct from conventional cigarettes. As such, it can be hypothesized that molecular differences observed here between conventional cigarettes and HRTPs may lie in the unique composition of HRTPs. Current work in our lab seeks to explore the relationship between developmental osteogenic outcomes and some of the known chemical components shared by conventional cigarettes and HRTPs. Our earliest results have found that some of these chemicals inhibit osteogenic differentiation with enhanced potency dependent on whether they are presented alone or in a combination with two or three other chemicals. As such, altering the chemical exposure profile between

conventional cigarettes and HRTPs may not actually reduce harm in developing osteoblasts but rather augment differentiation inhibition potency.

Results outlined in this thesis also infer that early exposure to Snus during cell specification events during osteogenesis can have lasting impacts on developing bone. Ongoing studies in our lab are investigating the extent of *in vivo* long-term impacts following developmental *in utero* exposure. Thus far, we have observed reduced bone mineral density in the skulls, ribs, and hips of *in utero* exposed offspring at 12 months of age as well as evidence of adipose metabolic dysfunction (Appendix Fig. 1.5.1-1.5.3). These early results suggest that HRTPs may impart an additional injury to health outcomes by disrupting key early events in embryonic development. These early results, however, only represent part of human exposure conditions for Snus as they are mediated through intravenous tail vein injection and feature a chemical profile that is restricted to only the aqueously soluble chemical components of Snus. Future follow-up studies, therefore, will be designed to verify similar osteotoxic outcomes under conditions that are closer to human physiological exposure circumstances.

In sum, we have successfully determined the comparative sensitivity of human and mouse pluripotent stem cells in embryotoxicity evaluations. We also utilized an *in vitro* developmental osteotoxicity screening model with human embryonic stem cells to successfully investigate embryotoxic mechanisms in conventional cigarettes and HRTPs. These assessments found harm-reduction cigarettes and Snus smokeless tobacco to elicit osteotoxic outcomes by differentiation inhibition and modulating cellular behaviors involved in key developmental events. The results presented here provide much needed

support for the use of hPSCS in mechanistic embryotoxicity assessments. Furthermore, findings from the presented studies on HRTPs address the current gaps in knowledge regarding HRTP-driven skeletal defects. Together, our results should be useful in advancing embryotoxicity screening efforts as well as for efforts to inform global health initiatives to reduce birth defects burdens.

APPENDICES

APPENDIX 1

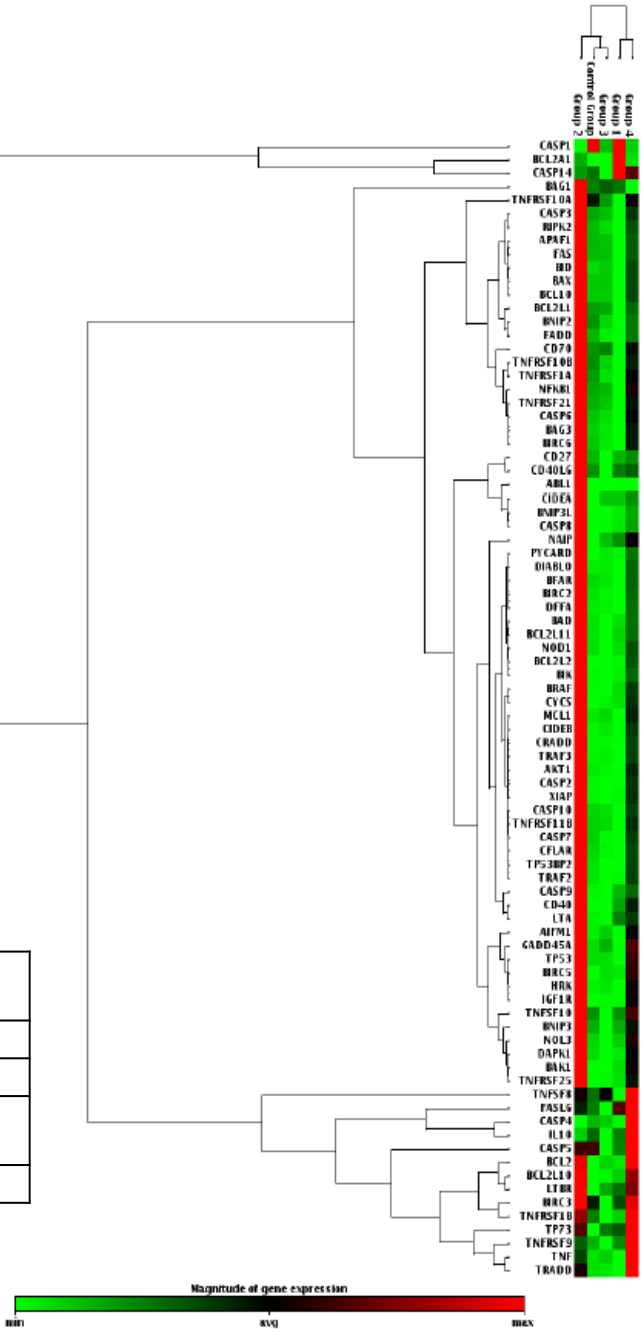

Control group	Untreated
Group 1	Camel SS non-effective dose
Group 2	Camel SS effective dose
Group 3	Camel Blue SS non-effective dose
Group 4	Camel Blue SS effective dose

Appendix Figure 1.4.1. Heatmap of candidate genes showing their regulation across all five treatments.

Chapter 5: Supplemental information

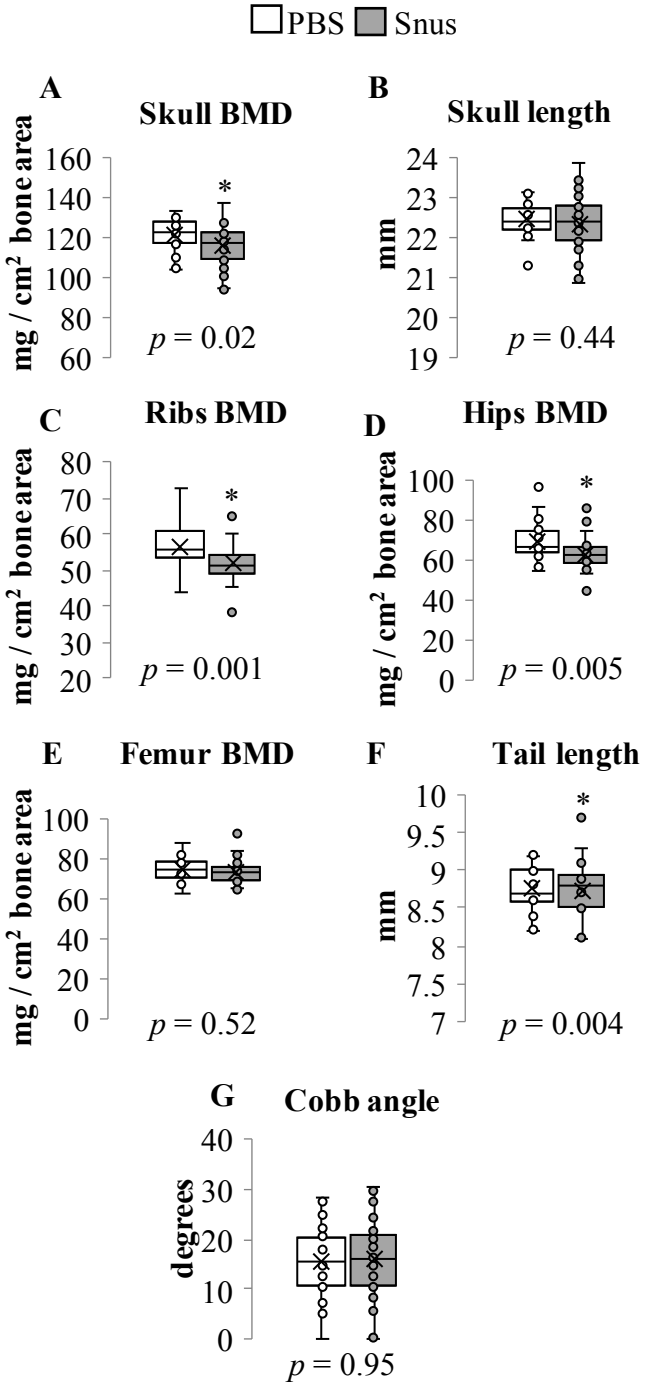

Appendix Figure 1.5.1. Snus-exposed mice demonstrated long-term skeletal impairment. (A, C, D) Bone mineral density was significantly reduced in the skulls, ribs, and hips of Snus-exposed mice. (B) Skull length was unchanged in Snus-exposed mice. (E) Femur bone mineral density did not differ between PBS and Snus-exposed mice. (F) Tail length was significantly reduced in Snus-exposed mice. Given that reduced bone mineral density has been associated with higher fat mass and serum lipids (29089152, 16400063), it is possible that Snus-exposure misregulates interconnected mechanisms that influence adipose tissue metabolism and osteogenesis. (G) Cobb angle measurement did not present a significant difference in spinal curvature between PBS and Snus mice. BMD, bone mineral density. PBS n = 29. Snus n = 47. $^{*}p<0.05$, represents a significant difference between PBS control mice and Snus-exposed mice.

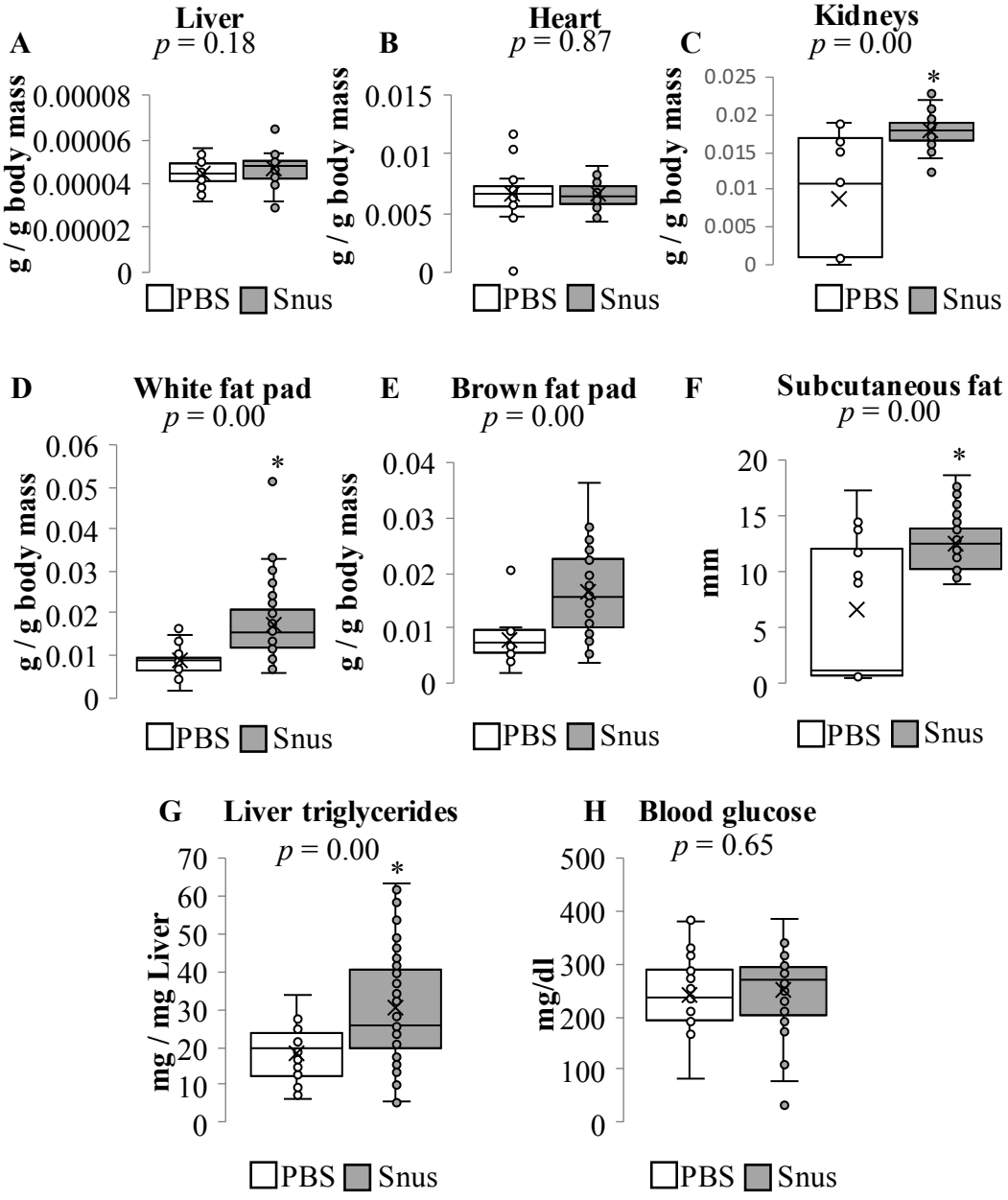
A
Liver
p = 0.18
g / g body mass
0.00008
0.00006
0.00004
0.00002
0
PBS
Snus
B
Heart
p = 0.87
g / g body mass
0.015
0.01
0.005
0
PBS
Snus
C
Kidneys
p = 0.00
g / g body mass
0.025
0.02
0.015
0.01
0.005
0
*
PBS
Snus
D
White fat pad
p = 0.00
g / g body mass
0.06
0.05
0.04
0.03
0.02
0.01
0
*
PBS
Snus
E
Brown fat pad
p = 0.00
g / g body mass
0.04
0.03
0.02
0.01
0
PBS
Snus
F
Subcutaneous fat
p = 0.00
mm
20
15
10
5
0
*
PBS
Snus
G
Liver triglycerides
p = 0.00
mg / mg Liver
70
60
50
40
30
20
10
0
*
PBS
Snus
H
Blood glucose
p = 0.65
mg/dl
500
400
300
200
100
0
PBS
Snus

Appendix Figure 1.5.2. 12-month-old *in utero* exposed mice possess increased adipose tissue and liver fat deposition. (A-C) Liver and heart mass were not significantly different between PBS and Snus exposed mice. Kidney mass, however, was significantly increased in Snus mice. (D-E) White and brown adipose tissue pads were significantly larger in Snus mice. (F) Subcutaneous fat, as measured by caliper, was significantly increased in Snus mice, compared to PBS mice. (G) Snus mice showed significantly increased liver triglyceride levels. (H) Blood glucose was not found to differ between PBS and Snus mice. Collectively, these results infer *in utero* Snus-exposed mice to possess impaired lipid metabolism and altered lipid deposition patterns. PBS n = 29. Snus n = 47. $^{*}p<0.05$, represents a significant difference between PBS control mice and Snus-exposed mice.

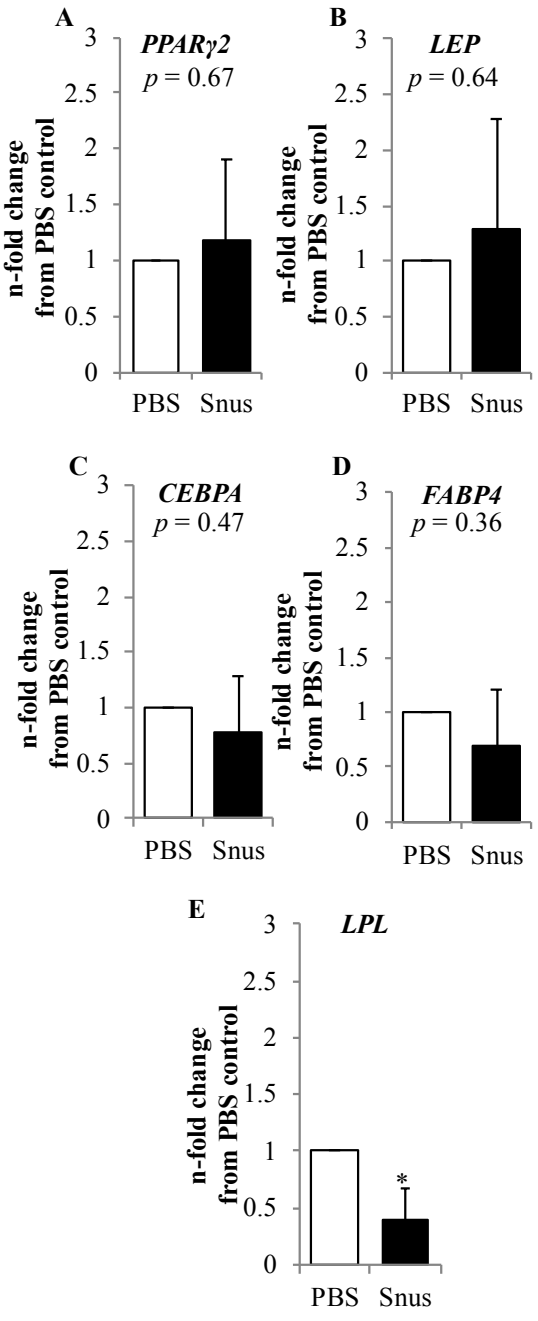
A
PPARγ2
p = 0.67
n-fold change from PBS control
3
2.5
2
1.5
1
0.5
0
PBS
Snus
B
LEP
p = 0.64
n-fold change from PBS control
3
2.5
2
1.5
1
0.5
0
PBS
Snus
C
CEBPA
p = 0.47
n-fold change from PBS control
3
2.5
2
1.5
1
0.5
0
PBS
Snus
D
FABP4
p = 0.36
n-fold change from PBS control
3
2.5
2
1.5
1
0.5
0
PBS
Snus
E
LPL
n-fold change from PBS control
3
2.5
2
1.5
1
0.5
0
*
PBS
Snus

Appendix Figure 1.5.3. qPCR analysis found significantly reduced expression of *LPL* mRNA in 12-month-old Snus-exposed mice. (A-D) No difference was observed for expression of genes associated with lipogenesis (*PPARγ2*, *CEBPA*) and fatty acid accumulation (*LEP*, *FABP4*) (E) mRNA expression of lipoprotein lipase enzyme (*LPL*) was significantly reduced in Snus-exposed mice. Together these data suggest that triglyceride lipolysis not adipogenesis is misregulated in Snus-exposed mice. PBS n = 4. Snus n = 7. $^{*}p<0.05$, represents a significant difference between PBS control mice and Snus-exposed mice. *CEBPA*, CCAAT enhancer binding protein alpha; *FABP4*, fatty acid binding protein 4; *LEP*, leptin; *LPL*, lipoprotein lipase; *PPARγ2*, peroxisome proliferator activated receptor gamma.

APPENDIX 2

Tobacco Product	Genes upregulated
Camel SS NED	*BCL2A1, BCL2L10, CASP1, CASP14, LTA, LTBR*
Camel SS ED	*ABL1, AIFM1, BAX, BCL2, BCL2A1, BCL2L10, BID, BIRC5, BNIP3L, CASP8, CASP9, CD27, CD40, CIDEA, CIDEB, CRADD, CYCS, DFFA, FASLG, GADD45A, HRK, LTA, LTBR, NAIP, TNF, TNFRSF10B, TNFRSF1B, TNFSF10, TP53, TP73, TRADD, TRAF2, TRAF3, XIAP*
Camel Blue SS NED	*AIFM1, BSC2L10, BIRC5, LTBR*
Camel Blue SS ED	*AIFM1, BAX, BCL2, BCL2A1, BCL2L10, BIRC5, BNIP3L, CASP4, CASP5, CASP8, CASP9, Casp14, CD27, CD40, CRADD, CYCS, DFFA, FASLG, HRK, IL10, LTA, LTBR, TNSFRSF9, TNFRSF10B, TNFRSF1B, TNFSF10, TP53, TP73, TRADD, TRAF2, TRAF3, XIAP*

Appendix Table 2.4.1. List of genes significantly regulated per treatment group compared to time-matched untreated cells as found with qPCR array.

29 common elements in Camel Snus NED and Camel Snus ED	Cyclin D1, FAK p53 (pT81), LYN, 14-3-3ζ/δ, Bax (N-term), Cyclin D1 (pT286), AKT1S1, p53 (pS20), 14-3-3ζ/δ (pT232), PTEN, MDM2, Tuberin, PP2Aα, IRS1, FAK (pS910), Paxillin, BAD (pS91/128), Gab1, MYT1, p53, PDK1, FAK (pY925), FAK (pY861), AKT1, AKT1 , eNOS (pS1177), FOXO1/3/4 (pT24/32), FOXO1A (pS329)
6 elements included exclusively in Camel Snus NED	p53 (pS6), IRS1 (pS612), BAD (pS112), p53 (pS315), IKKα/β (pS180/181)
18 elements included exclusively in Camel Snus ED	p70S6K, AKT (pS473), PI3K p85α/γ (pY467/Y199), FOXO1 (pS256), p53 (pS46), PDK1 (pS241), PTEN, p70S6K (pS424), IRS1 (pS312), AKT2 (pS474), SYK (inter), S6 Ribosomal Protein (pS235), PFKFB2 (inter), FOXO1 (pS319), PTEN (pS380/T382/T383), JAK1 (pY1022), GSK3β (pS9), FOXO1A/3A (pS322/325)

Appendix Table 2.5.1. List of proteins significantly misregulated per treatment group on AKT phospho protein array.